Atmospheric Nucleation: Measurements, Mechanisms, and Dynamics

A DISSERTATION
SUBMITTED TO THE FACULTY OF THE GRADUATE SCHOOL
OF THE UNIVERSITY OF MINNESOTA
BY

Chongai Kuang

IN PARTIAL FULFILLMENT OF THE REQUIREMENTS
FOR THE DEGREE OF
DOCTOR OF PHILOSOPHY

Peter H. McMurry, Alon V. McCormick

September 2009

Table of Contents

List of Tables

List of Figures

Chapter 1 : Introduction

1.1 Atmospheric Nucleation

Atmospheric nucleation occurs when stable molecular clusters are formed spontaneously from the gas-phase. The photochemically-driven formation and growth of stable atmospheric clusters is believed to occur through multi-component processes that often include sulfuric acid. New particle formation (NPF) occurs when these nucleated clusters grow to a detectable size. These nucleation events are then usually identified by increases in the concentrations of gas-phase sulfuric acid followed by increases in the concentrations of nanoparticles above the size detection limit which, until recently, was about 3 nm [*Stolzenburg and McMurry*, 1991]. Using these criteria, atmospheric nucleation events have been observed year-round in global, diverse locations including urban, rural, marine, and biogenic environments [*Kulmala et al.*, 2004b].

New particle formation by nucleation of gas-phase species significantly influences the size distributions and number concentrations of atmospheric aerosols. These nucleated particles are formed at rates that are orders of magnitude higher than were predicted by early models [*Weber et al.*, 1996] and grow at rates that are typically ten times faster than can be explained by the condensation of sulfuric acid alone [*Weber et al.*, 1997; *Mäkelä et al.*, 2001; *Wehner et al.*, 2005]. The resultant aerosols exert a significant impact on global climate by affecting the earth's radiation balance directly through the scattering and absorption of incident solar radiation, and indirectly through their role as cloud condensation nuclei (CCN) [*Albrecht*, 1989; *Charlson et al.*, 1992]. High formation rates and fast growth to CCN sizes ensure that NPF contributes significantly to the global CCN population [*Ghan et al.*, 2001; *Spracklen et al.*, 2008].

Since the highest uncertainties in the current estimates for global radiative forcing are associated with these direct and indirect aerosol effects [*IPCC*, 2007; *Chin et al.*, 2009], it is essential to develop a detailed, mechanistic understanding of processes that affect the ambient aerosol population. As these particles are first produced from the

formation of stable molecular clusters and subsequently grow to a CCN-active size, they undergo various processes that enhance and deplete the particle population such as the condensation of gas-phase species and particle-particle coagulation, respectively. It is the primary goal of the research described in this thesis to develop robust models, *constrained by measurement*, for the sequential formation of CCN from the nucleation of gas-phase precursors. To this end, my thesis focuses on four topics: [1] the development of nucleation rate parameterizations from correlations between formation rates of 1 nm particles (assumed nucleated particle size) and gas-phase sulfuric acid concentrations in diverse environments; [2] the development of a cluster formation mechanism incorporating energetic barriers at the smallest clusters; [3] the derivation of a simple, dimensionless criterion determining whether or not NPF would occur on a particular day; and [4] the determination of the survival probability of newly formed particles (3 nm) as they grow to a CCN-active size (100 nm). A schematic diagram of an aerosol size distribution measured during a nucleation event is shown in Figure 1.1, overlaid with the particle size ranges corresponding to each of the above-mentioned thesis topics. While the results of this work pertain to atmospheric nucleation, the methods of analysis and applied numerical techniques apply to gas-phase nucleation in general.

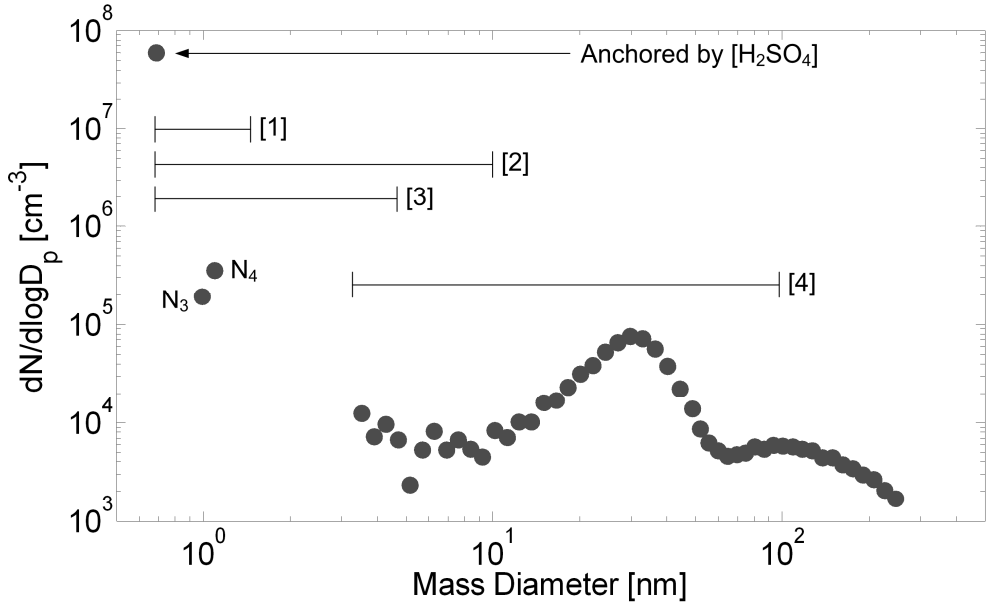

Figure 1.1 Aerosol size distribution measured during nucleation event observed on 08/06/08 in the Manitou Experimental Forest (Manitou Springs, Colorado). The size distribution is anchored at the smallest size by measured [H_2SO_4] and includes the cluster species $(H_2SO_4)_3$ and $(H_2SO_4)_4$ (N_3 and N_4 on the figure, respectively) as well as nanoparticles from 3 – 300 nm. Sulfuric acid monomer and cluster measurements were obtained with a prototype cluster mass spectrometer [*Zhao et al.*, 2009]. Nanoparticle measurements were acquired with a conventional particle size distribution instrument [*Woo et al.*, 2001]. The aerosol size range of interest for each thesis topic (in square brackets) is also shown, referenced in section 1.1.

1.2 Thesis Overview

In chapter 2, correlations between measured concentrations of newly formed particles and [H_2SO_4] were analyzed for nucleation events measured in diverse environments. A simple parameterization for atmospheric nucleation rates (J_1) was obtained, $J_1 = K \cdot [H_2SO_4]^P$, that could be easily implemented in regional and chemical transport models [*Spracklen et al.*, 2008]. The nucleation exponent P was shown to be equal to 2 (indicating a critical cluster containing two sulfuric acid molecules [*Oxtoby*, 1998]) and the pre-factor K varied from 1 – 4 orders magnitude beneath the hard-sphere collision limit. These reduced cluster formation rates suggested the presence of a significant barrier to small cluster formation.

In chapter 3, the effect of this cluster formation barrier on the dynamics of a nucleating aerosol was explored with a cluster population balance model [*Kuang et al.*, 2009e]. This formation barrier was modeled with an accommodation coefficient (varying between 0 and 1) which was calculated using bimolecular reaction rate theory, predicting a decrease in energized cluster stability with decreasing cluster size. Comparisons between measured cluster concentrations and the resulting modeled cluster concentrations assuming varying degrees of energy accommodation yielded the first direct estimates of this barrier to cluster formation.

In chapter 4, a simple dimensionless criterion was developed that determined whether or not NPF would occur on a particular day. The criterion L_Γ determines the probability that a nucleated particle will grow to a detectable size before being lost by coagulation with the pre-existing aerosol. Using measured aerosol size distributions and particle growth rates, the boundary value for L_Γ which separated NPF events and non-events (characterized by growth of the pre-existing aerosol without new particle formation) was shown to be nominally 1, with an empirically determined value of 0.7.

In chapter 5, CCN production from the growth of newly formed particles was determined by analytically solving the aerosol general dynamic equation for a nucleated aerosol population growing from 3 to 100 nm. Using measured aerosol size distributions

and growth rates, the probability of a 3 nm particle surviving to a CCN-active size (assumed to be 100 nm) was determined to be 1 – 10%, with pre-existing CCN concentrations being enhanced by factors of 2 – 9 due to new particle formation.

In chapter 6, future work is presented in which the developed cluster population balance model can yield kinetic and thermodynamic cluster parameters using measured cluster concentrations. Furthermore, the cluster model can be used to validate nucleation rate parameterizations and provide criteria for consistent, accurate date reduction. Continuing work is also described regarding the development, characterization, and implementation of a new condensation particle counter using oleic acid as the working fluid.

Chapter 2 : Dependence of Nucleation Rates on Sulfuric Acid Vapor Concentration in Diverse Atmospheric Locations

2.1 Synopsis

Correlations between concentrations of newly formed particles and sulfuric acid vapor were analyzed for twenty one nucleation events measured in diverse continental and marine atmospheric environments. A simple power law model for formation rates of 1 nm particles, $J_1 = K \cdot [H_2SO_4]^P$, where P and K are least-squares parameters, was tested for each environment. We found that, to within experimental uncertainty, $P = 2$. Constraining P to 2, the pre-factor $K_{kinetic}$ ranges from 10^{-14} – 10^{-11} cm^3s^{-1}. According to the nucleation theorem, an exponent value of 2 indicates that the critical cluster contains two sulfuric acid molecules. Existing nucleation rate expressions based on classical nucleation theory predict significantly larger values of P. The pre-factor values vary with environment and are 1 – 4 orders of magnitude below the hard-sphere collision limit. These results provide a simple, robust parameterization for atmospheric new particle formation that could be used in chemical and regional transport models.

2.2 Introduction

New particle formation by nucleation of gas phase species significantly influences the size distributions and number concentrations of atmospheric aerosol particles. These aerosol particles are believed to exert a considerable impact on global climate by affecting the earth's radiation balance directly through the scattering of solar radiation or indirectly through their role as cloud condensation nuclei [*IPCC*, 2007]. Several recent field campaigns [*Lihavainen et al.*, 2003; *Kerminen et al.*, 2005; *Laaksonen et al.*, 2005] and modeling efforts [*Ghan et al.*, 2001; *Spracklen et al.*, 2008] have directly implicated newly formed particles from atmospheric nucleation events as an important source of cloud condensation nuclei. It is essential that new particle formation by sufficiently well

understood since global climate models require accurate prediction of atmospheric new particle formation in order to realistically capture aerosol radiative effects.

New particle formation in the atmospheric boundary layer has been frequently observed in diverse locations including boreal forests, European coastal environments, and rural and urban continental regions in North America [*Kulmala et al.*, 2004a]. Field studies conducted at remote marine and continental sites have shown that sulfuric acid vapor is involved with new particle formation and that the maximum measured new particle formation rates at those locations varied in proportion to $[H_2SO_4]^2$ [*Weber et al.*, 1996]. Analysis of two European measurement campaigns by *Sihto et al.* [2006] and *Riipinen et al.* [2007] have further explored this correlation between sulfuric acid and the concentration of newly formed particles (nominally 3 – 6 nm) and have demonstrated a simple power law relationship between observed particle formation rates and sulfuric acid vapor concentration where the exponent $[H_2SO_4]$ varies between 1 and 2. These parameterizations were able to quantitatively explain many features of the observed nucleation events and have subsequently been implemented in the off-line chemical transport model of *Spracklen et al.* [2008] and the one-dimensional aerosol formation model of *Boy et al.* [2006].

The present study was motivated by similar correlations between concentrations of sulfuric acid vapor and newly formed particles measured in various continental and marine locations: Tecamac, Mexico [*Iida et al.*, 2008b]; Atlanta, Georgia [*McMurry et al.*, 2005]; Macquarie Island [*Weber et al.*, 1998a]; Hyytiälä, Finland [*Fiedler et al.*, 2005; *Sihto et al.*, 2006]; Boulder, CO [*Eisele et al.*, 2006; *Iida et al.*, 2006]; Idaho Hill, CO [*Weber et al.*, 1997]; and Mauna Loa, HI [*Weber et al.*, 1995]. Simultaneous concentration measurements of sulfuric acid vapor and newly formed particles were analyzed from this diverse set of atmospheric locations.

The nucleation rate of critical clusters was a central quantity in this analysis and was estimated as the formation rate of 1 nm particles (J_1). Because critical clusters formed by atmospheric nucleation events cannot yet be measured (minimum detectable size ~ 3 nm), J_1 was extrapolated from the formation rate of 3 nm particles (J_3), which

was obtained from measured particle size distributions. The functional dependence of J_1 on $[H_2SO_4]$ was studied by assuming a simple power law model for new particle formation where $J_1 = K \cdot [H_2SO_4]^P$. An unconstrained least-squares fit between measured values of J_1 and $[H_2SO_4]$ yielded best-fit parameters P and K. The nucleation exponent P and pre-factor K provide insight into the nucleation mechanism, where P values of 1 and 2 correspond to the activation [*Kulmala et al.*, 2006] and kinetic models [*McMurry and Friedlander*, 1979; *McMurry*, 1980; 1983] for new particle formation, respectively. The activation model assumes that nucleation occurs through the activation of small clusters containing one H_2SO_4 molecule through one of several mechanisms including heterogeneous nucleation and heterogeneous chemical reactions. The kinetic model assumes that critical clusters are formed through bimolecular collisions of sulfuric acid containing clusters. The pre-factors for both models contain chemical and physical details of the nucleation process. The resulting best-fit nucleation exponent and corresponding pre-factor provide a simple parameterization for atmospheric new particle formation that could be used in large-scale transport models.

2.3 Apparatus and Techniques

2.3.1 Campaign Sites

The data from Hyytiälä were acquired by the research team from the University of Helsinki [*Sihto et al.*, 2006] while the other measurements were carried out by the group from the University of Minnesota and the National Center for Atmospheric Research. A summary of pertinent parameters from each measurement campaign is listed in Table 2.1. Mauna Loa and Macquarie Island are marine sites in the Pacific Ocean while Tecamac, Atlanta, Boulder, Idaho Hill, and Hyytiälä are various urban and rural continental sites in North American and Europe. Detailed descriptions of the physical and meteorological conditions at each site can be found in the cited references.

Table 2.1 Summary of measurement campaign parameters

Location	Air Mass Type	Measurement Platform	Month/Year	No. of Events	Reference
Tecamac, Mexico	City	Land	03/06	9	*Iida et al.* [2008b]
Atlanta, Georgia	City	Land	07 – 08/02	2	*McMurry et al.* [2005]
Boulder, Colorado	Small city	Land	09/04	5	*Iida et al.* [2006]
Hyytiälä, Finland	Boreal forest	Land	03/03	2	*Sihto et al.* [2006]
Idaho Hill, CO	Mountain forest	Land	09/93	1	*Weber et al.* [1997]
Mauna Loa, HI	Marine/volcanic	Land	07/92	1	*Weber et al.* [1995]
Macquarie Island	Marine/biogenic	Aircraft	11/95	1	*Weber et al.* [1998a]

2.3.2 Measurement Instrumentation

Various instruments from each measurement campaign enabled extensive characterization of aerosols and major gas-phase compounds. The aerosol instrumentation allowed for evaluation of the particle size distribution and aerosol surface area, while the gas-phase instrumentation provided continuous measurements of [H_2SO_4] and numerous meteorological parameters. A summary of the pertinent instruments utilized during each measurement campaign is listed in Table 2.2. Details of the measurement techniques are discussed in the cited references.

Table 2.2 Summary of pertinent measurement instrumentation

Location	$[H_2SO_4]$	Particle Size Distribution
Tecamac; Atlanta; Boulder	SI-CIMS[a]	Nano-SMPS[b]; SMPS[c]; OPC[d]
Idaho Hill; Mauna Loa	SI-CIMS	PHA[e]; SMPS
Macquarie Island	SI-CIMS	PHA; CPC[f]
Hyytiälä	CIMS[g]	DMPS[h]

[a]SI-CIMS: selected ion chemical ionization mass spectrometer [*Eisele and Tanner*, 1993]; *Sjostedt et al.* [2007] describes instrument from Tecamac campaign in detail.

[b]Nano-SMPS: nano scanning mobility particle sizer (3 – 40 nm) [*Stolzenburg and McMurry*, 1991; *Chen et al.*, 1998].

[c]SMPS: scanning mobility particle sizer (20 – 250 nm) [*Wang and Flagan*, 1990].

[d]OPC: optical particle counter (0.1 – 2 μm), Lasair Model 1002.

[e]PHA: pulse height analysis method (3 – 4 nm) [*Saros et al.*, 1996; *Weber et al.*, 1998b] using an ultrafine condensation particle counter (UCPC) [*Stolzenburg and McMurry*, 1991].

[f]CPC: condensation particle counter (> 10 nm), TSI Model 3020.

[g]CIMS: chemical ionization mass spectrometer [*Reiner and Arnold*, 1993; *Hanke et al.*, 2002].

[h]DMPS: differential mobility particle sizer (3 – 500 nm) [*Birmili et al.*, 1999].

2.3.3 Data Analysis

The rate (J_3) at which particles grow past the minimum detectable size (~ 3 nm) by vapor condensation is:

$$[1] \qquad J_3 \equiv \left.\frac{dN}{dD_p}\right|_3 \cdot \left.\frac{dD_p}{dt}\right|_3 ,$$

where dN / dD_p and dD_p / dt are the aerosol size distribution and particle diameter growth rate, respectively, at 3 nm. This exact expression was then approximated as [*Weber et al.*, 1996]:

[2] $$J_3 \cong \frac{\Delta N_{NFP}}{\Delta D_p} \cdot GR_{1-3},$$

where ΔD_p is the diameter size range of newly formed particles associated with the following measurement techniques listed in Table 2.2: PHA (3 – 4 nm) and Nano-SMPS (3 – 6 nm), ΔN_{NFP} is the number concentration of newly formed particles in these size ranges, and GR_{1-3} is the particle growth rate from 1 to 3 nm. The approximations in equation [2] assume that the distribution function dN / dD_p is constant within the diameter size range and does not vary with time, which introduces some uncertainty in J_3.

The PHA technique measures ultrafine aerosols defined as particles in the narrow size range from 3 nm, the lower detection limit of the ultrafine condensation particle counter (UCPC), to nominally 4 nm in diameter [*Weber et al.*, 1998b]. The Nano-SMPS diameter size range was chosen to be small enough to be considered newly formed but large enough to achieve good Poisson counting statistics [*McMurry*, 2000]. Values of ΔN_{NFP} were obtained from size distribution measurements while GR_{1-3} was estimated from the observed time shift (Δt) between increasing [H_2SO_4] and ΔN_{NFP}, which is often interpreted as the time required for a critical cluster of roughly 1 nm diameter to grow to the lower detection limit of 3 nm [*Weber et al.*, 1997; *Kulmala et al.*, 2004b; *Fiedler et al.*, 2005; *Sihto et al.*, 2006]. As *Sihto et al.* [2006] had previously done, the appropriate Δt was determined from the time delay which maximized the correlation coefficient between both ΔN_{NFP} and [H_2SO_4], and ΔN_{NFP} and [H_2SO_4]^2 over the duration of the nucleation event. The event was assumed to begin when [H_2SO_4] began to rise sharply, and to end either when ΔN_{NFP} began to decrease significantly or when there was indication of an abrupt change in particle concentration, typically in the 10 – 50 nm range, indicating that the measurement site was being impacted by a strong source of emissions or was sampling a different air mass. As is explained later, values of Δt that were obtained from correlations with [H_2SO_4]^2 differed at most by 15% from those

obtained from correlations with [H_2SO_4]. Therefore, values of Δt obtained from the correlation with [H_2SO_4] were used to estimate GR_{1-3}.

Assuming a steady-state cluster distribution between 1 and 3 nm particles, the nucleation rate of 1 nm particles (J_1) was extrapolated from time-shifted values of J_3 by incorporating the probability that a particle would grow from 1 to 3 nm by vapor condensation before being scavenged by the pre-existing aerosol according to the relation [*Weber et al.*, 1997; *McMurry et al.*, 2005]:

$$[3] \qquad J_1(t) = J_3(t+\Delta t)\cdot \exp\left[\frac{1}{2}\cdot\frac{A_{Fuchs}}{GR_{1-3}}\cdot\sqrt{\frac{48k_BT}{\pi^2\rho}}\cdot\left(\frac{1}{\sqrt{D_{p1}}}-\frac{1}{\sqrt{D_{p3}}}\right)\right],$$

where A_{Fuchs} is the median value of the Fuchs surface area of the pre-existing aerosol during the time interval [t, $t + \Delta t$], k_B is the Boltzmann constant, T is the temperature, ρ is the aerosol density, and D_{p1} and D_{p3} correspond to the initial (1 nm) and final (3 nm) particle size. Values of the exponential in equation [3] typically range from 2 to 10 for the analyzed nucleation events. This expression assumes that the removal of particles in the 1 to 3 nm range by coagulation with the pre-existing aerosol can be calculated by using the Fuchs-Sutugin transition regime condensation expression [*Fuchs and Sutugin*, 1971]. In calculating A_{Fuchs} with this expression, we used a mean free path of 0.1 μm. This value was chosen by comparing "condensation" rates of 1 – 3 nm particles using the Fuchs-Sutugin transition regime expression with coagulation rates of 1 – 3 nm particles calculating using Fuchs' transition regime coagulation equation [*Fuchs*, 1964], which is the most accurate method available for calculating these removal rates. The value of 0.1 μm for the mean free path leads to overall loss rates that are within 10% of the values that would be obtained using Fuchs' transition regime coagulation expression. The analyses of *Sihto et al.* [2006] and *Riipinen et al.* [2007] use a similar expression connecting J_1 and J_3 in which the quantity CS' behaves analogously as A_{Fuchs} [*Kerminen and Kulmala*, 2002]. Our re-analysis of their published results makes use of the following relationship between CS' and A_{Fuchs} as described in [*McMurry et al.*, 2005]:

[4] $$CS' = \frac{\overline{c}_1 A_{Fuchs}}{16\pi D},$$

where $\overline{c}_1$ is the condensing monomer mean thermal speed and D is the condensing vapor (sulfuric acid) diffusivity. Uncertainties in J_1 inevitably arise due to uncertainties in the exponential of equation [3], but it will be shown in section 2.4.3 that, under certain assumptions, these uncertainties affect only the pre-factor K and not the nucleation exponent P.

These estimated values of J_1 were fit by the method of least-squares to the corresponding values of [H_2SO_4] according to a simple power law expression of the form:

[5] $$J_1 = K \cdot [H_2SO_4]^P,$$

where both the exponent P and the pre-factor K were unconstrained fitting parameters. For measurement campaigns where more than one nucleation event was measured, this fitting approach was applied to the campaign as a whole. The resulting cumulative data set contained measured values of J_1 and [H_2SO_4] from all nucleation events observed at a particular location, enabling a wider dynamic range over which the unconstrained least-squares fit could be applied. Applying this cumulative fitting method over the entire measurement campaign would then generate one set of best-fit parameters P and K that characterized nucleation events for a particular location. Implicit in this approach is the assumption that nucleation events occur by the same mechanism during each measurement campaign, though there may be variability in daily meteorological conditions and gas-phase species concentrations.

For each cumulative data set, we examined the sensitivity of P to the length of the fitting time intervals over which the least-squares fit was applied. In one case, the cumulative data set contained values of J_1 and [H_2SO_4] from time intervals spanning the entire day for each nucleation event that was observed. In the other case, the cumulative data set contained values of J_1 and [H_2SO_4] from time intervals during which particle production was obviously taking place, starting at the initial rise in ΔN_{NFP} and ending

either when ΔN_{NFP} decreased significantly or when there was indication of an abrupt change in particle concentration, typically in the 10 – 50 nm range. *Riipinen et al.* [2007] also investigated the relationship between J_1 and [H_2SO_4] for nucleation events measured in Hyytiälä and Heidelberg, Germany. Their fitting approach was applied to individual nucleation events as opposed to the campaign as a whole. They fit their measured J_1 and [H_2SO_4] assuming constrained nucleation exponent values of 1, 2, or 3 and allowed their pre-factors to vary freely. Our approach both examines time interval sensitivity and analyzes the campaign data set as a whole while allowing both the nucleation exponent and pre-factor to vary as free parameters.

2.4 Results and Discussion

2.4.1 Growth Rate Calculation from [H_2SO_4] and ΔN_{NFP} Correlations

The correlation between time-shifted ΔN_{NFP} and both [H_2SO_4] and [H_2SO_4]^2 was clearly observed during each of the land-based measurement campaigns. Representative examples of correlations with both [H_2SO_4] and [H_2SO_4]^2 from the Tecamac and Atlanta campaigns are shown in Figure 2.1. In these nucleation events, the time-shifted ΔN_{NFP} generally tracks the rise and fall in both [H_2SO_4] and [H_2SO_4]^2. Differences between values of Δt determined from correlating with either [H_2SO_4] or [H_2SO_4]^2 were no more than 15%. Therefore, time-shifted ΔN_{NFP} was correlated with [H_2SO_4] and the corresponding correlation coefficients and resulting values for Δt and GR_{1-3} from each analyzed nucleation event are listed in Table 2.3. Four nucleation events from Tecamac, Mexico yielded no discernible time shift, implying that, in those cases, the particle growth from the size of the initial nuclei to the particle detection limit was faster than that typically observed in rural, remote, and most other urban environments [*Stolzenburg et al.*, 2005]. For two of these events, the diameter growth rates were estimated from size-dependent charge fractions [*Iida et al.*, 2008b]. The growth rates for the remaining two

events were calculated assuming a Δt equal to the measurement time resolution for particle size distributions, yielding a lower limit to the actual growth rate.

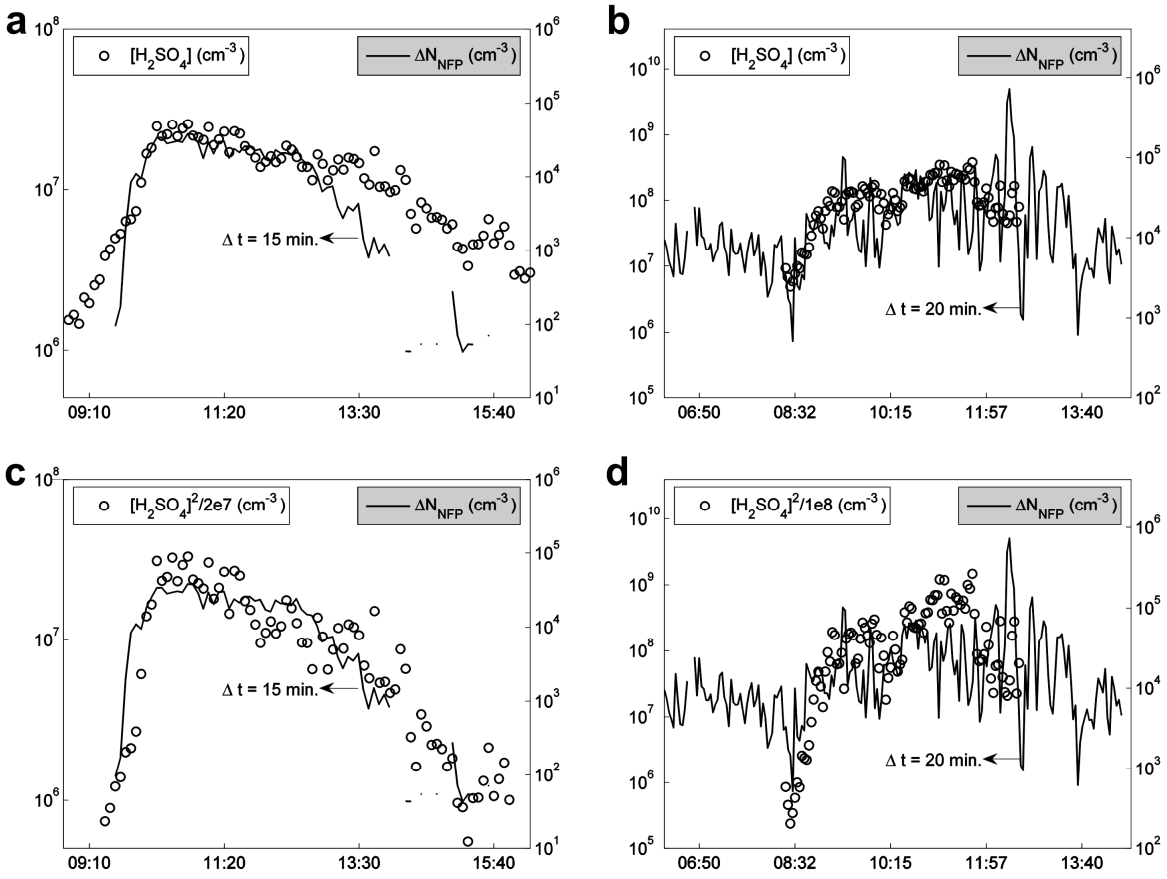

Figure 2.1 Correlations between time-shifted ΔN_{NFP} and both $[H_2SO_4]$ and scaled $[H_2SO_4]^2$ as a function of local time for nucleation events measured during the Tecamac campaign on 03/22/06 ((a) and (c)) and during the Atlanta campaign on 07/31/02 ((b) and (d)). Corresponding values of the time-shift Δt and direction of shift are shown.

Table 2.3 Calculated quantities for correlation analysis between $[H_2SO_4]$ and ΔN_{NFP}

Location[d]	Event Date (mm/dd/yy)	Δt (min)	GR_{1-3} (nm/h)	R[a]
Tecamac	03/15/06	10	20	0.66
	03/16/06	—[b]	26	0.93
	03/21/06	—[b]	20	0.83
	03/22/06	15	13	0.88
	03/23/06	5	39	0.77
	03/26/06	—[c]	≥ 39	0.90
	03/29/06	25	7.8	0.82
	03/30/06	—[c]	≥ 39	0.85
	03/31/06	20	9.7	0.89
Atlanta	07/31/02	20	9.7[e]	0.73
	08/05/02	10	20[e]	0.84
Boulder	09/02/04	55	3.5	0.84
	09/07/04	40	4.9	0.86
	09/08/04	20	9.7	0.77
	09/09/04	25	7.8	0.66
	09/14/04	40	4.9	0.61
Hyytiälä	03/25/03	140	1.3	0.97
	03/26/03	40	4.9	0.91
Idaho Hill	09/21/93	60	2.4	0.95
Mauna Loa	07/15/92	20	8.3	0.93

[a]Correlation coefficient between $[H_2SO_4]$ and ΔN_{NFP}.

[b]Correlation analysis yielded $\Delta t = 0$; growth rate estimated from size-dependent charge fractions [*Iida et al.*, 2008b].

[c]Correlation analysis yielded $\Delta t = 0$; lower limit to growth rate calculated assuming Δt equal to measurement time resolution.

[d]Correlation analysis not performed for Macquarie Island nucleation event due to relatively constant $[H_2SO_4]$ profile that accompanied measured particle burst; growth rate estimated based on transport time from island to measurement location [*Weber et al.*, 1998a].

[e]Growth rates are in good agreement with modal growth rates calculated by [*Stolzenburg et al.*, 2005].

The nucleation event measured at Macquarie Island was unique in the analyzed data set since evidence of new particle formation involving biogenic gas-phase species was observed via aircraft-based measurements as opposed to land-based measurements of photochemically-driven nucleation events [*Weber et al.*, 1998a]. This intense burst of particle formation was detected downwind of a penguin colony but not in immediately adjoining air, which led to the conclusion that biogenic emissions from the colony contributed to new particle formation. A rough correlation between ΔN_{NFP} and [H_2SO_4] was observed, but values for Δt and GR_{1-3} were not obtained from a correlation analysis due to the relatively constant [H_2SO_4] profile that accompanied the particle burst. Instead, ΔN_{NFP} was not time-shifted with respect to [H_2SO_4] and the particle growth rate was estimated to be 4 nm/hr based on the transport time from the coast to the measurement location, assuming the island was the starting point for growth [*Weber et al.*, 1998a].

2.4.2 Sensitivity of P to Fitting Time Intervals

The value of the nucleation exponent P was sensitive to the lengths of the fitting time intervals, varying from approximately 1 when fitting over the entire day to 2 when fitting only over the duration of the nucleation events. This sensitivity is illustrated in Figure 2.2 and Figure 2.3, where J_1 is plotted versus [H_2SO_4] for the cumulative Tecamac measurement campaign and for two nucleation events from the Hyytiälä measurement campaign, respectively. For the Tecamac campaign, applying a cumulative least-squares fit over time intervals spanning the entire day yielded a P value and corresponding 90% confidence interval of 0.85 ± 0.05 as shown in Figure 2.2a, while applying the cumulative fit over time intervals spanning only the duration of the nucleation events yielded a P value of 1.99 ± 0.09 as shown in Figure 2.2b. The corresponding plots for the analyzed events from the Hyytiälä campaign are shown in Figure 2.3a and Figure 2.3b, where the P value varies from 1.15 ± 0.08 to 1.99 ± 0.11 as the fitting time intervals are restricted from spanning the entire day to only the duration of the nucleation events. This convergence of P toward 2 was consistently

observed when examining multi- and single-event data sets from the various campaigns. This dependence of the nucleation exponent on the length of the fitting time interval can be attributed to the inclusion of J_1 and [H_2SO_4] values that were measured from sources not associated with nucleation, such as pre-existing background aerosol, plume transport, and vertical down-mixing associated with the morning development of the boundary layer. These best-fit values of P and K, generated from choosing fitting time intervals that span only the duration of the nucleation events, were chosen as the parameters that most accurately characterize nucleation rates for a particular location.

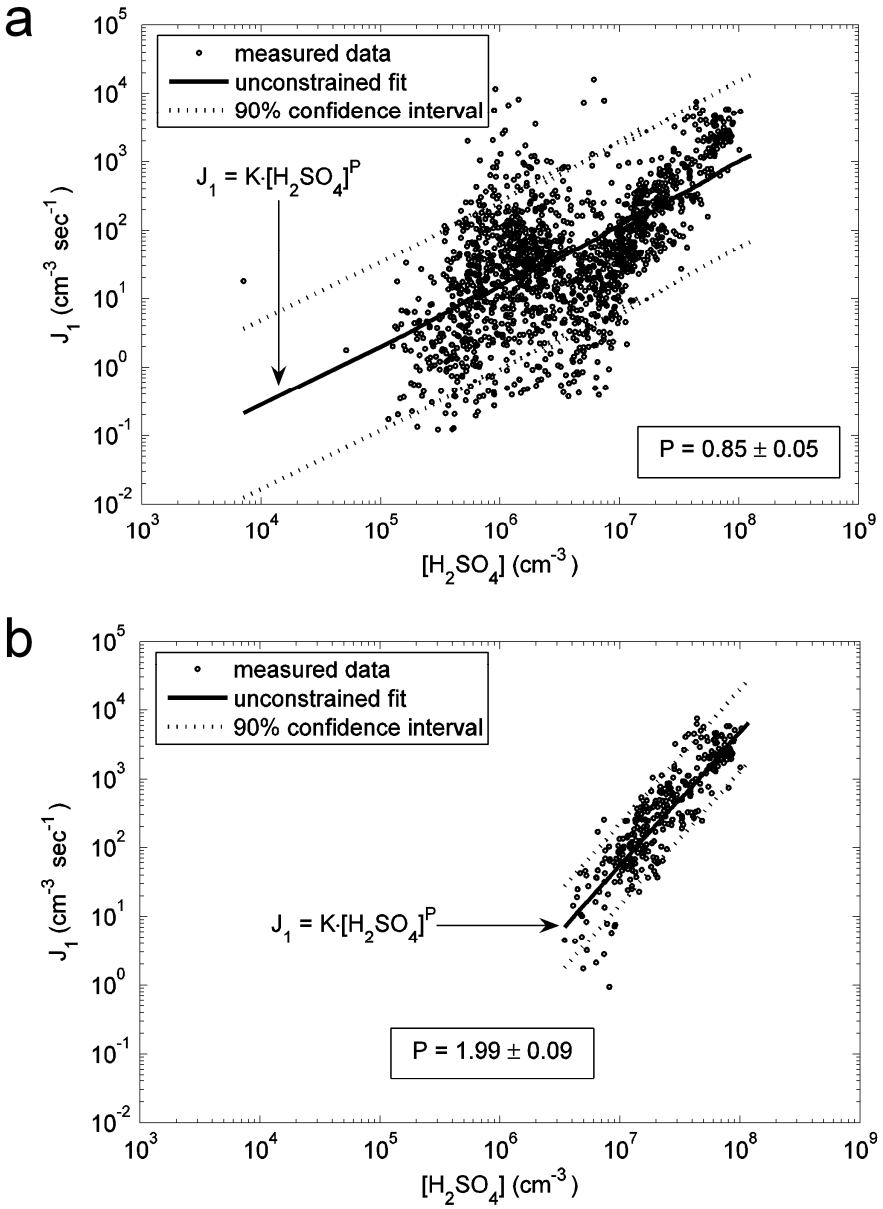

Figure 2.2 Values of J_1 extrapolated from particle measurements versus measured $[H_2SO_4]$ during the Tecamac measurement campaign. The unconstrained fits over time intervals spanning (a) the entire day and (b) only the nucleation events are shown along with the resulting best-fit nucleation exponent P and corresponding 90% confidence interval. The power law model relating J_1 and $[H_2SO_4]$ is shown for reference.

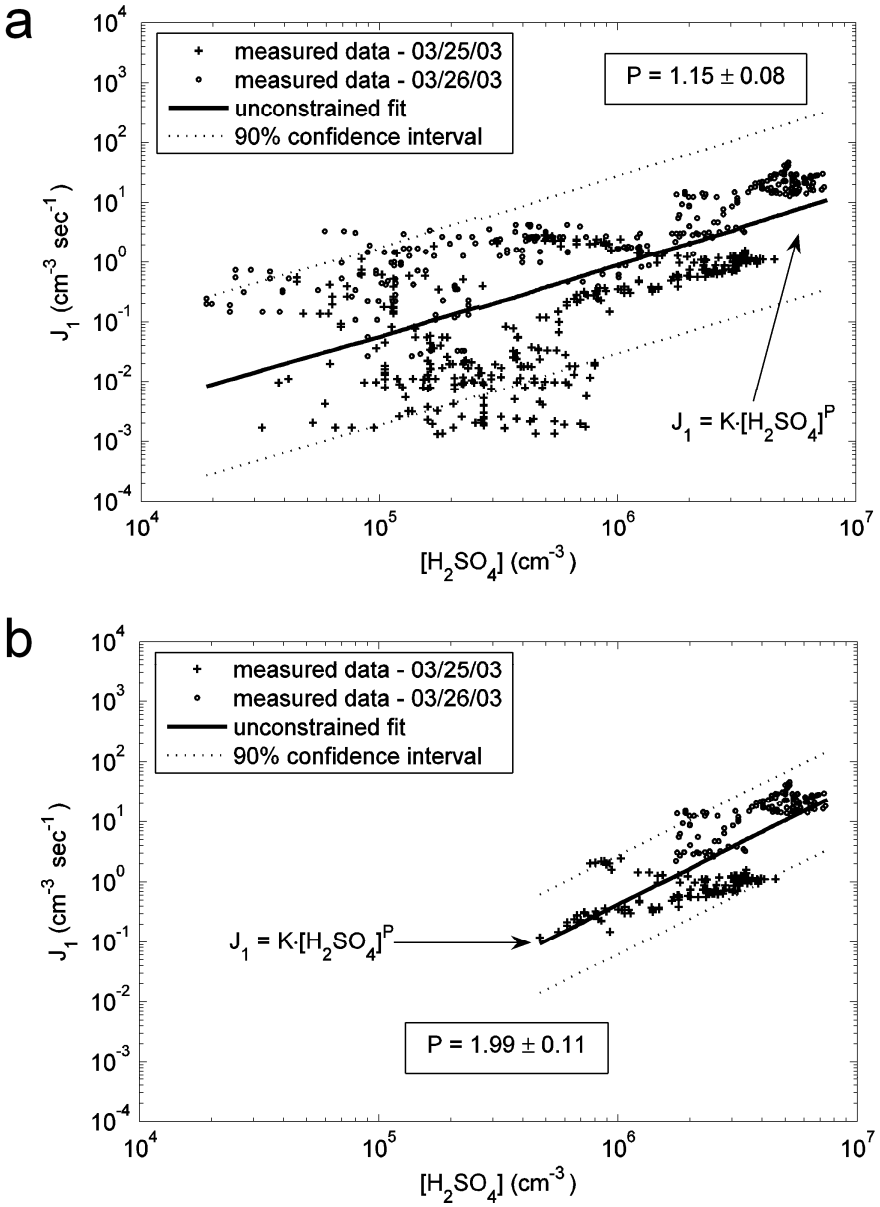

Figure 2.3 Values of J_1 extrapolated from particle measurements versus measured $[H_2SO_4]$ for two nucleation events measured during the Hyytiälä campaign on 03/25/03 and 03/26/03. The unconstrained fits over time intervals spanning (a) the entire day and (b) only the nucleation events are shown along with the resulting best-fit nucleation exponent P and corresponding 90% confidence interval. The power law model relating J_1 and $[H_2SO_4]$ is shown for reference.

2.4.3 Best Fit Parameters P and K

Values for the best-fit parameters P, K, and $K_{kinetic}$ (the resulting kinetic pre-factor when $P = 2$) and the corresponding 90% confidence intervals are listed for each measurement campaign in Table 2.4. The nucleation exponent P varies narrowly from 1.98 ± 0.23 to 2.04 ± 0.27 for the different atmospheric environments. To within experimental uncertainty, these results support the conclusion that $P = 2$. According to the nucleation theorem for multicomponent systems [*Oxtoby and Kashchiev*, 1994], an exponent value of 2 indicates that the critical cluster contains two sulfuric acid molecules. This result is supported by the work of *Hanson and Eisele* [2002] in which their measurements of prenucleation molecular clusters indicate a critical cluster containing 2 H_2SO_4 molecules. Our results suggest that current classical, binary, and ternary nucleation theories do not correctly predict these atmospheric observations, since they predict a critical cluster containing more than two sulfuric acid molecules. A critical cluster containing two sulfuric acid molecules can be formed through a kinetically limited nucleation process where a collision between 2 H_2SO_4 molecules or H_2SO_4 containing clusters is the rate-limiting step in the formation of a stable critical cluster.

Table 2.4 Least-squares fit results

Location	Air Mass Type	P [a]	$\log K$ [a,b]	$\log K_{kinetic}$ [b,c]
Tecamac	City	1.99 ± 0.09	-12.2 ± 0.68	-12.2 ± 0.59
Atlanta	City	2.01 ± 0.35	-13.9 ± 2.77	-13.8 ± 0.98
Boulder	Small city	1.98 ± 0.23	-13.3 ± 1.63	-13.4 ± 0.83
Hyytiälä	Boreal forest	1.99 ± 0.11	-12.3 ± 0.73	-12.4 ± 0.49
Idaho Hill	Mountain forest	2.04 ± 0.27	-11.0 ± 0.37	-10.8 ± 1.03
Mauna Loa	Marine/volcanic	2.00 ± 0.16	-12.3 ± 0.42	-12.3 ± 0.40
Macquarie Island	Marine/biogenic	2.00 ± 1.94	-14.0 ± 12.6	-14.0 ± 0.90

[a]Unconstrained results with 90% confidence intervals.

[b]log K shown instead of K due to linearization of power law model.

[c]Constrained results where $P = 2$ with 90% confidence intervals; $K_{kinetic}$ has units of $cm^3 s^{-1}$.

A similar approach was followed by *Sihto et al.* [2006] when analyzing nucleation events measured in the Boreal forests in Hyytiälä, where constrained nucleation exponent values of both 1 and 2 were shown to adequately model nucleation rates. *Riipinen et al.* [2007] arrived at a similar conclusion for their nucleation exponent when analyzing a more recent campaign at the same location. Our re-analysis of the published results of *Sihto et al.* [2006], while focusing on the time interval starting at the initial rise in ΔN_{NFP} and ending after the peak value in ΔN_{NFP}, yielded an unconstrained P value of 1.99 $\pm$ 0.11 and $K_{kinetic}$ value of 3.86 x 10^{-13} cm^3s^{-1}, which is in reasonable agreement with the published mean pre-factor value of 5.7 x 10^{-13} cm^3s^{-1} for that location assuming a kinetic model [*Sihto et al.*, 2006]. While a P value of 1.99 best fits the measured nucleation rates and sulfuric acid vapor concentrations for the composite data set as seen in Figure 2.3b, it is worth noting that the best-fit slopes of J_1 versus [H_2SO_4] are different when the nucleation events are analyzed individually, with $P = 1.30 \pm 0.14$ for the nucleation event measured on 03/25/03 and $P = 1.92 \pm 0.13$ for the nucleation event measured on 03/26/03. It may be significant that sulfuric acid vapor concentrations on 03/25/03 extended to values as low 4 x 10^5 cm^{-3}, which is the lowest value of [H_2SO_4] at which new particle formation was observed in these studies. The lowest values for the other nucleation events were typically > 2 x 10^6 cm^{-3}.

Uncertainties in the extrapolated values of J_1, primarily from uncertainties in the estimated value of GR_{1-3} and their subsequent propagation in equations [2] and [3], represent the largest source of error when determining these best-fit parameters. However, under certain assumptions, it can be shown that uncertainties in GR_{1-3} affect only the value of the pre-factor K and not the value of the nucleation exponent P. These assumptions are: [1] uncertainties in GR_{1-3} are constant from event to event in a campaign; [2] values of A_{Fuchs} are constant during a nucleation event; and [3] values of the ratio A_{Fuchs} / GR_{1-3} are constant from event to event in a campaign. The resulting effect of uncertainties in GR_{1-3} is to then shift the values of the quantity log J_1 by a

constant offset. The value of the nucleation exponent P is therefore not affected, while the value of log K is offset by a constant factor. Our analysis focuses only the short time period during which new particle formation is observed and the corresponding values of A_{Fuchs} from our analyzed nucleation events deviate by at most 20% during a campaign. The ratio A_{Fuchs} / GR_{1-3} gives an indication of whether new particle formation occurs on a particular day and for the nucleation events that were analyzed in each measurement campaign, the values of the ratio varied by at most 30%. With these variabilities in A_{Fuchs} and A_{Fuchs} / GR_{1-3}, a 50% uncertainty in GR_{1-3} results in uncertainties in values of P and log K that are within the 90% confidence intervals calculated assuming no uncertainty in GR_{1-3}.

The pre-factor $K_{kinetic}$ spans nearly 3 orders of magnitude from $10^{-14} - 10^{-11}$ cm^3s^{-1} across the different measurement campaigns. Comparison with the hard-sphere collision frequency (~ 4×10^{-10} cm^3s^{-1}) suggests that not every bimolecular collision between H_2SO_4 containing clusters results in the formation of a stable critical cluster. These values for $K_{kinetic}$ are in the typical range of bimolecular gas-phase reaction rate constants. There are several reasons why such reaction rates are less than the hard-sphere collision frequency, which include steric requirements for a successful collision trajectory between approaching clusters, and energetic requirements for stable cluster formation. This energetic barrier to stable cluster formation can be understood within the context of bimolecular reaction rate theory [*Dean*, 1985] where the rate of stable cluster formation is governed by the competition between stabilization and decay of an energetically unstable complex formed from the collision of two H_2SO_4 containing clusters. The variability in $K_{kinetic}$ with environment points to a possible dependence on gas-phase species that co-nucleate with sulfuric acid vapor and stabilize the critical cluster. The identity and concentration of these species, which could vary significantly with environment, would influence their ability to accommodate the cluster collision energy. Further work in developing a bimolecular nucleation mechanism and quantifying the degree of energy accommodation during cluster formation is detailed in the next chapter.

2.5 Conclusions

Correlations between concentrations of newly formed particles and sulfuric acid vapor have been analyzed for nucleation events measured at various atmospheric locations. Unconstrained least-squares fits between measured formation rates of 1 nm particles and corresponding sulfuric acid vapor concentrations yielded a nucleation exponent of 2 in different environments, suggesting a kinetically limited nucleation mechanism in which the critical cluster contains two sulfuric acid molecules. Analyzing multi-event campaigns as a whole enabled a more robust data set with a wider dynamic range in J_1 and [H_2SO_4] over which the fitting method was applied. Restricting the fitting time intervals to only the duration of nucleation events ensured that the resulting best-fit parameters would accurately characterize the nucleation event. Best-fit $K_{kinetic}$ values were 1 – 4 orders of magnitude below the hard-sphere collision limit, suggesting a strong barrier to critical cluster formation that can be rationalized within the context of energy accommodation during the cluster formation process. Factors that lead to variability in $K_{kinetic}$ with environment need to be investigated further and may be influenced by co-nucleating species which stabilize the critical cluster to varying degrees based on their identity and concentration. This analysis provides a simple power law parameterization of atmospheric new particle formation that could be implemented in chemical and regional transport models.

2.6 Acknowledgements

This work was supported in part by the IGERT Program of the National Science Foundation under Award Number DGE-0114372. Support for P. H. McMurry was provided by NSF Award Number ATM-0500674. We thank L. G. Huey and coworkers from the School of Earth and Atmospheric Sciences at the Georgia Institute of Technology for providing us with the data for sulfuric acid vapor concentrations from the Tecamac, Mexico measurement campaign.

Chapter 3 : Cluster Energy Non-Accommodation and Barriers to Small Cluster Formation

3.1 Synopsis

The role of cluster energy non-accommodation in small cluster formation was investigated using bimolecular quantum Rice-Ramsperger-Kassel (QRRK) theory. In the context of this theory, stable cluster formation occurs through a sequence of three steps: [1] bimolecular collision yielding an energetically unstable cluster complex, followed either by [2] decay back into starting reactants or [3] stabilization by collision with a third body. This competition between decay and stabilization was shown to introduce a significant barrier to stable cluster formation, with the cluster accommodation coefficient (fraction of collisions yielding a stable cluster) quickly decreasing with decreasing cluster size. This model for cluster energy non-accommodation was applied to a sulfuric acid aerosol system that starts with the formation of the dimer species $(H_2SO_4)_2$, yielding a dimer accommodation coefficient P_2 ranging from 2 x 10^{-1} to 2 x 10^{-3}. The effects of a dimer formation barrier on aerosol concentrations were investigated by comparing measured concentrations of $(H_2SO_4)_n$ (n = 1, 3, and 4) and nanoparticles (3 – 10 nm) with predictions from a newly developed cluster population balance model. A dimer accommodation coefficient of α = 3 x 10^{-2} yielded the best-fit between measured and modeled concentrations, while a value of α = 1 (perfect accommodation) overestimated cluster concentrations by 10 – 40 X. This empirically obtained value of the dimer accommodation coefficient (α = 3 x 10^{-2}) falls in the range predicted by QRRK theory and is in qualitative agreement with values of P_2 obtained from correlations of measured $[H_2SO_4]$ and extrapolated nucleation rates.

3.2 Introduction

The details of cluster formation from gaseous precursors are of fundamental and practical interest to the study of gas-particle conversions, playing a definitive role in

diverse fields including novel materials synthesis, catalysis, vapor deposition, and atmospheric aerosol formation [*Friedlander*, 1977; *Seinfeld and Pandis*, 1998]. A detailed knowledge of cluster formation mechanisms would enable the accurate prediction of particle nucleation rates, which, when combined with accurate knowledge of particle growth rates, would fully characterize the time and size-dependent dynamics of an evolving aerosol system. Classical nucleation theory (CNT) and subsequent versions of it have been traditionally used to model cluster formation [*Volmer and Weber*, 1926; *Becker and Doring*, 1935; *Frenkel*, 1946], treating clusters as spherical droplets with bulk properties and assuming that the rate of monomer addition to a cluster is given by the hard-sphere collision rate multiplied by an accommodation coefficient that is usually set to unity [*Friedlander*, 1977]. Over the past two decades, the cluster thermodynamics predicted by CNT have been critically revised with molecular-based modeling methods [*McGraw and Laaksonen*, 1996; *Ford*, 1997; *Oxtoby*, 1998; *Schenter et al.*, 1999]. The kinetics of cluster formation predicted by CNT have also been re-examined in experimental studies [*Weber et al.*, 1996; *Lehtinen et al.*, 2004; *McMurry et al.*, 2005; *Kuang et al.*, 2008] and theoretical studies [*Venkatesh et al.*, 1995; *Zahoransky et al.*, 1995; *Okada and Hara*, 2007] indicating that the net formation rate of small clusters may be significantly smaller than the hard-sphere collision rate.

This barrier to small cluster formation can be understood within the context of elementary reaction kinetics where, in the early stages of cluster formation, bimolecular collisions rarely lead to stable clusters, due to the exothermal nature of the reactions providing sufficient energy for dissociation [*Holbrook et al.*, 1996]. The energetically unstable collision complex that forms immediately dissociates back into reactants, unless that complex is first de-energized by collision with a third body that removes the excess energy. CNT neglects the energetics inherent in the cluster collision process and assumes that every cluster-cluster collision leads to stable cluster formation, which can overestimate the cluster formation rate and the resulting cluster concentrations. It is reasonable to believe that this competition between collision complex decay and collisional stabilization can decrease the rate of small cluster formation below the hard-

sphere collision limit. The probability that a cluster-cluster collision results in stable cluster formation can be described by an accommodation coefficient, which is expected to be small for monomer- monomer collisions and to asymptotically approach unity as cluster size increases [*Venkatesh et al.*, 1995]. Substantial energy non-accommodation would result in a relatively small accommodation coefficient.

A particularly relevant system to which this concept of energy non-accommodation can be applied is the formation of sulfuric acid clusters and their subsequent growth to detectable sizes. *Kurtén et al.* [2009], using quantum chemically calculated vibrational frequencies and anharmonic coupling constants for small sulfuric-acid containing clusters, calculated an accommodation coefficient for the collision of two H_2SO_4 molecules that is at least 0.15 at the very least and likely equal to unity. While the calculated vibrational frequencies and coupling constants of *Kurtén et al.* [2009] are sufficiently accurate, the calculated range (0.15 – 1) in accommodation coefficients is based on a crude assumption regarding dimer dissociative properties (which will be addressed in subsequent sections) and can lead to an overestimation of the accommodation coefficient by several orders of magnitude.

Recent measurements of ambient sulfuric acid clusters by *Zhao et al.* [2009] during a nucleation event have provided an exciting opportunity to obtain cluster kinetic and thermodynamic properties. Using a newly developed cluster mass spectrometer (Cluster-CIMS), *Zhao et al.* [2009] were able to measure the cluster species $(H_2SO_4)_n$ (n = 1, 3, and 4) in conjunction with conventional aerosol instrumentation measuring down to 3 nm during a nucleation event. These ambient cluster measurements are the first of their kind. These cluster measurements can, in principle, yield empirically obtained accommodation coefficients in conjunction with a cluster population balance model, providing the first estimate of a $(H_2SO_4)_n$ formation barrier using measured cluster concentrations.

In this study, a model was developed for calculating size-dependent cluster accommodation coefficients for a nucleating aerosol system using basic reaction rate theory. This model for cluster energy non-accommodation was applied to a sulfuric acid

aerosol system driven by formation of the dimer species $(H_2SO_4)_2$. The effects of a dimer formation barrier on aerosol concentrations were investigated by comparing measured concentrations of $(H_2SO_4)_n$ (n = 1, 3, and 4) [*Zhao et al.*, 2009] and nanoparticles (3 – 10 nm) with predictions from a newly developed cluster population balance model [*Kuang et al.*, 2009e]. An empirically obtained value for the dimer accommodation coefficient was then compared with QRRK predictions and corresponding accommodation coefficients obtained from correlations of measured $[H_2SO_4]$ and extrapolated nucleation rates [*Kuang et al.*, 2008].

3.3 Theory

The mechanism of cluster formation can be readily formulated within the context of elementary reaction kinetics. In the early stages of cluster formation, few bimolecular collisions lead to stable clusters, due to the exothermal nature of the reactive collisions providing sufficient energy for cluster dissociation. Stable clusters will only form when third bodies collide with and remove excess energy from transient cluster complexes formed from previous bimolecular collisions.

This competition between cluster dissociation and stabilization can be modeled as a set of three reactions with bimolecular quantum Rice-Ramsperger-Kassel (QRRK) theory [*Dean*, 1985], an extension to the unimolecular QRRK theory developed by Rice and Ramsperger [*Rice and Ramsperger*, 1927; 1928] and Kassel [*Kassel*, 1928a; b]. Bimolecular QRRK considers the formation of a *j*-sized cluster through monomer addition to occur via the sequence:

[1] $A_1 + A_{j-1} \xrightarrow{k_f f(E)} A_j^*(E)$

[2] $A_j^*(E) \xrightarrow{k_d(E)} A_1 + A_{j-1}$

[3] $A_j^*(E) + M \xrightarrow{\beta k_s} A_j + M$,

where A_1 is the monomer, $A_j^*(E)$ is an energetically unstable collision complex with energy E, and M is a non-reactive third body. In equation [1], species A_1 and A_{j-1}

reactively collide to form an energetically unstable collision complex $A_j^*(E)$, where k_f is the cluster-monomer collision rate constant and $f(E)$ is the energy distribution function of the resulting complex. This energetic complex $A_j^*(E)$ can then either dissociate back into starting reactants as shown in equation [2] with energy-dependent decay rate constant $k_d(E)$, or be stabilized by collision with M as shown in equation [3] where k_s is the stabilization rate constant and β is a collisional deactivation efficiency. In principle, the quantities k_f, $f(E)$, $k_d(E)$, and k_s are functions of cluster size *j*, and their size explicit size-dependence will be defined in subsequent sections. A schematic energy diagram for this reaction sequence is shown in Figure 3.1, where E_o is the binding (dissociation) energy, the minimum energy required for cluster dissociation to occur. Application of a pseudo steady-state condition to $A_j^*(E)$ and integrating over cluster energy E yields the net formation rate constant k_{net} of the cluster A_j:

$$[4] \qquad k_{net} = \int_{E_o}^{\infty} \beta k_s [M] \frac{k_f f(E)}{\beta k_s [M] + k_d(E)} dE .$$

The energized complex $A_j^*(E)$ contains an excess of energy relative to its stable ground state A_j, as illustrated in Figure 3.1. The decay rate of this complex can be described by unimolecular QRRK reaction rate theory, which treats this excess cluster energy as quantized vibrational energy. In the simplest form of unimolecular QRRK theory, a cluster is assumed to be composed of s identical harmonic oscillators (vibrational modes) having the same vibrational frequency ν, usually calculated as a geometric mean $\langle \nu \rangle$ of the cluster's actual vibrational frequency distribution [*Holbrook et al.*, 1996]. In order for cluster dissociation to occur, the critical energy E_o must be localized in a single oscillator. This critical energy is then expressed as $E_o = mh\langle \nu \rangle$ and the total energy of the cluster is expressed as $E = nh\langle \nu \rangle$, where m is the number of vibrational quanta that are equivalent to the critical energy and n is the total number of

vibrational quanta possessed by the cluster [*Holbrook et al.*, 1996]. For a cluster complex $A_j^*(E)$ possessing s oscillators and n vibrational quanta, the probability P_d that a single critical oscillator has m critical quanta is determined by an application of straightforward combinatorial statistics [*Steinfeld et al.*, 1989]:

[5] $$P_d(n) = \frac{n!(n-m+s-1)!}{(n-m)!(n+s-1)!}.$$

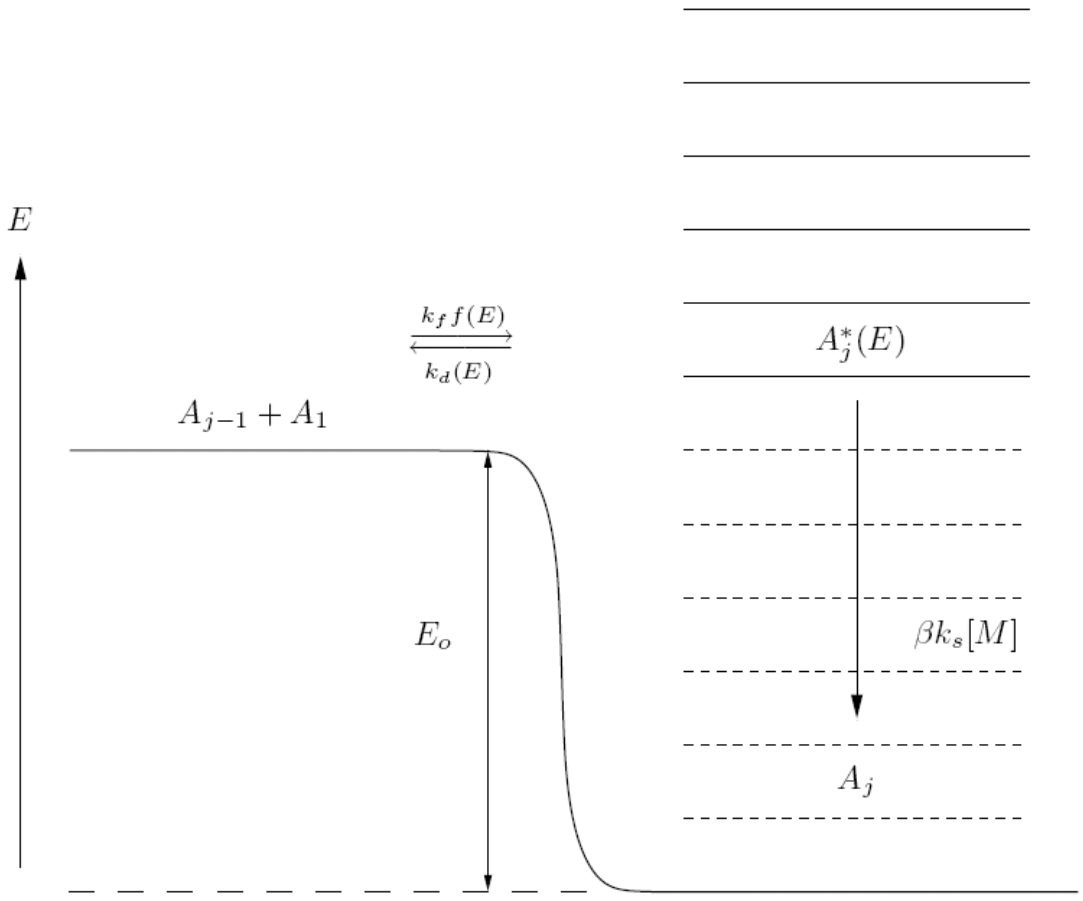

Figure 3.1 Energy diagram for cluster growth through monomer addition via the sequence: monomer A_1 reactively colliding with cluster A_{j-1} to form energetically unstable complex $A_j^*(E)$ which can either dissociate into reactants A_1 and A_{j-1} or be stabilized by collision with third body M to form stable cluster A_j with binding energy E_o. Refer to text for definitions of accompanying rate constants.

This expression for single oscillator decay can be extended to describe multiple oscillator decay, where the probability $P_{c,d}$ that *c* critical oscillators contain *m* critical quanta is given by the expression:

[6] $$P_{c,d}(n) = \left[-\frac{-\bar{\Gamma}(1+c+n)\bar{\Gamma}(m)+\bar{\Gamma}(1+n)\bar{\Gamma}(c+m)}{c(-1+c)!\bar{\Gamma}(1+n)\bar{\Gamma}(m)} \right] \Bigg/ \left[\frac{(n+s-1)!}{n!(s-1)!} \right],$$

where $\bar{\Gamma}$ is the gamma function.

For a cluster possessing n vibrational quanta, the probability of cluster decay decreases with increasing oscillator number s since the cluster energy quanta n is distributed among more vibrational degrees of freedom and the resulting probability of isolating the critical quanta m in a single oscillator consequently decreases. Naturally, the decay probability would also decrease with increasing cluster size j since the oscillator number s (vibrational degrees of freedom) is linearly dependent on cluster size j through the relation [*McQuarrie and Simon*, 1997]:

[7a] $s(j) = 3j - 5$ for linear clusters

[7b] $s(j) = 3j - 6$ for non-linear clusters,

For monomers containing N polyatomic molecules, the cluster size j is substituted with the quantity Nj in equations [7a] and [7b]. For the case of single oscillator decomposition, the rate constant $k_d(j,n)$ for the decomposition of $A_j^*(n)$ is then equal to the product of $P_d(n)$ and a proportionality constant A_∞, the Arrhenius pre-exponential factor for dissociation of A_j in the high-pressure limit, yielding [*Holbrook et al.*, 1996]:

[8] $$k_d(j,n) = A_\infty \frac{n!(n-m+s(j)-1)!}{(n-m)!(n+s(j)-1)!}.$$

Obtaining an accurate value for the pre-exponential factor A_∞ is often difficult, as it requires detailed knowledge of the cluster transition state [*Gilbert and Smith*, 1990]. In the absence of such data, this parameter is usually obtained either from available literature data or estimated from group contribution methods [*Benson*, 1968]. For

reactions involving simple fission of complex molecules (analogous to cluster dissociation), the transition state tends to be "loose" with a very shallow activation energy yielding values of A_∞ that fall in the range 10^{15} s^{-1} < A_∞ < 10^{17} s^{-1} [*Gilbert and Smith*, 1990; *Holbrook et al.*, 1996]. In *Kurtén et al.* [2009], the calculation of $k_d(j,n)$ involved setting A_∞ equal to the geometric mean frequency $\langle\nu\rangle$, which is usually in the range 10^{13} – 10^{14} s^{-1} and in the case of $(H_2SO_4)_2$ equals 2.6 x 10^{13} s^{-1}. However, $\langle\nu\rangle$ is known to underestimate measured values of A_∞ by 2 – 4 orders of magnitude [*Steinfeld et al.*, 1989; *Gilbert and Smith*, 1990; *Holbrook et al.*, 1996]. This would then lead to a dramatic underestimation of the cluster decay rate and, subsequently, the cluster stability. For this analysis, the reported range in A_∞ for simple fission reactions (10^{15} s^{-1} < A_∞ < 10^{17} s^{-1}) will be used to calculate a range in $k_d(j,n)$. The dependence of k_d on the cluster size j for a monatomic model system (N = 1) is shown in Figure 3.2 for a set of model cluster parameters. As expected, the rate of cluster decay decreases as cluster size increases since there are a greater number of vibrational modes over which the cluster vibrational quanta n can be distributed.

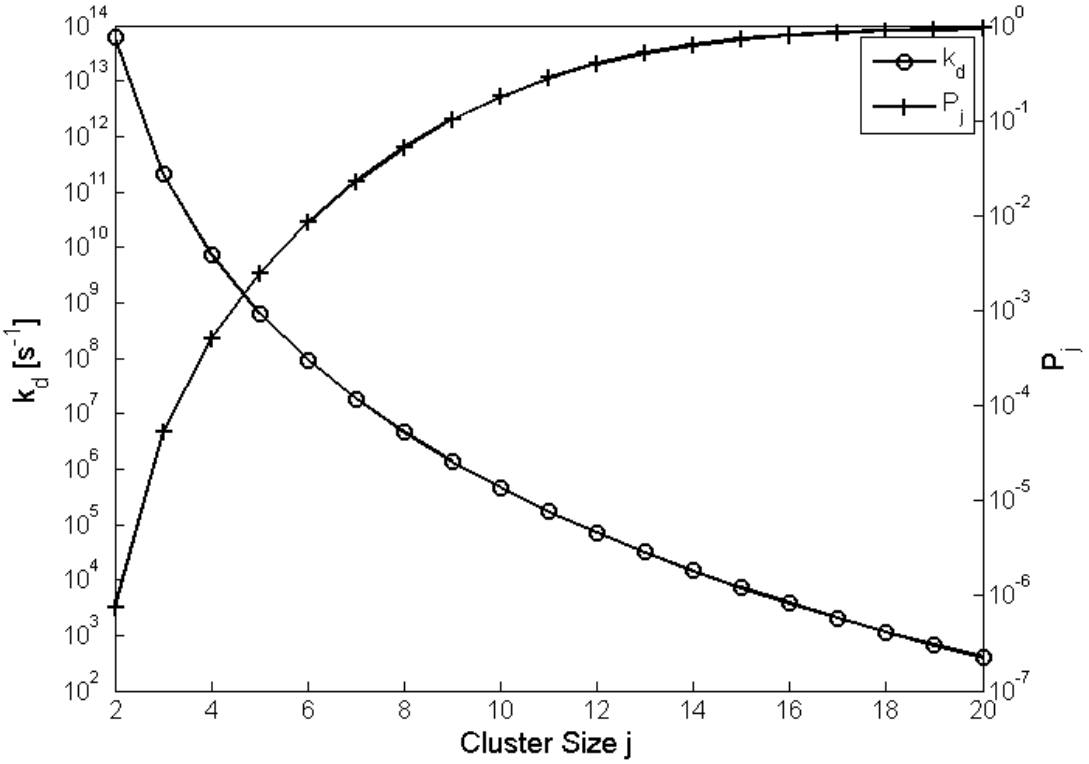

Figure 3.2 Cluster decay rate k_d of a j-sized cluster and the resulting accommodation coefficient P_j for the formation of a *j*-sized cluster from the collision of a monomer with a *j*-1 sized cluster. Calculations were performed using bimolecular QRRK theory [*Dean*, 1985] for a monatomic monomer system with the following cluster input parameters: critical quanta $m = 5$, vibrational quanta $n = 10$ (for calculation of k_d), A_∞ = 1 x 10^{16} s^{-1}, ε = 100 cm^{-1}, $-\langle \Delta E_{coll} \rangle$ = 500 cm^{-1}, and geometric mean vibrational frequency $\langle \nu \rangle$ = 1000 cm^{-1}.

The rate constant k_f that is associated with formation of the initial collision complex $A_j^*(n)$ can be described by hard-sphere collision theory [*Benson*, 1968]:

[9] $$k_f = p_{steric} Z \exp\left[-\frac{E_{act}}{k_B T}\right],$$

where p_{steric} is the fraction of collisions that have the proper orientation for reaction, Z is the hard-sphere collision rate constant, and E_{act} is the activation energy barrier to initial cluster formation. For cluster systems in which intermolecular interactions are characterized by weak, non-directional bonding and where no significant bond rearrangement takes place during collision, it would be reasonable to set the steric factor to unity and the activation energy to zero [*Gilbert and Smith*, 1990]. Under these conditions, the initial cluster formation step in equation [1] becomes a barrier-less process and, for a collision between a monomer and a *j*-sized cluster, equation [9] reduces to the hard-sphere limit expression Z, defined as [*Friedlander*, 1977]:

[10] $$Z = \left(\frac{3}{4\pi}\right)^{1/6} \left(\frac{6k_B T}{\rho}\right)^{1/2} \upsilon_1^{1/6} \left(1+\frac{1}{j-1}\right)^{1/2} \left[1+(j-1)^{1/3}\right]^2,$$

where υ_1 is the monomer volume, T is the temperature, k_B is Boltzmann's constant, and ρ is the cluster density. This expression for Z is equivalent to that of β_{1j} defined in *Friedlander* [1977]. With the cluster energy now quantized, the resulting distribution function $f(j,n)$ for the collision complex $A_j^*(n)$ is calculated by applying the principle of detailed balance to the energized cluster formation process, yielding:

[11] $$f(j,n) = \frac{k_d(j,n) P(j,n)}{\sum_{n=m}^{\infty} k_d(j,n) P(j,n)},$$

where $P(j,n)$ is the quantized thermal energy distribution derived by *Kassel* [1928b] that defines the probability that an energized cluster of size *j* has n vibrational quanta with geometric mean vibrational frequency $\langle \nu \rangle$ distributed among s harmonic oscillators, given by the expression [*Holbrook et al.*, 1996]:

[12] $$P(j,n) = \exp\left[-\frac{nh\langle\nu\rangle}{k_B T}\right]\left(1-\exp\left[-\frac{h\langle\nu\rangle}{k_B T}\right]\right)^{s(j)} \frac{(n+s(j)-1)}{n!(s(j)-1)!}.$$

Values of the stabilization rate constant k_s are computed with Lennard-Jones collision theory, yielding:

[13] $$k_s = 2.708 Z \left(\frac{\varepsilon}{k_B T}\right)^{1/3},$$

where Z is the hard-sphere collision rate constant (see equation [10]) and ε is the well depth of the interaction potential between the cluster and colliding third body M, usually an inert gas [*Gilbert and Smith*, 1990]. A collisional deactivation efficiency β has been applied to modify the traditional but incorrect strong-collision assumption that every collision between $A_j^*(n)$ and M results in the removal of all the excess energy from $A_j^*(n)$ [*Westmoreland et al.*, 1986]. By analyzing the collisional energy transfer with master-equation methods, the temperature dependence of β can be fit with the equation:

[14] $$\frac{\beta}{1-\sqrt{\beta}} = \frac{-\langle\Delta E_{coll}\rangle}{F(E) k_B T},$$

where $-\langle\Delta E_{coll}\rangle$ is the average amount of energy transferred per collision and $F(E)$ is an energy-dependent factor that has a median value of 1.15 over the temperature range 300 - 2500 K for a series of reactions [*Troe*, 1977a; b]. This approach modifies the strong collision assumption so that not every collision is deactivating, but when deactivation does occur, it is complete, and all the excess energy is lost.

The accommodation coefficient P_j for a monomer-cluster collision that yields a cluster of size j can then be defined as the ratio of the net formation rate constant k_{net} to the rate constant assuming every collision is effective, k_f (hard-sphere collision rate constant), yielding:

[15] $$P_j = \sum_{n=m}^{\infty} \frac{\beta k_s [M] f(j,n)}{\beta k_s [M] + k_d(j,n)}.$$

The dependence of the cluster accommodation coefficient with cluster size at atmospheric pressure for monatomic model system is shown in Figure 3.2 for a set of model cluster parameters. The accommodation coefficient increases with increasing cluster size due to the accompanying decrease in the decay rate of the energized cluster complex k_d. The lifetime of the cluster complex increases to the point where third body collisions with M are frequent enough to stabilize the complex. This competition between cluster decay and stabilization creates a "bottleneck" to cluster formation at the smallest sizes, and could potentially account for the reduced rates of measured cluster formation when compared to model predictions.

In order to make predictions of cluster non-accommodation in a nucleating system, one then needs the following species dependent parameters: the geometric mean of the cluster complex's vibrational frequencies $\langle \nu \rangle$, the pre-exponential factor A_∞ (in this study, ranging from 1 x 10^{15} – 1 x 10^{17} s^{-1}), the number of vibrational degrees of freedom s of the cluster complex (calculated from cluster geometry), the cluster binding energy E_o, the Lennard-Jones interaction well depth ε between cluster complex and third body (estimated from tabulated values), and the average transferred per collision with the third body $-\langle \Delta E_{coll} \rangle$ (estimated from tabulated values).

3.4 Model Application

3.4.1 Non-Accommodation in $(H_2SO_4)_2$ Formation

A particularly interesting and relevant test system that is amenable to this model for cluster energy non-accommodation is the formation of the stable dimer $(H_2SO_4)_2$ from the collision of two sulfuric acid molecules. Diverse measurement campaigns have indicated the critical role that sulfuric acid plays in atmospheric nucleation [*Weber et al.*, 1996; *Eisele and McMurry*, 1997; *Riipinen et al.*, 2007; *Kuang et al.*, 2008]. In these same studies, the formation rates of the smallest clusters were shown to be 1 – 4 orders of magnitude below the hard-sphere collision limit, indicating the presence of a barrier to cluster formation. If this "bottleneck" to cluster formation is assumed to occur at the

formation of the sulfuric acid dimer (which is reasonable as the effects of non-accommodation diminish rapidly with increasing cluster size), then cluster non-accommodation can provide a physical basis for the observation that extrapolated cluster formation rates are orders of magnitude below the collision limit.

It is important to note that non-accommodation is not the only process that can lead to reduced rates of cluster formation, as cluster evaporation would have the same qualitative effect, reducing net cluster formation rates and concentrations. Also, it is speculated that the cluster formation process could involve species other than sulfuric acid (e.g. ammonia or amines), leading to multi-component interactions that can have substantial effects on cluster stability [*Weber et al.*, 1997; *Kulmala et al.*, 2000; *Kurten et al.*, 2008]. A method for obtaining empirical estimates of the dimer evaporation coefficient from cluster measurements is described in section 6.1.2.

While four minimum-energy structures of the sulfuric acid dimer have been identified [*Salonen et al.*, 2009], the c1 isomer was chosen for this study as a test case for non-accommodation. Model inputs for the c1 isomer include the anharmonic cluster frequencies calculated by *Kurten et al.* [2009], a zero-point corrected binding energy of 6255 cm^{-1} calculated by *Salonen et al.* [2009], and collisional energy parameters ε and $-\langle \Delta E_{coll} \rangle$ obtained from *Troe* [1979] and *Gilbert and Smith* [1990] assuming O_2 as the third body. Based on their anharmonic frequency calculations and visualizations of dimer dissociation, *Kurten et al.* [2009] determined that there were 22 vibrational modes that were coupled to the dimer dissociative mode ($s = 22$). Even though this number is less than the 36 total vibrational modes expected based on cluster geometry, it is consistent with the observation that often the best fit to experimental results is obtained by taking the number of accessible modes to be roughly half the total number of vibrational modes [*Holbrook et al.*, 1996]. With the harmonic oscillator number $s = 22$, the geometric mean $\langle \nu \rangle$ of the corresponding vibrational frequency distribution was calculated to be 900 cm^{-1}. With this value for $\langle \nu \rangle$ and the reported cluster binding energy, the critical vibrational quanta was calculated to be 6. Because of the uncertainty

in the Arrhenius parameter A_∞, the dimer accommodation coefficient was calculated using the measured range in A_∞ (10^{15} s^{-1} < A_∞ < 10^{17} s^{-1}) associated with simple fission reactions [*Holbrook et al.*, 1996]. These types of reactions are often characterized by potential surfaces without a pronounced energetic barrier [*Gilbert and Smith*, 1990], which is not an unreasonable assumption for the dissociation of a sulfuric acid dimer [*Kurtén et al.*, 2009]. All calculations were performed at a temperature of 298 K, at a pressure of 1 atmosphere, and assuming bulk particle properties of sulfuric acid for the calculation of collision parameters utilizing cluster volume.

3.4.2 Effect of Non-Accommodation on Modeled $(H_2SO_4)_n$ Concentrations

Recent measurements by *Zhao et al.* [2009] of ambient sulfuric acid cluster concentrations during a nucleation event have provided a unique opportunity to test for the presence of a cluster formation barrier; such a "bottleneck" at the smallest cluster sizes would reduce the cluster formation rate and the resulting cluster concentrations. The concentration measurements of sulfuric acid clusters were acquired during atmospheric nucleation events observed in an urban (Boulder, CO) and forested site (Manitou Experimental Forest) using a newly developed cluster chemical ionization mass spectrometer (Cluster-CIMS) [*Zhao et al.*, 2009].

These concentration measurements of sulfuric acid clusters $(H_2SO_4)_n$ (n = 1, 3, and 4) were compared with modeled cluster concentrations using a recently developed aerosol population balance model [*Kuang et al.*, 2009e]. The model was used to simulate the dynamics of a single-component aerosol system driven by sulfuric acid nucleation with simultaneous coagulation and condensation. In this model, the evolution of the dimer concentration N_2 (smallest cluster) was described with the following balance equation:

[16] $$\frac{dN_2}{dt} = \alpha k_f N_1^{\,2} - \Gamma \beta_{12} N_1 N_2 - N_2 \sum_{i=2}^{\infty} \beta_{2i} N_i \,,$$

where N_1 is the measured concentration of sulfuric acid monomer, Γ is a growth enhancement factor that parameterizes the condensation of vapor phase species other than sulfuric acid that contribute to the measured particle growth rate [*Kuang et al.*, 2009e], and β_{ij} is the collision frequency function between clusters of size *i* and *j* calculated from the Fuchs transition regime expression [*Fuchs*, 1964]. The second and third terms on the RHS of equation [16] defined the depletion of the dimer through condensational growth past the dimer and through coagulation with the pre-existing aerosol, respectively. Cluster growth rates were parameterized from measured growth rates of 5 – 25 nm particles and the measured contribution from sulfuric acid condensation [*Kuang et al.*, 2009e]. The first term on the RHS is the rate at which the dimer is produced from the bimolecular collision of two sulfuric acid monomers, where the hard-sphere collision rate k_f is reduced by an empirical parameter α $(0 < \alpha < 1)$ in order to simulate the presence of a barrier to cluster formation. This parameter α was then decreased from 1 (no barrier) to 1 x 10^{-4} so as to explore the sensitivity of the resulting modeled cluster concentrations to an increasing barrier to cluster formation. The value of α that provided the best model fit to measured cluster concentrations was then compared with predictions from bimolecular QRRK theory and with inferred values calculated from parameterized dimer formation rate constants [*Kuang et al.*, 2008].

3.5 Results and Discussion

3.5.1 Theoretical $(H_2SO_4)_2$ Accommodation Coefficient

To illustrate the sensitivity of the magnitude of non-accommodation to input cluster parameters, the accommodation coefficient P_2 for the formation of the c1 isomer of $(H_2SO_4)_2$ was calculated for a range in two input quantities: [1] the number of accessible vibrational modes s, and [2] the Arrhenius pre-factor A_∞. Depending on the strength of intermolecular interactions within the sulfuric acid dimer, s can range from 6 (weakly bound cluster) to 36 vibrational modes (strongly bound cluster) [*Kurtén et al.*,

2009]. The resulting sensitivity of the dimer accommodation coefficient to the vibrational mode number s is shown in Figure 3.3, where P_2 ranges from 1 x 10^{-5} (weakly bound cluster) to 1 x 10^{-1} (strongly bound cluster) given a geometric mean value of the Arrhenius pre-factor A_∞ = 1 x 10^{-16} s^{-1}. This increase in energy accommodation with increasing s is expected as there are a greater number of vibrational modes over which the excess collision energy can be distributed, yielding an energized cluster complex with a longer lifetime that can be subsequently stabilized by collision with a third body.

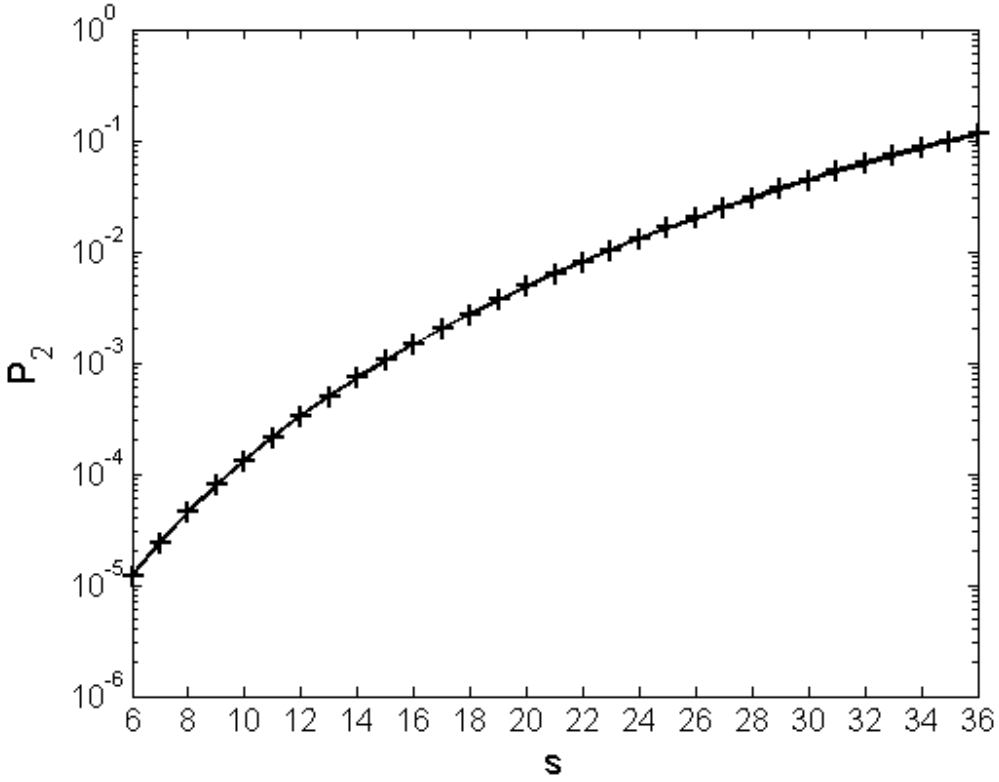

Figure 3.3 The dimer accommodation coefficient P_2 as a function of the number of accessible vibrational modes s for the c1 isomer of $(H_2SO_4)_2$. P_2 defines the probability that a monomer-monomer collision will result in the formation of a stable dimer. The vibrational mode number s varies from 6 (weakly bound cluster) to 36 (strongly bound cluster) and defines the number of vibrational modes that are coupled to the dimer dissociative mode. Calculations were performed using bimolecular QRRK theory [*Dean*, 1985] and vibrational frequencies from Kurtén et al. [2009] with the following input parameters for the c1 isomer of $(H_2SO_4)_2$: critical quanta 6, $A_\infty = 1 \times 10^{16}$ s^{-1}, $\varepsilon = 78$ cm^{-1}, $-\langle \Delta E_{coll} \rangle = 501$ cm^{-1}, number of critical oscillators = 3, and $\langle \nu \rangle = 900$ cm^{-1}.

Qualitatively, the pre-factor A_∞ describes the frequency at which the energized cluster complex dissociates and for the simple fission of complex molecules into two relatively large fragments, this pre-factor falls in the range 10^{15} $s^{-1} < A_\infty < 10^{17}$ s^{-1} [*Holbrook et al.*, 1996]. Using a vibrational mode number of $s = 27$ (an upper limit determined by *Kurtén et al.* [2009]), the sensitivity of the dimer accommodation coefficient to the given range in A_∞ was explored, as shown in Figure 3.4, with P_2 decreasing from 2 x 10^{-1} to 2 x 10^{-3} as A_∞ is increased from 1 x 10^{15} to 1 x 10^{17} s^{-1}. This decrease in accommodation is expected since an increase in A_∞ results in a faster cluster decay rate (see equation [8]), leading to a reduced lifetime for the energized complex, which then decays before it can be stabilized by collision with a third body. This calculated range in dimer accommodation is at least an order of magnitude smaller than that calculated by *Kurtén et al.* [2009], due to the much smaller value of A_∞ that is used.

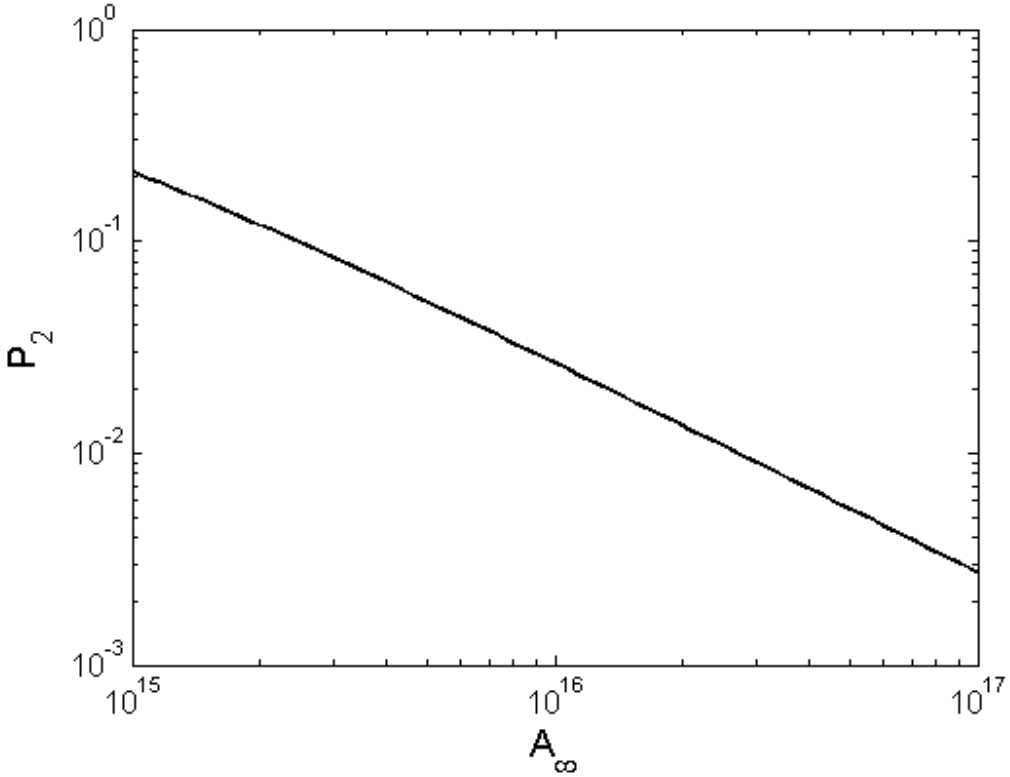

Figure 3.4 The dimer accommodation coefficient P_2 as a function of the Arrhenius pre-factor A_∞ for the c1 isomer of $(H_2SO_4)_2$. P_2 defines the probability that a monomer-monomer collision will result in the formation of a stable dimer. The pre-factor A_∞ varies in the range 10^{15} $s^{-1} < A_\infty < 10^{17}$ s^{-1}, corresponding to the measured range in A_∞ associated with simple fission reactions with no pronounced activation barrier [*Gilbert and Smith*, 1990; *Holbrook et al.*, 1996]. Calculations were performed using bimolecular QRRK theory [*Dean*, 1985] and vibrational frequencies from Kurtén et al. [2009] with the following input parameters for the c1 isomer of $(H_2SO_4)_2$: critical quanta 6, $s = 27$, ε = 78 cm^{-1}, $-\langle \Delta E_{coll} \rangle$ = 501 cm^{-1}, number of critical oscillators = 3, and $\langle \nu \rangle$ = 900 cm^{-1}.

3.5.2 Empirical $(H_2SO_4)_2$ Accommodation Coefficient

Measured concentrations of $(H_2SO4_4)_n$ (n = 1, 3, and 4) and nanoparticles (3 – 10 nm) produced during a nucleation event were compared with predictions from an aerosol dynamics model, as shown in Figure 3.5. Modeled results are shown for the case of perfect accommodation (α = 1) and for the value of α (α = 3 x 10^{-2}) that yielded the best fit with measured cluster and nanoparticle concentrations. The modeled results are anchored by the measured sulfuric acid concentration. Both model results utilize the same size-dependent growth enhancement factor Γ parameterized from the measured growth rate of 3 – 25 nm particles and the measured contribution to growth from the condensation of sulfuric acid. A size-dependent Γ was used that increased linearly from 1 at the dimer to 20 at a cluster size of 100 (~ 3 nm). When perfect dimer accommodation is assumed, concentrations of $(H_2SO_4)_3$, $(H_2SO_4)_4$, and 3 – 10 nm particles are overestimated by at least factors of 40, 10, and 20, respectively, when compared to their measured values. Reasonable agreement between measured and modeled concentrations is only obtained when α is decreased to a value of 3 x 10^{-2}; only 3% of sulfuric acid monomer-monomer collisions yield stable dimer formation. This inferred value of the dimer accommodation coefficient falls within the range (2 x 10^{-1} to 2 x 10^{-3}) predicted by bimolecular QRRK theory.

This best-fit value of the dimer accommodation coefficient (α = 3 x 10^{-2}) can also be compared with location-dependent dimer accommodation coefficients obtained from correlations of measured $[H_2SO_4]$ and extrapolated nucleation rates [*Kuang et al.*, 2008]. In *Kuang et al.* [2008], location-dependent accommodation coefficients were calculated, varying in range from 10^{-4} – 10^{-2}, suggesting the presence of a barrier to dimer formation. In that work, a dimer accommodation coefficient of 4 x 10^{-2} was obtained for nucleation rates measured at Idaho Hill, a forested site in the Colorado Front Range Mountains that is similar to the Manitou Experimental Forest where these cluster measurements were obtained. The qualitative agreement between these two values of the dimer accommodation coefficient (3 x 10^{-2} vs. 4 x 10^{-2}) is encouraging, given the

different methods through which they were obtained. Results from this study, combined with the non-accommodation results from *Kuang et al.* [2008], further point to the presence of a barrier to small cluster formation in sulfuric acid-driven nucleation systems.

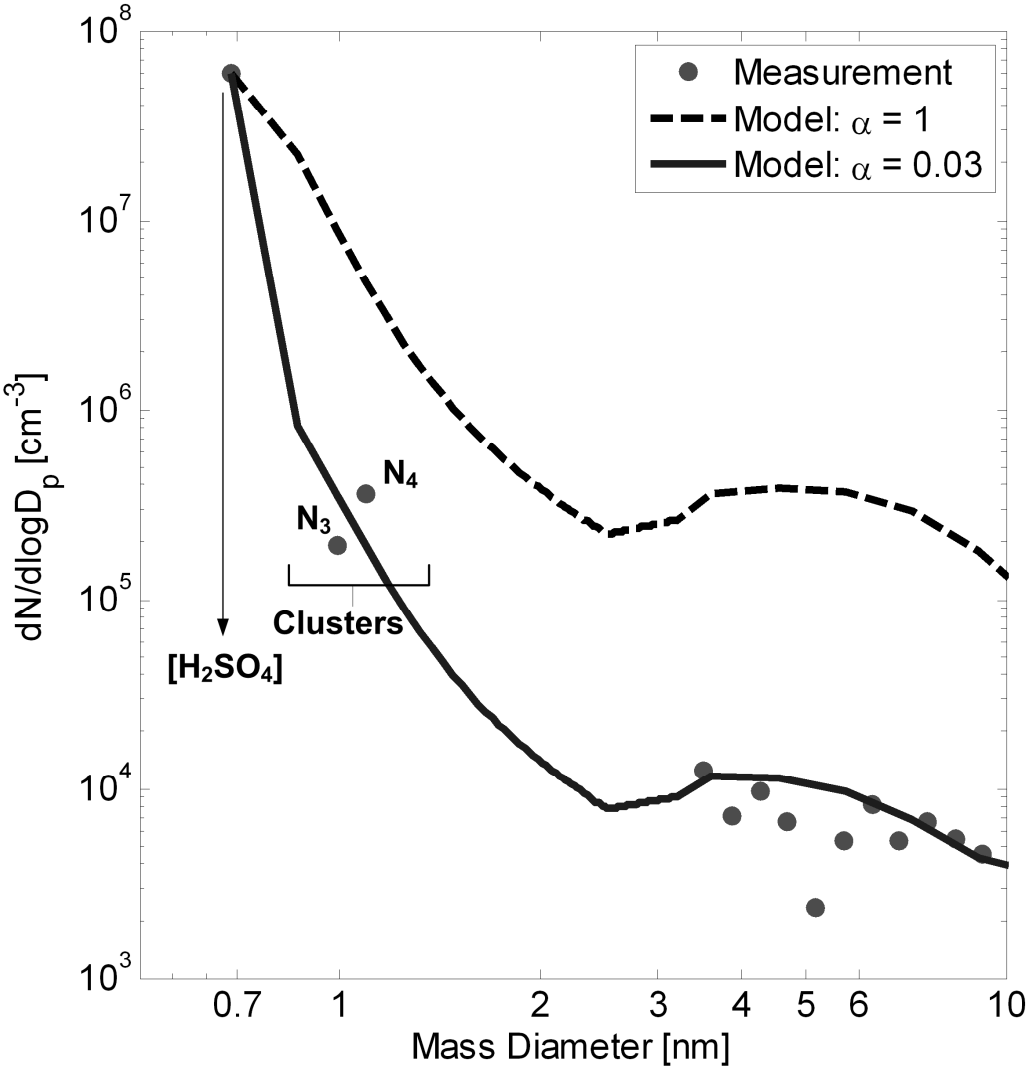

Figure 3.5 Comparison of measured concentrations of $(H_2SO_4)_n$ (n = 1, 3, and 4) and nanoparticles (3 – 10 nm) with time-dependent predictions from an aerosol dynamics model assuming perfect accommodation (α = 1) and using a value of α (α = 0.03) that yielded the best fit with measured cluster and nanoparticle concentrations. Measured data were obtained during a nucleation event measured at 12:30 PM local time in the Manitou Experimental Forest. Concentrations of $(H_2SO_4)_n$ were obtained with a Cluster-CIMS [*Zhao et al.*, 2009] while concentrations of 3 – 10 nm particles were obtained with a conventional SMPS system [*Wang and Flagan*, 1990]. The model results are anchored by the measured concentration of H_2SO_4.

3.6 Conclusions

Using bimolecular QRRK theory, a model for cluster energy non-accommodation was developed which predicted the presence of a barrier to small cluster formation. This barrier arises from the competition between decay of the energetic cluster and collisional stabilization of the energetic cluster with a third body. The resulting cluster accommodation coefficient (fraction of collisions yielding a stable cluster) was shown to be a strong function of cluster size, asymptotically approaching unity as cluster size increased due to the increased number of vibrational modes over which the excess collision energy can be distributed. This model for cluster energy non-accommodation was applied to a sulfuric acid aerosol system driven by formation of the dimer species $(H_2SO_4)_2$, yielding a dimer accommodation coefficient P_2 ranging from 2×10^{-1} to 2×10^{-3}. An empirical best-fit value of the dimer accommodation coefficient ($\alpha = 3 \times 10^{-2}$) was shown to yield the best agreement between measured concentrations of $(H_2SO_4)_n$ (n = 1, 3, and 4) and nanoparticles (3 – 10 nm) with predictions from a newly developed cluster population balance model. A value of $\alpha = 1$ (perfect accommodation) overestimated cluster concentrations by 10 – 40 X. This empirically obtained value of the dimer accommodation coefficient falls in the range predicted by QRRK theory and is in qualitative agreement with inferred values of the dimer accommodation coefficient obtained in similar environments.

3.7 Acknowledgements

Financial support from the IGERT Program of the National Science Foundation (DGE-0114372) and computational resources from the Minnesota Supercomputing Institute are gratefully acknowledged.

Chapter 4 : An Improved Criterion for New Particle Formation in Diverse Atmospheric Environments

4.1 Synopsis

A dimensionless theory for boundary layer new particle formation (NPF) was developed, using an aerosol population balance model incorporating recent developments in nucleation rates and measured particle growth rates. Based on this theoretical analysis, it was shown that a dimensionless parameter L_Γ, characterizing the ratio of the scavenging loss rate to the particle growth rate, exclusively determined whether or not NPF would occur on a particular day. This parameter determines the probability that a nucleated particle will grow to a detectable size before being lost by coagulation with the pre-existing aerosol. Cluster-cluster coagulation was shown to contribute negligibly to this survival probability under conditions pertinent to the atmosphere. Data acquired during intensive measurement campaigns in Tecamac (MILAGRO), Altanta (ANARChE), Boulder, and Hyytiälä (QUEST II and QUEST IV) were used to test the validity of L_Γ as an NPF criterion. Measurements included aerosol size distributions down to 3 nm and gas-phase sulfuric acid concentrations. The model was applied to forty-eight NPF events and five non-events (characterized by growth of pre-existing aerosol without NPF) measured in diverse environments with broad ranges in sulfuric acid concentrations, ultrafine number concentrations, and particle growth rates (nearly two orders of magnitude). Across this diverse data set, a nominal value of $L_\Gamma = 1$ was found to determine the boundary for the occurrence of NPF, with NPF occurring when $L_\Gamma < 1$ and being suppressed when $L_\Gamma > 1$. Calculation of L_Γ for measured events and non-events yielded an empirical value of 0.7 as the boundary for NPF. Moreover, more than 65% of measured L_Γ values associated with NPF fell in the relatively narrow range of $0.23 < L_\Gamma < 0.42$.

4.2 Introduction

Atmospheric aerosols contribute significantly to the net radiative forcing that drives the earth's energy balance, directly through the scattering and absorption of incident solar radiation, and indirectly through their role as potential cloud condensation nuclei (CCN) [1992]. Boundary layer new particle formation (NPF), an important source of atmospheric particles, occurs frequently in diverse locations [*Kulmala et al.*, 2004b], and is also an important source of CCN, as demonstrated in various measurement campaigns [*Kerminen et al.*, 2005; *Laaksonen et al.*, 2005] and modeling efforts [*Spracklen et al.*, 2008; *Kuang et al.*, 2009b]. Since the highest uncertainties in the current estimates for global radiative forcing are associated with these direct and indirect aerosol effects [*Chin et al.*, 2009], it is essential to understand processes that determine new particle formation (NPF) rates.

NPF occurs when nucleated particles grow to a size that can be detected. Until recently, the minimum detectable size was about 3 nm [*Stolzenburg and McMurry*, 1991], but recent developments have extended detection limits to sizes below 2 nm [*Iida et al.*, 2008a; *Sipilä et al.*, 2009]. While nucleation potentially occurs every day, NPF only occurs when particle growth to the detection limit dominates over particle losses from coagulation with the pre-existing aerosol. Analysis with aerosol dynamics models [*McMurry and Friedlander*, 1979; *McMurry*, 1983; *Kerminen and Kulmala*, 2002] have indicated that conditions favorable to NPF include high growth rates and low concentrations of pre-existing aerosol (low scavenging rates). These conditions have also been correlated with measured NPF events observed in diverse field campaigns [*Fiedler et al.*, 2005; *McMurry et al.*, 2005]. The development of a simple, quantitative, and universal criterion for NPF would form an important component of predictive models for aerosol formation, and would also characterize the relative importance of these processes that influence aerosol dynamics as the nucleated particles grow to the detection limit.

Past and recent efforts to model boundary layer NPF from the gas-phase have focused on simulating the dynamics of a nucleating aerosol growing through condensation and coagulation [*McMurry*, 1983; *Lehtinen and Kulmala*, 2003; *Korhonen*

et al., 2004; *Gaydos et al.*, 2005]. In light of the broad range (at least an order of magnitude) in the measured nucleation rates, in the pre-existing aerosol concentrations and in the particle growth rates associated with NPF, it is logical to take a non-dimensional approach in modeling NPF so as to obtain universally applicable results. This approach was used by *McMurry et al.* [1983] in developing a simple dimensionless loss parameter L, which is the ratio of the particle loss rate due to scavenging to the particle growth rate, determining whether or not NPF can occur. This parameter L was then calculated for NPF events measured in the sulfur-rich environment of Atlanta where it was shown that NPF was observed when $L<1$ but not when $L>1$ [*McMurry et al.*, 2005].

This NPF criterion, however, was derived assuming a steady-state, single-component system which greatly limits its application when modeling ambient aerosols. Cluster concentrations may not reach steady-state since atmospheric new particle formation is photochemically driven and therefore diurnal and dynamic. The derivation of the criterion assumes that both nucleation and growth are single-component processes, where every monomer-monomer collision generates a stable cluster (collision-limited nucleation), and where condensation of the monomer (gas-phase sulfuric acid) accounts for all the particle growth. A collision-limited model for nucleation, however, yields particle formation rates that are several orders of magnitude larger than observations [*Weber et al.*, 1996; *Kuang et al.*, 2008]. Also, sulfuric acid condensation accounts for only 10% of the measured particle growth [*Weber et al.*, 1997; *Mäkelä et al.*, 2001; *O'Dowd et al.*, 2002; *Wehner et al.*, 2005; *Iida et al.*, 2008b; *Smith et al.*, 2008]. Not only are nucleation and growth multi-component processes, but species that are responsible for the growth of newly formed particles are likely different from those that participate in nucleation. In these environments, the old L criterion greatly underestimates the particle growth rate and consequently underestimates the nucleated particle survival probability and subsequent frequency of NPF.

To address these limitations, we have developed a new aerosol population balance model that predicts new particle formation in a time-dependent system, incorporating

recent developments in nucleation rates, parameterizing them as power-law functions of sulfuric acid concentration, [*Sihto et al.*, 2006; *Riipinen et al.*, 2007; *Kuang et al.*, 2008], and recent work in determining the contribution of sulfuric acid condensation to measured nanoparticle growth rates [*Stolzenburg et al.*, 2005; *Sihto et al.*, 2006; *Riipinen et al.*, 2007; *Iida et al.*, 2008b]. This model adapts a single-component formulation for aerosol dynamics to include a multi-component representation through the use of measured nucleation and growth rates. This model explicitly incorporates the competition between particle loss due to cluster self-coagulation and scavenging by the pre-existing aerosol and particle gain due to measured growth, using measured aerosol size distributions and sulfuric acid concentrations. Model analysis yielded a new dimensionless parameter L_Γ, characterizing the ratio of the particle loss rate to the measured particle growth rate, which determined whether or not NPF would occur on a particular day. This criterion was validated against forty-eight NPF events and five non-events (characterized by growth of pre-existing nanoparticles without observed NPF) measured during various campaigns.

4.3 Experiment

This analysis utilized measurements of aerosol size distributions and gas-phase sulfuric acid concentrations from forty-eight new particle formation events and five non-events observed during an environmentally diverse set of measurement campaigns: MILAGRO (Tecamac, Mexico) [*Iida et al.*, 2008b], ANARChE (Atlanta, Georgia) [*McMurry et al.*, 2005], Boulder, CO [*Iida et al.*, 2006], QUEST II (Hyytiälä , Finland) [*Sihto et al.*, 2006], and QUEST IV (Hyytiälä , Finland) [*Riipinen et al.*, 2007]. The measurements from the QUEST II and IV campaigns in Hyytiälä were acquired by the research team from the University of Helsinki while the other measurements were carried out by the research team from the University of Minnesota and the National Center for Atmospheric Research. Descriptions of the physical and meteorological conditions at Tecamac, Atlanta, and Boulder as well as a summary of the pertinent aerosol and gas-phase instrumentation can be found in *Kuang et al.* [2008].

4.4 Theory

Currently, the photochemical nucleation and growth of stable atmospheric clusters is believed to occur through multi-component processes that often include sulfuric acid. New particle formation occurs when these nucleated clusters grow to a detectable size, typically about 3 nm [*Stolzenburg and McMurry*, 1991]. The probability of these clusters surviving to 3 nm depends on the relative rates of cluster growth and loss due to cluster-cluster coagulation and scavenging by the pre-existing aerosol. For a steady-state system, *McMurry* [1983] developed a simple, limiting criterion for whether or not new particle formation would occur by comparing rates at which clusters grow by condensation and are lost by coagulation with the pre-existing aerosol. It is the goal of this work to extend this criterion to more environmentally diverse systems where other gas-phase species besides sulfuric acid may contribute both to nucleation and growth by developing a cluster balance model that incorporates measurements and observationally constrained parameterizations for growth and nucleation, respectively.

The dynamics of an aerosol driven by simultaneous nucleation, condensation, and coagulation can be described by a set of dimensional population balance equations for discrete cluster sizes *k* [*McMurry*, 1983; *Lehtinen and Kulmala*, 2003]:

[1] $$\frac{dN_{k^\dagger}}{dt} = J^\dagger - \beta_{1k^\dagger} N_1 N_{k^\dagger} - N_{k^\dagger} \sum_{i=k^\dagger}^{\infty} \beta_{k^\dagger i} N_i - \frac{\overline{c}_1 A_{Fuchs}}{4} \frac{N_{k^\dagger}}{\sqrt{k^\dagger}}$$

[2] $$\frac{dN_k}{dt} = N_1 \left(\beta_{1k-1} N_{k-1} - \beta_{1k} N_k \right) - N_k \sum_{i=k}^{\infty} \beta_{ki} N_i + \frac{1}{2} \sum_{\substack{i \geq k^\dagger \\ i+j=k}}^{k} \beta_{ij} N_i N_j - \frac{\overline{c}_1 A_{Fuchs}}{4} \frac{N_k}{\sqrt{k}},$$

where equation [1] is the balance equation for the nucleating critical cluster ($k = k^\dagger$) and equation [2] is the balance equation for clusters larger than the critical cluster ($k > k^\dagger$). In these equations, N_k is the number concentration for newly formed *k*-sized clusters, N_1 is the number concentration of the condensing vapor-phase species, β_{ij} is the collision frequency function between clusters of size *i* and *j* (the free-molecular expression is used since the particles of interest are much smaller than the mean free path of air), A_{Fuchs} is the pre-existing aerosol surface area corrected for diffusion to transition regime particles

[*Fuchs and Sutugin*, 1971], and $\bar{c}_1 = \sqrt{(8kT)/(\pi\rho\upsilon_1)}$ (mean monomer thermal speed) where υ_1 is the molecular volume of the condensing species. In equation [1], formation of the critical cluster is defined by the nucleation rate $J^\dagger$, while depletion occurs through condensational growth past the critical cluster size, cluster-cluster coagulation, and coagulation with the pre-existing aerosol. In equation [2], cluster production processes include condensational growth and coagulation of smaller clusters while loss mechanisms include condensational growth of the cluster, cluster-cluster coagulation, and coagulation with the pre-existing aerosol.

In order to model the cluster dynamics of observed boundary layer nucleation events, recent developments regarding nucleation rates and growth rates are incorporated into equations [1] and [2]. For atmospheric boundary layer nucleation, studies have shown that the nucleation rate can be modeled as a power-law function of gas-phase sulfuric acid concentration [H_2SO_4]:

[3] $$J^\dagger = K \cdot [H_2SO_4]^P,$$

where K is a measurement campaign-specific pre-factor and the exponent P varies between 1 and 2 [*Weber et al.*, 1996; *Sihto et al.*, 2006; *Riipinen et al.*, 2007; *Kuang et al.*, 2008]. Based on the work of *Kuang et al.* [2008], a value of $P = 2$ and the corresponding pre-factor K are used in this analysis and this power-law expression for nucleation is substituted for $J^\dagger$ in equation [1]. Growth rates based solely on sulfuric acid vapor condensation have been shown to significantly underestimate the measured growth rate [*Weber et al.*, 1997], largely because organic compounds are responsible for up to 90% of the growth [*Mäkelä et al.*, 2001; *O'Dowd et al.*, 2002; *Iida et al.*, 2008b; *Smith et al.*, 2008]. A growth enhancement factor Γ is included in equations [1] and [2] as a multiplier of the condensational growth rate due to sulfuric acid in order to capture the condensation of other vapor-phase species that contribute to the measured particle growth rate. The growth enhancement factor Γ is obtained by dividing the measured growth rate, GR_{MEAS}, by the growth rate assuming free-molecule condensation of sulfuric acid, GR_{SA}, defined by the equation [*Weber et al.*, 1997]:

[4] $$GR_{SA} = \frac{1}{2}\upsilon_1 N_1 \bar{c}_1,$$

where N_1 is the number concentration of gas-phase sulfuric acid, υ_1 is the corresponding sulfuric acid molecular volume (estimated to be 1.7 x 10^{-22} cm^3), and $\bar{c}_1$ is the mean thermal speed of the condensing sulfuric acid (calculated to be 240 ms^{-1}). This yields the following cluster population balance equations:

[5] $$\frac{dN_{k^\dagger}}{dt} = K \cdot {N_1}^2 - \Gamma\beta_{1k^\dagger} N_1 N_{k^\dagger} - N_{k^\dagger}\sum_{i=k^\dagger}^{\infty}\beta_{k^\dagger i} N_i - \frac{\bar{c}_1 A_{Fuchs}}{4}\frac{N_{k^\dagger}}{\sqrt{k^\dagger}}$$

[6] $$\frac{dN_k}{dt} = \Gamma N_1\left(\beta_{1k-1}N_{k-1} - \beta_{1k}N_k\right) - N_k\sum_{i=k^\dagger}^{\infty}\beta_{ki}N_i + \frac{1}{2}\sum_{\substack{i\geq k^\dagger \\ i+j=k}}^{k-k^\dagger}\beta_{ij}N_i N_j - \frac{\bar{c}_1 A_{Fuchs}}{4}\frac{N_k}{\sqrt{k}}.$$

While the growth enhancement factor Γ incorporates the effects of multi-component condensation, equations [5] and [6] are still based on a single-component formulation since Γ is calculated assuming a condensing molecular volume of sulfuric acid; Γ essentially becomes a multiplier of the sulfuric acid concentration It is assumed in this analysis that particles smaller than 3 nm undergo the same enhancement to growth, even though Γ is obtained from aerosol measurements larger than 3 nm and there is evidence that growth rates depend on size [*Kulmala et al.*, 2004a]

With the appropriate dimensional scaling following a method analogous to that of *McMurry and Friedlander* [1979], equations [5] and [6] can be cast into dimensionless form by making the following substitutions:

[7] $$N_k = \bar{N}_k\sqrt{\frac{K\left(N_m\right)^2}{\beta_{11}}}$$

[8] $$t = \tau\sqrt{\frac{1}{K\left(N_m\right)^2\beta_{11}}}$$

[9] $$\beta_{ij} = c_{ij}\beta_{11}$$

[10] $$N_1 = \bar{N}_1 N_m$$

[11] $$L_1 = \frac{\bar{c}_1 A_{Fuchs}}{4\sqrt{K\left(N_m\right)^2 \beta_{11}}},$$

where K is the pre-factor associated with the nucleation exponent $P = 2$, N_m is the peak value of [H_2SO_4] during the nucleation event, and L_1 is a dimensionless parameter characterizing the scavenging rate scaled by the maximum nucleation rate, $K\left(N_m\right)^2$. The variables $\bar{N}_k$, τ, c_{ij}, and $\bar{N}_1$ are the dimensionless analogues of N_k, t, β_{ij}, and N_1, where c_{ij} is defined in *McMurry and Friedlander* [1979]; β_{11} is the monomer-monomer coagulation coefficient and is calculated assuming a molecular volume of sulfuric acid. The dimensionless forms of equations [5] and [6] are then:

[12] $$\frac{d\bar{N}_{k^\dagger}}{d\tau} = \left(\bar{N}_1\right)^2 - \Gamma\sqrt{\frac{\beta_{11}}{K}} c_{1k^\dagger} \bar{N}_1 \bar{N}_{k^\dagger} - \bar{N}_{k^\dagger} \sum_{i=k^\dagger}^{\infty} c_{k^\dagger i} \bar{N}_i - L_1 \frac{\bar{N}_{k^\dagger}}{\sqrt{k^\dagger}}$$

[13] $$\frac{d\bar{N}_k}{d\tau} = \Gamma\sqrt{\frac{\beta_{11}}{K}} \bar{N}_1 \left(c_{1k-1}\bar{N}_{k-1} - c_{1k}\bar{N}_k\right) - \bar{N}_k \sum_{i=k^\dagger}^{\infty} c_{ki}\bar{N}_i + \frac{1}{2}\sum_{\substack{i\geq k^\dagger \\ i+j=k}}^{k-k^\dagger} c_{ij}\bar{N}_i\bar{N}_j - L_1\frac{\bar{N}_k}{\sqrt{k}},$$

where the processes of nucleation, growth, and scavenging are fully decoupled and their effects on the concentration of newly formed particles can be explored. Scaling equations [5] and [6] by the maximum nucleation rate not only reduces the computational load during simulation but also reveals two key dimensionless parameters, L_1 and Γ_1, where Γ_1 defined as:

[14] $$\Gamma_1 = \Gamma\sqrt{\frac{\beta_{11}}{K}},$$

which, respectively, drive the scavenging and growth processes in equations [12] and [13]. In subsequent sections, it will be shown that these two parameters provide a strategy to develop a simple, robust criterion for new particle formation.

4.5 Model Application

Analysis begins by verifying that the set of dimensionless cluster balance equations [12] and [13] can adequately model the measured number concentration N_{3-4}, at the detection limit (3 – 4 nm) during a new particle formation event. For a particular event, measured inputs into the model include the peak sulfuric acid concentration N_m, the corresponding scaled sulfuric acid concentration profile $\bar{N}_1$, the growth enhancement factor Γ, the Fuchs surface area A_{Fuchs}, and the nucleation rate pre-factor K. While the pre-factor K is campaign specific, the growth enhancement factor Γ is event-specific and obtained by dividing the measured growth rate by the growth rate assuming only the condensation of sulfuric acid at concentration N_m. The measured growth rate is estimated either from the time delay between $[H_2SO_4]$ and measured ultrafine particle concentrations (3 - 6 nm) [*Weber et al.*, 1997; *Fiedler et al.*, 2005; *Sihto et al.*, 2006; *Riipinen et al.*, 2007; *Kuang et al.*, 2008] or from size-dependent charge fractions of 3 – 25 nm aerosol [*Iida et al.*, 2008b]. The Fuchs surface area is calculated by integrating over the measured aerosol size distribution according to the method of *McMurry et al.* [2005]. The nucleation rate pre-factor K for each analyzed campaign is obtained from a least-squares fitting of measured $[H_2SO_4]$ with nucleation rates extrapolated from the particle production rate at the detection limit [*Sihto et al.*, 2006; *Riipinen et al.*, 2007; *Kuang et al.*, 2008].

Equations [12] and [13] are then solved with the initial condition of $\bar{N}_k = 0$ ($k \geq k^\dagger$). The output dimensionless number concentrations $\bar{N}_k$ are then dimensionalized according to equation [7] for comparison with concentration measurements of 3 – 4 nm mobility diameter particles. The corresponding range in geometric (mass) diameter is approximately 2.7 – 3.7 nm, based on the work of *Ku and de la Mora* [2009]. This conversion between mobility and geometric diameter is necessary when comparing measured and modeled results. Assuming spherical clusters, the cluster sizes k

corresponding to this geometric size range are calculated according to the relation [*McMurry*, 1980]:

[15] $$D_p = \left(\frac{6k\upsilon_1}{\pi} \right)^{1/3}.$$

The analysis is simplified by focusing only on the peak values of N_{3-4} when comparing measured and modeled number concentrations. Consequently, the input values of Γ and A_{Fuchs} are those corresponding to the measured peak value of N_{3-4}. Sensitivity of the modeled N_{3-4} to the peak sulfuric acid concentration N_m is explored by using a range of concentrations taken 15 minutes before and after the peak sulfuric acid concentration. Uncertainty in the measured peak N_{3-4} is calculated as Poisson error from the finite number of particles detected by the instruments in the corresponding size range. It is expected that the modeled and measured values of peak N_{3-4} would be in qualitative agreement since the nucleation expression that drives the model in equation [5] is parameterized from measured values of N_{3-4}.

After model verification, the competing effects of scavenging and growth on new particle formation were explored by calculating the peak dimensionless particle flux $\bar{J}_3$ (3 nm) as a function of parameters L_1 and Γ_1 calculated from the measured ranges in A_{Fuchs}, N_m, and growth enhancement Γ for each measurement campaign. Each campaign simulation is initialized with input parameters K (campaign specific nucleation rate pre-factor) and N_m (event specific peak [H_2SO_4]); equation [8] is used to map the time resolution associated with measured $\bar{N}_1$ onto the dimensionless time scale τ. Sensitivity of the modeled peak $\bar{J}_3$ to the range in N_m measured during a campaign was investigated and compared with the result using a mean value for the peak [H_2SO_4] measured during a campaign, defined as $\bar{N}_m$. $\bar{J}_3$ is defined as:

[16] $$\bar{J}_3 = \Gamma \sqrt{\frac{\beta_{11}}{K}} c_{1k_3} \bar{N}_1 \bar{N}_{k_3},$$

where k_3 is the cluster size associated with the detection limit at 3 nm (see equation [15]). Critical values of L_1 and Γ_1 at which new particle formation was suppressed were identified from this model analysis and compared with earlier work [*McMurry*, 1983]. A dimensionless parameter was then derived based on these critical L_1 and Γ_1, and was subsequently validated as an NPF criterion against measurements of both NPF events and non-events. In this analysis, non-events are characterized by periods where growth of pre-existing nanoparticles was observed but new particle formation was not.

4.6 Solution Procedure

Following the methods of *Rao and McMurry* [1989] and *Wu and Flagan* [1988], equations [12] and [13] are solved via a discrete-sectional method so as to reduce the computational burden when solving a system of discrete population balance equations. In this study, discrete equations were solved for clusters of size $k \leq 100$ (calculated to overlap with the lower detection limit at 3 nm), and a sectional representation was used for larger clusters [*Gelbard et al.*, 1980]. Numerical diffusion associated with condensation is mitigated by the use of a number conserving expression for condensation fluxes between adjacent sections following *Warren and Seinfeld* [1985]. Accuracy of the discrete-sectional method when applied to equations [12] and [13] was checked by comparing the numerical and analytical results for the time-dependent cluster number concentrations for the special case of a size-independent collision frequency function. Agreement was within 0.01%. Aerosol dynamic simulations were run on a Sun Fire Linux cluster requiring a typical simulation time of 5 seconds per nucleation event. This short computational time enables the efficient exploration of the fairly large parameter space for L_1 and Γ_1 needed to satisfactorily determine the sensitivity of the particle flux to the measured range in scavenging and growth rates associated with a particular field campaign.

4.7 Results and Discussion

Relevant modeled and measured parameters for each campaign and NPF event are listed in Table 4.1: K (campaign-specific nucleation rate pre-factor), $\overline{N}_m$ (campaign average of peak [H_2SO_4]), Γ (event-specific growth enhancement factor), N_m (peak [H_2SO_4] during NPF event), A_{Fuchs} (Fuchs aerosol surface area averaged over duration of NPF event), and J_m (maximum nucleation rate calculated from N_m and equation [3]). The calculated values of the growth enhancement factor Γ span the range from 1 (Atlanta and Hyytiälä) to 25 (Tecamac), emphasizing the multi-component nature of particle growth where the condensation of sulfuric acid accounts only for a fraction of the measured particle growth. The input data into the model span several orders of magnitude (2.4×10^6 cm^{-3} < N_m < 3.6×10^8 cm^{-3}; 7.5 μm^{2}cm^{-3} < A_{Fuchs} < 570 μm^{2}cm^{-3}; 0.43 cm^{-3}s^{-1} < J_m < 6600 cm^{-3}s^{-1}), demonstrating the insights that might be afforded by a dimensionless theory that quantify the relative contributions of nucleation, cluster growth, cluster-cluster coagulation, and cluster scavenging by the pre-existing aerosol.

Table 4.1 Summary of relevant model inputs derived from measured aerosol size distributions and sulfuric acid concentrations acquired during analyzed measurement campaigns. See text for input parameter descriptions and calculations.

Campaign	K ($cm^3 s^{-1}$)	$\overline{N}_m$ (cm^{-3})	Date (mm/dd/yy)	Γ	N_m (cm^{-3})	A_{Fuchs} ($\mu m^2 cm^{-3}$)	J_m ($cm^{-3} s^{-1}$)
MILAGRO	6.3E-13	4.25E+07	03/15/06	14	1.77E+07	217	1.97E+02
			03/16/06	4	8.05E+07	571	4.08E+03
			03/21/06	4	5.48E+07	350	1.89E+03
			03/22/06	7	2.45E+07	361	3.78E+02
			03/23/06	5	1.02E+08	441	6.57E+03
			03/26/06	11	4.70E+07	336	1.39E+03
			03/29/06	5	2.12E+07	207	2.82E+02
			03/30/06	25	1.77E+07	208	1.98E+02
			03/31/06	7	1.73E+07	256	1.88E+02
ANARChE	1.6E-14	2.12E+08	07/31/02	1	3.58E+08	356	2.03E+03
			08/01/02	4	4.97E+07	267	3.91E+01
			08/05/02	1	2.27E+08	266	8.20E+02
Boulder	4.0E-14	2.21E+07	09/02/04	2	2.94E+07	97	3.44E+01
			09/07/04	2	3.16E+07	122	3.98E+01
			09/08/04	5	1.69E+07	80	1.14E+01
			09/09/04	7	1.24E+07	64	6.12E+00
			09/14/04	3	2.03E+07	90	1.64E+01
QUEST II	4.0E-13	6.41E+06	03/20/03	3	3.35E+06	10	4.46E+00
			03/21/03	1	6.34E+06	19	1.60E+01
			03/23/03	3	3.06E+06	22	3.73E+00
			03/25/03	2	4.77E+06	11	9.06E+00
			03/26/03	3	6.91E+06	40	1.90E+01
			03/28/03	2	3.49E+06	8	4.85E+00
			03/31/03	2	3.20E+06	15	4.08E+00
			04/01/03	4	5.02E+06	23	1.00E+01
			04/02/03	3	5.23E+06	36	1.09E+01
			04/03/03	1	1.85E+07	48	1.36E+02
			04/04/03	1	6.41E+06	12	1.64E+01
			04/06/03	2	3.02E+06	12	3.62E+00
			04/07/03	1	1.32E+07	16	6.95E+01
			04/08/03	2	7.16E+06	20	2.04E+01
QUEST IV	5.5E-14	9.31E+06	04/12/05	6	1.60E+07	21	1.41E+01
			04/13/05	2	1.30E+07	27	9.30E+00
			04/16/05	6	3.90E+06	23	8.37E-01
			04/17/05	9	5.80E+06	18	1.85E+00
			04/18/05	1	1.10E+07	23	6.66E+00
			04/24/05	3	5.70E+06	55	1.79E+00
			04/25/05	2	7.70E+06	35	3.26E+00
			04/26/05	1	1.40E+07	50	1.08E+01
			04/27/05	4	1.80E+07	66	1.78E+01
			04/30/05	4	2.80E+06	25	4.31E-01
			05/02/05	1	2.30E+07	41	2.91E+01
			05/08/05	8	4.90E+06	31	1.32E+00
			05/11/05	12	5.20E+06	29	1.49E+00
			05/12/05	1	8.00E+06	23	3.52E+00
			05/13/05	20	3.60E+06	25	7.13E-01
			05/14/05	20	5.70E+06	24	1.79E+00
			05/16/05	4	9.90E+06	50	5.39E+00

The modeled and measured peak values of N_{3-4} for each of the analyzed new particle formation events are compared in Figure 4.1, with vertical bars representing the sensitivity of the modeled peak N_{3-4} to the measured peak sulfuric acid concentration and with horizontal bars representing the measured particle counting uncertainties. The modeled and measured peak values of N_{3-4} are in qualitative agreement with each other spanning three orders of magnitude in number concentration. This agreement between model and measurement is somewhat expected since the power-law nucleation model used to drive the aerosol simulation was parameterized from measured ultrafine particle concentrations. Scatter in the modeled peak N_{3-4} (under and over-estimations of the measured N_{3-4}) can be partially attributed to the use of a single campaign-specific nucleation rate pre-factor K, which has an associated confidence interval [*Sihto et al.*, 2006; *Riipinen et al.*, 2007; *Kuang et al.*, 2008]. Underestimations of the measured peak N_{3-4} by the model can also be due to the contributions of particle source processes not accounted for in the model (e.g. ion-induced nucleation). In spite of this scatter, this model verification result is significant in that the use of a single campaign-specific K value can reasonably model the peak ultrafine particle concentrations observed at a particular location.

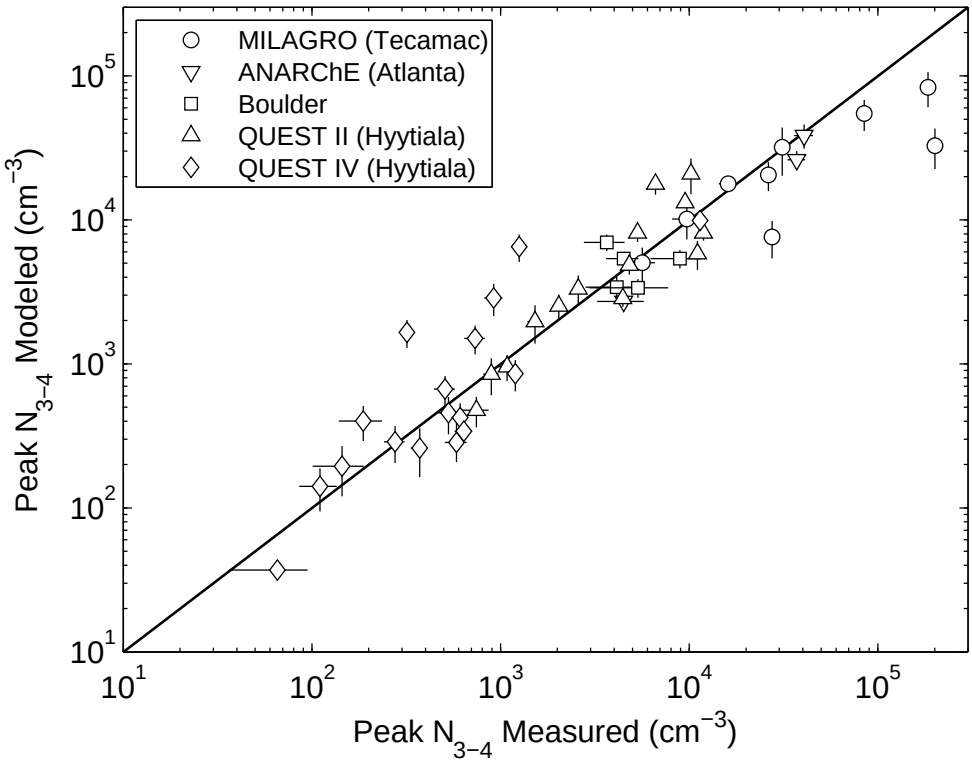

Figure 4.1 Comparison of measured and modeled peak ultrafine particle number concentrations (N_{3-4}) for forty-eight new particle formation events measured during the field campaigns (location) listed in the figure legend. The solid diagonal line represents perfect agreement between model results and measurements. Vertical and horizontal bars represent ranges associated with the maximum sulfuric acid concentration and uncertainties associated with the measured particle counts, respectively.

After model verification, the effect of scavenging and growth on new particle formation was investigated, focusing primarily on the dimensionless particle flux $\bar{J}_3$ as a function of the dimensionless quantities L_1 (scavenging parameter) and Γ_1 (growth parameter). By definition, $\bar{J}_3$ is also equivalent to the dimensional particle production rate J_3 scaled by the maximum dimensional nucleation rate J_m, which is a representative value for the probability that a nucleated particle will grow to the detection limit. As an example, a contour plot of the modeled peak $\bar{J}_3$ as a function of measured ranges in L_1 and Γ_1 is shown in Figure 4.1 for the MILAGRO campaign. This result was obtained using the mean peak sulfuric acid concentration $\bar{N}_m$ to initialize the model, as opposed to calculating a $\bar{J}_3$ contour for each event. Use of campaign-averaged inputs was justified since event-specific inputs yielded results within an absolute error of less than 1 % compared to the results obtained with the campaign-averaged $\bar{N}_m$. Similar model results were observed for the other campaign models. Model inputs for each campaign analysis are listed in Table 4.1.

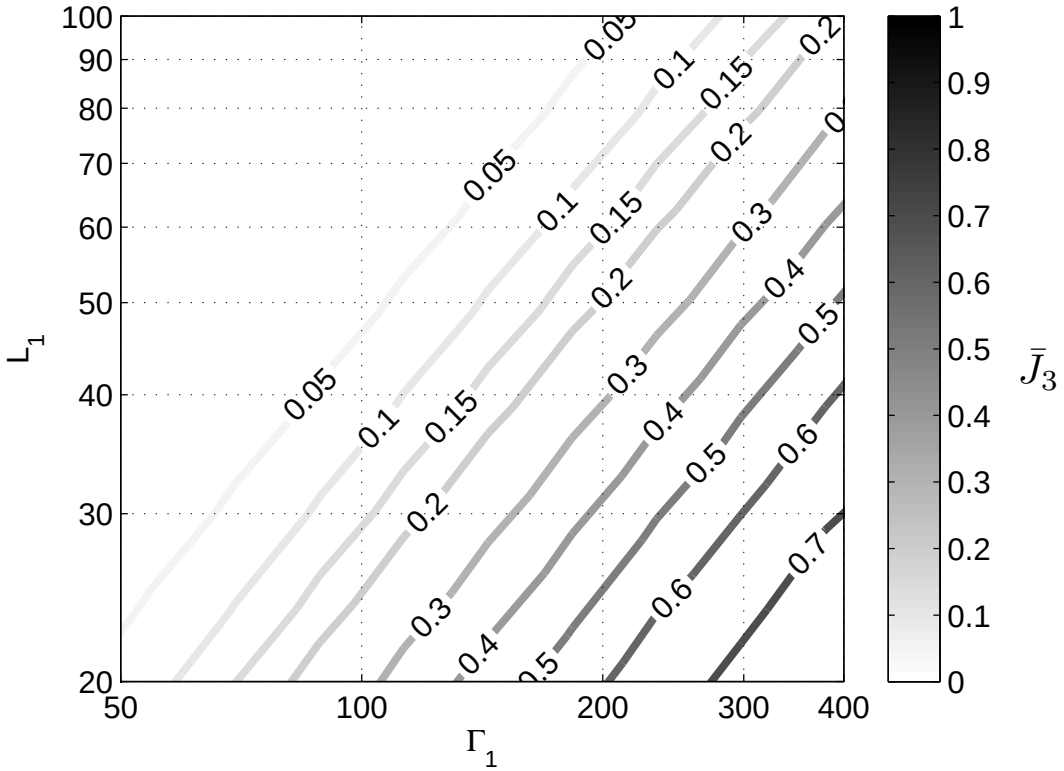

Figure 4.2 Contour plot of modeled peak $\bar{J}_3$ (0.05 – 0.70) as a function of measured ranges in cluster scavenging parameter L_1 and cluster growth parameter Γ_1 for the MILAGRO campaign (Tecamac); $\bar{J}_3$ is equivalent to the survival probability of a nucleated particle growing to the detection limit (3 nm). Model input parameters K and $\bar{N}_m$ are listed in Table 4.1.

Generally, the peak values of $\bar{J}_3$ are seen to increase with increasing Γ_1 at a given value of L_1, and to decrease with increasing L_1 at a given value of Γ_1. These trends are expected as cluster growth and scavenging are source and sink processes, respectively, for ultrafine particles. From Figure 4.2, contours of constant peak $\bar{J}_3$ were identified along with their corresponding pairs of L_1 and Γ_1. The linearity of those contours over the measured ranges in L_1 and Γ_1 suggests a linear log-log relationship between L_1 and Γ_1 for a given value of $\bar{J}_3$: $\log L_1 = M \log \Gamma_1 + B$, where M and B are least-squares fit parameters obtained for each value of $\bar{J}_3$. Least-squares analysis yielded an average M value of 1.03 ± 0.02 (95% confidence) over the range of modeled peak $\bar{J}_3$. With M essentially equal to one, the parameter B is then equal to the ratio L_1 / Γ_1. Since each line of constant $\bar{J}_3$ has a unique intercept B, $\bar{J}_3$ is then seen to depend only on the ratio L_1 / Γ_1. This result suggests that the effect of cluster-cluster coagulation (as both a source and sink process from equations [12] and [13]) contributes negligibly to the evolution of the cluster distribution. Identical behavior was also observed in the model results for the other measurement campaigns. The apparent inconsistency of this result with the observation that substantial coagulation was observed in Atlanta [*Stolzenburg et al.*, 2005] and Mexico City [*Kuang et al.*, 2009b] is resolved by noticing that the contribution of coagulation is a strong function of cluster size. The contribution of cluster-cluster coagulation would be nearly negligible up to the detection limit, yet would be significant at larger sizes. A more detailed analysis of the contribution of cluster-cluster coagulation to the cluster survival probability will be included in a subsequent paper [*Kuang et al.*, 2009d] focusing on intercomparisons of nucleation rate parameterizations [*Weber et al.*, 1997; *Kerminen and Kulmala*, 2002; *Lehtinen et al.*, 2007].

The negligible contribution from cluster-cluster coagulation and the fact that $\bar{J}_3$ depends only on the ratio L_1 / Γ_1 (hereafter renamed L_Γ) indicates that L_Γ is the

controlling parameter that exclusively determines the probability that a nucleated particle grows to the detection limit. From equations [11] and [14], L_Γ is defined as:

$$[17] \qquad L_\Gamma = \frac{\overline{c}_1 A_{Fuchs}}{4\Gamma\beta_{11}N_m},$$

which is essentially a ratio of the scavenging loss rate to the measured growth rate. This new dimensionless parameter is nearly identical in form to the L parameter of *McMurry and Friedlander* [1979]:

$$[18] \qquad L = \frac{\overline{c}_1 A_{Fuchs}}{4\beta_{11}N_1},$$

which was reasonably successful in predicting the occurrence of NPF in the sulfur-rich environment of Atlanta during the ANARChE measurement campaign. There, it was shown that sulfuric acid condensation accounted for nearly all of the growth early in the nucleation event. Under those conditions, the growth enhancement factor Γ is equal to one (see Table 4.1) and the parameters L_Γ and L become functionally equivalent. The advantage of this new parameter L_Γ is that it is derived from a more general form of the aerosol population balance equations that can incorporate the observed range in experimentally parameterized nucleation rates and measured growth rates. It is worth noting that L_Γ is independent of the nucleation rate pre-factor K and nucleation exponent P from equation [3]. Therefore, any nucleation rate expression of the form $J^\dagger = K \cdot [\mathrm{H_2SO_4}]^P$ can be used.

With L_Γ as the controlling parameter, the results from Figure 4.2 can then be recast in a more compact form, where the modeled peak $\overline{J}_3$ is now plotted only as a function of L_Γ for each measurement campaign, as shown in Figure 4.3. The results from each campaign at each value of L_Γ are nearly identical, deviating by less than 5% from each other. This similarity is a remarkable result given that the measured inputs into the model vary over several orders of magnitude across the different campaigns. This location-independent result further indicates that the contribution of cluster-cluster

coagulation up to 3 nm is nearly negligible, even in polluted environments like Tecamac and Atlanta, where significant coagulation might have been expected to occur. From Figure 4.3, $\bar{J}_3$ is seen to asymptotically approach unity in the limit of $L_\Gamma << 1$, which is consistent with the fact that at fast enough growth rates ($\Gamma_1 >> L_1$), all nucleated particles survive to 3 nm and the particle flux at the detection limit approaches the nucleation rate. $\bar{J}_3$ is also seen to decrease with increasing L_Γ ($L_1 >> \Gamma_1$), approaching a survival probability of 0.2% at $L_\Gamma = 1$, where new particle formation is effectively suppressed. New particle formation would then occur only for values of $L_\Gamma < 1$.

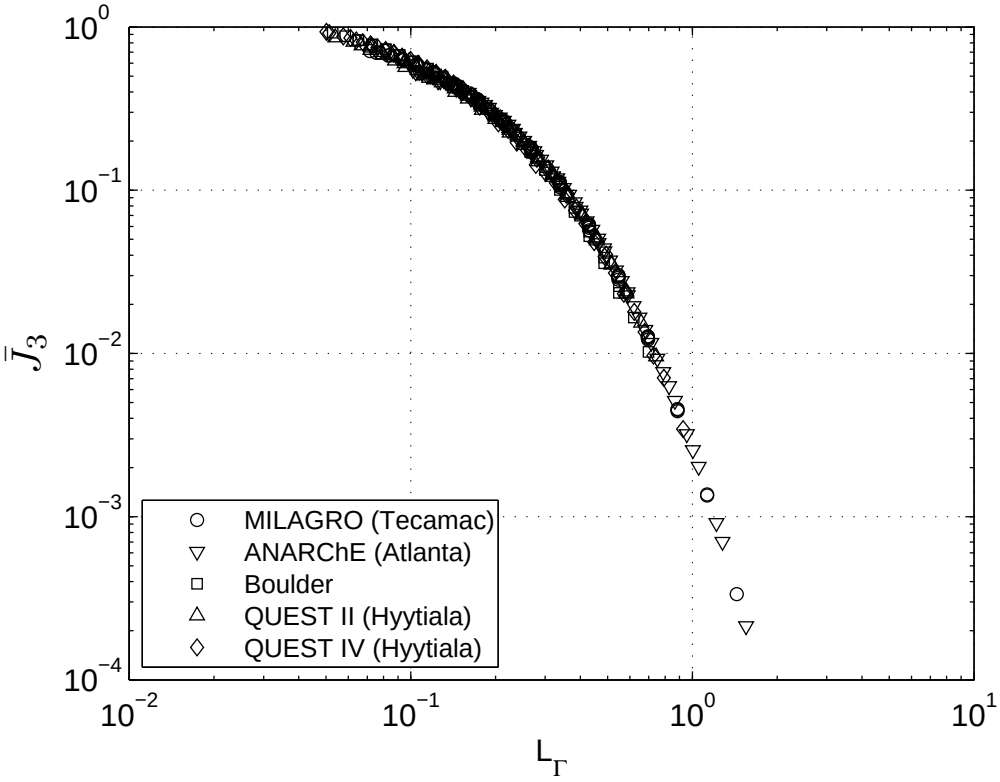

Figure 4.3 Modeled peak $\bar{J}_3$ as a function of L_Γ ($L_\Gamma = L_1 / \Gamma_1$) for the analyzed measurement campaigns (locations), where L_1 is the dimensionless scavenging parameter (equation [11]) and Γ_1 is the dimensionless growth parameter (equation [14]).

This limiting criterion was then tested against measured new particle formation events by calculating L_Γ from the scavenging and growth parameters L_1 and Γ_1 associated with the measured values of peak N_{3-4} for each of the forty-eight new particle formation events that were analyzed. L_Γ values were also calculated for non-events where nanoparticle growth of the pre-existing aerosol was observed but NPF was not: three from the QUEST IV campaign, one from the ANARChE campaign, and one from the Boulder campaign. Only five of these non-events were identified due to the analysis requirement of measurable growth of the pre-existing aerosol mode so that a growth enhancement factor Γ can be obtained. Relevant modeled and measured parameters for these non-events are detailed in Table 4.2, with values of the growth enhancement Γ ranging from 3 – 6, average peak sulfuric acid concentrations ranging from 4 x 10^5 – 4 x 10^6 cm^{-3}, Fuchs surface area ranging from 10 – 300 $\mu m^2 cm^{-3}$, and calculated nucleation rates ranging from 6 x 10^{-3} – 4 x 10^{-1} $cm^{-3}s^{-1}$. The importance of these non-events where pre-existing aerosol growth occurs without NPF has not been discussed in the literature and represents a crucial subset of aerosol measurements against which the $L_\Gamma > 1$ criterion (where NPF is suppressed) can be tested. Without such observations, only half of the NPF criterion can be verified. The results from this analysis are shown as a histogram in Figure 4.4, where L_Γ values associated with NPF and non-events are displayed. All NPF events fell in the range $0.03 < L_\Gamma < 0.4$ corresponding to survival probabilities in the range $15\% < \bar{J}_3 < 90\%$, while non-events fell in the range $1.0 < L_\Gamma < 4.0$ corresponding to survival probabilities much less than l %. L_Γ values associated with NPF all fell below the $L_\Gamma = 1$ boundary, where the model predicts NPF should occur. Conversely, four of the five L_Γ values associated with non-events fell well above the boundary $L_\Gamma = 1$. Though the remaining non-event had a value of $L_\Gamma = 0.96$, the corresponding low predicted particle survival probability to 3 nm ($\bar{J}_3 \sim 0.2\%$) reasonably suggests NPF suppression. An empirically determined value of $L_\Gamma = 0.7$

appears to separate all events from all non-events. This universal behavior across different measurement campaigns indicates that L_Γ is a robust parameter that can be used to predict the frequency and strength of NPF events.

Table 4.2 Summary of relevant model inputs derived from measured aerosol size distributions and [H_2SO_4] for non-events, characterized by the growth of pre-existing nanoparticles without new particle formation. See text for input parameter descriptions and calculations.

Campaign	K (cm^3s^{-1})	Date (mm/dd/yy)	Γ	N_m (cm^{-3})	A_{Fuchs} (μm^2cm^{-3})	J_m ($cm^{-3}s^{-1}$)
ANARChE	1.6E-14	08/07/02	6	2.01E+06	303	6.40E-02
Boulder	4.0E-14	06/11/04	4	3.91E+05	39	6.07E-03
QUEST IV	5.5E-14	04/28/05	3	3.94E+06	103	8.73E-01
		05/01/05	3	8.37E+05	33	3.94E-02
		05/15/05	3	7.03E+05	11	2.78E-02

From Figure 4.4, L_Γ values associated with 65% of the NPF events span the relatively narrow range $0.23 < L_\Gamma < 0.42$, corresponding to a nucleated particle survival probability to 3 nm of between 10 and 30%. This narrow range suggests a self-regulating process in the boundary layer where high growth rates for sub 3 nm particles, which increase survival probability, are often accompanied by a large pre-existing aerosol surface area, which depletes the newly formed particle population and decreases the survival probability, as observed in Tecamac and vice versa as observed in Hyytiälä. Analogous self-regulating behavior for the production of CCN (~100 nm) from newly formed particles was observed in simulation results [*Spracklen et al.*, 2008] and constrained models [*Kuang et al.*, 2009b].

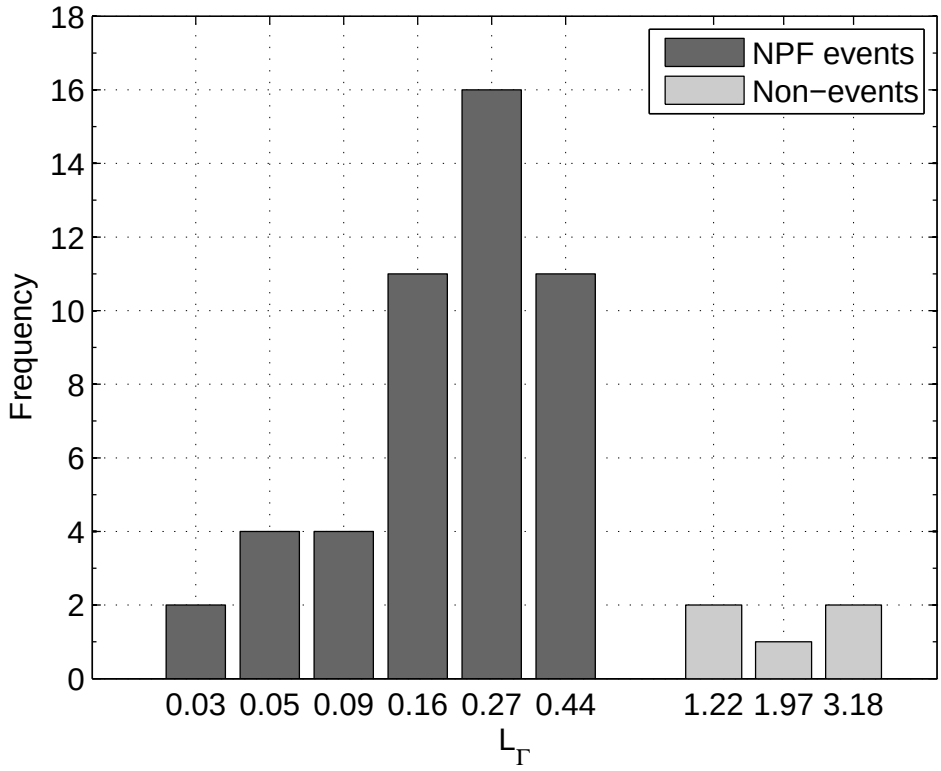

Figure 4.4 Histogram of measured L_Γ values associated with forty-eight NPF events and five non-events, where $L_\Gamma = L_1 / \Gamma_1$: L_1 is the dimensionless scavenging parameter (equation [11]) and Γ_1 is the dimensionless growth parameter (equation [14]).

To accurately predict NPF, it is imperative to incorporate the measured enhancement to the particle growth rate Γ, since L_Γ scales with $1/\Gamma$. Assuming no enhancement to particle growth ($\Gamma = 1$) compared with a typical enhancement of $\Gamma = 10$ leads to an overestimation of L_Γ by a factor of 10. For NPF events with L_Γ values greater than 0.1 (>80% of analyzed NPF events), assuming that sulfuric acid accounts for all the growth ($\Gamma = 1$) yields L_Γ values that are greater than 1, where NPF is not predicted to occur. Therefore, assuming that sulfuric acid accounts for the all the measured growth leads to a dramatic underestimation of both the frequency of NPF events and the associated particle production rates.

4.8 Conclusions

A dimensionless cluster population balance model was developed to analyze new particle formation from a nucleating system growing by condensation and coagulation in the presence of a pre-existing aerosol. The model incorporates recent developments in boundary layer nucleation rates parameterized as power-law functions of gas-phase sulfuric acid and recent work in nanoparticle growth rates. Model results were validated against forty-eight measured new particle formation events, yielding good agreement between modeled and measured ultrafine particle number concentrations. Model analysis indicated that nucleated particle survival probability depends only on a simple dimensionless parameter L_Γ. L_Γ was shown to determine exclusively whether or not new particle formation could occur on a particular day and was validated against measured NPF events and non-events characterized by measurable growth of pre-existing nanoparticles without NPF. New particle formation was shown to occur only at values of $L_\Gamma < 1$, and was suppressed for values of $L_\Gamma > 1$, with an empirically determined boundary at $L_\Gamma = 0.7$. Measured values of L_Γ and corresponding survival probabilities fell in a relatively narrow range, suggesting a self-regulating process in the boundary layer where enhancements from high growth rates are mitigated by depletions from a substantial pre-existing aerosol surface area, and vice versa.

4.9 Acknowledgements

Financial support from the National Science Foundation (DGE-0114372 and ATM-050067), the Department of Energy (DE-FG02-05ER63997), and the Guggenheim Foundation (PHM), and computational resources from the Minnesota Supercomputing Institute are gratefully acknowledged.

Chapter 5 : The Production of Cloud Condensation Nuclei from New Particle Formation Events

5.1 Synopsis

An analytical expression has been developed that accurately models the population dynamics of an aerosol growing from the detection limit (3 nm) to CCN size (100 nm), quantifying the contributions of size and time-dependent source and sink terms such as coagulation of smaller particles and scavenging by the pre-existing aerosol. These model inputs were calculated from measured aerosol size distributions and growth rates acquired during intensive measurement campaigns in Boulder, CO, Atlanta, GA, and Tecamac, Mexico. Twenty CCN formation events from these campaigns were used to test the validity of this model. Measured growth rates ranged from 3 – 22 nm/h. The modeled and measured CCN production probabilities agreed well with each other, ranging from 1 – 20%. The pre-existing CCN number concentration increased on average by a factor of 3.8 as a result of new particle formation.

5.2 Introduction

Atmospheric aerosols exert a significant impact on global climate by affecting the earth's radiation balance directly through the scattering and absorption of solar radiation and indirectly through their role as cloud condensation nuclei (CCN) [*Albrecht*, 1989; *Charlson et al.*, 1992]. This indirect effect of aerosols contributes the largest uncertainty to estimates of global radiative forcing [*IPCC*, 2007]. Accurate assessment of the relationship between CCN and forcing in global climate models requires understanding processes that determine CCN concentrations. Several field campaigns [*Kerminen et al.*, 2005; *Laaksonen et al.*, 2005] have implicated newly formed particles from atmospheric nucleation events as an important source of CCN.

New particle formation in the atmospheric boundary layer and subsequent growth to 100 nm, a representative CCN-active diameter at 0.2% supersaturation (typical of

stratocumulus clouds) [*Seinfeld and Pandis*, 1998], has been observed in the continental troposphere [*Stolzenburg et al.*, 2005]. As these newly formed particles grow from 3 nm to 100 nm, they undergo processes that enhance and deplete the growing population, such as coagulation production and scavenging by the pre-existing aerosol, respectively [*Stolzenburg et al.*, 2005]. Reducing the uncertainty in the CCN number population due to the growth of newly formed particles depends on accurately accounting for these sources and sinks, which depend on particle size and growth rate.

Recent modeling efforts incorporating aerosol microphysics have studied the effect of boundary layer new particle formation on CCN concentrations using an off-line chemical transport model [*Spracklen et al.*, 2008] and a particle growth model [*Pierce and Adams*, 2007]. The model inputs included parameterized new particle formation rates [*Spracklen et al.*, 2008] and simulated size distributions and growth rates [*Pierce and Adams*, 2007]. In the present work, a model for CCN formation was developed based on measured new particle formation events, yielding an analytical expression for the number distribution of nucleated particles that grew to 100 nm based on measured aerosol size distributions and growth rates. The model was applied to twenty CCN formation events measured in three North American locations: Boulder, CO [*Iida et al.*, 2006]; Atlanta, GA [*McMurry et al.*, 2005]; and Tecamac, Mexico [*Iida et al.*, 2008b]. The results of these calculations are compared with observations. Enhancements to pre-existing CCN number concentrations due to new particle formation were also calculated.

5.3 Measurements and Techniques

Data from the three measurement campaigns were acquired by researchers from the University of Minnesota and the National Center for Atmospheric Research. Detailed descriptions of the physical and meteorological conditions at each site as well as a summary of pertinent aerosol instrumentation can be found in *Kuang et al.* [2008]. This analysis utilized measurements of aerosol size distributions.

For a measured CCN formation event, the size distribution of 100 nm particles was modeled by following a population of newly formed particles as they grew from 3 to

100 nm, and accounting for how various aerosol sources and sinks added to and depleted the population during growth. An example of such an event is shown in Figure 5.1, where new particle production occurred just before 12:00 on 09/02/08 and was followed by nearly continuous particle growth approaching 100 nm in diameter over the next 33 hours. It is the goal of this work to develop a simple analytical expression that accurately models the size distribution of the nucleated particles as they grow to 100 nm using measured size distributions and growth rates to account for sources and sinks.

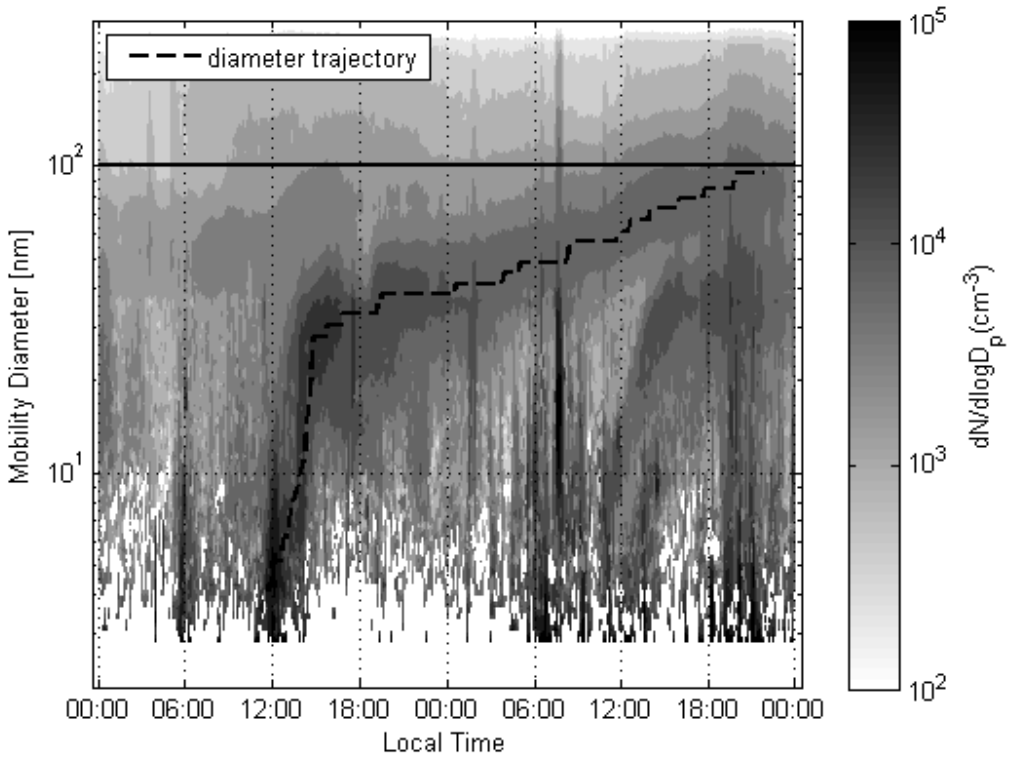

Figure 5.1 Contour plot of aerosol size distribution versus mobility diameter and local time for a new particle formation event resulting in formation of CCN (assumed to be 100 nm – solid black line) measured at Boulder, CO over the period 09/02/08 – 09/03/08. Included is a representative diameter trajectory of a subset of the growing aerosol population.

The dynamics of an aerosol population growing by condensation and coagulation are described by the particle size distribution *n* evolving through size and time according to the general dynamic equation [*Seinfeld and Pandis*, 1998]:

$$\frac{\partial}{\partial t}\left[n\left(D_p,t\right)\right] = -\frac{\partial}{\partial D_p}\left[GR\left(D_p,t\right)\cdot n\left(D_p,t\right)\right]$$
$$+ D_p{}^2\cdot\int_0^{D_p/2^{1/3}} K\left(\psi,\tilde{D}_p\right)\cdot n\left(\psi,t\right)\cdot n\left(\tilde{D}_p,t\right)\cdot\frac{d\tilde{D}_p}{\psi^2}, \qquad [1]$$
$$- n\left(D_p,t\right)\cdot\int_0^{\infty} K\left(D_p,\tilde{D}_p\right)\cdot n\left(\tilde{D}_p,t\right)\cdot d\tilde{D}_p$$

where $GR\left(D_p,t\right)$ is the particle diameter growth rate, $\psi = \left(D_p{}^3 - \tilde{D}_p{}^3\right)^{1/3}$, and $K\left(\psi,D_p\right)$ is the coagulation coefficient for particles of diameter ψ and D_p. There are well-established analytical [*Ramabhadran et al.*, 1976] and numerical [*Gelbard and Seinfeld*, 1978] methods of solving equation [1] and obtaining *n*. In this work however, equation (1) is solved only for a subset of the aerosol population $n^\dagger$ that follows a diameter trajectory $D_p^\dagger$, defined as the path through diameter space that a growing particle follows according to the measured growth rate, a representative example of which is shown in Figure 5.1. After expanding the growth term in equation [1] and grouping similar terms, equation [1] is reduced to an ordinary differential equation along $D_p^\dagger$ by the method of characteristics:

$$\frac{d}{dt}\left[n^\dagger(t)\right] = D_p^{\dagger 2}\cdot\int_0^{D_p^\dagger/2^{1/3}} K\left(\psi,\tilde{D}_p\right)\cdot n\left(\psi,t\right)\cdot n\left(\tilde{D}_p,t\right)\cdot\frac{d\tilde{D}_p}{\psi^2}$$
$$- n^\dagger(t)\cdot\left\{\int_0^{\infty} K\left(D_p^\dagger,\tilde{D}_p\right)\cdot n\left(\tilde{D}_p,t\right)\cdot d\tilde{D}_p + \frac{d}{dD_p}\left[GR\left(D_p^\dagger\right)\right]\right\}, \qquad [2]$$

which defines the size and time-dependent sources and sinks of $n^\dagger$ as it grows along the measured diameter trajectory $D_p^\dagger$. On the RHS of equation [2], the first term defines contributions to $n^\dagger$ from coagulation of smaller particles that yield a larger particle of

size $D_p^\dagger$, the second term defines losses due to scavenging by the pre-existing aerosol, and the third term defines losses due to size-dependent growth. For the CCN formation events analyzed, the loss from self-coagulation of $n^\dagger$ was calculated to be negligible. Equation [2] is then integrated along $D_p^\dagger$, yielding an analytical expression for $n^\dagger$:

$$[3] \qquad n^\dagger(t) = \exp\left[-\tau_{loss}(t)\right] \cdot \left\{ n_3 + \int_0^t F_{coag}(t) \cdot \exp\left[\tau_{loss}(t)\right] \cdot dt \right\}$$

$$[4] \qquad \tau_{loss}(t) = \int_0^t \left\{ \int_0^\infty K\left(D_p^\dagger, \tilde{D}_p\right) \cdot n\left(\tilde{D}_p, t\right) \cdot d\tilde{D}_p + \frac{d}{dD_p}\left[GR\left(D_p^\dagger\right)\right] \right\} \cdot dt$$

$$[5] \qquad F_{coag}(t) = D_p^{\dagger 2} \cdot \int_0^{D_p^\dagger / 2^{1/3}} K\left(\psi, \tilde{D}_p\right) \cdot n(\psi, t) \cdot n\left(\tilde{D}_p, t\right) \cdot \frac{d\tilde{D}_p}{\psi^2},$$

where n_3 is the value of the measured distribution function at the start of growth (nominally 3 nm), τ_{loss} is a sink term characterizing the various loss mechanisms that deplete $n^\dagger$, and F_{coag} is a source term representing all collisions of smaller particles that yield larger particles with sizes equal to the diameter trajectory $D_p^\dagger$. To determine the size distribution for 100 nm particles ($n^\dagger = n_{100}$), equation [3] is evaluated at a time *t* along the diameter trajectory where $D_p^\dagger$ = 100 nm. This approach is an extension of earlier methods [*Weber et al.*, 1997; *McMurry et al.*, 2005] where particle growth from 3 to 100 nm is now examined and where time and size-dependent particle sources, sinks, and growth rates are now included. This is particularly important during periods of substantial new particle formation, where the aerosol number concentration and surface area (from which sources and sinks are calculated) can change significantly. In this analysis, the percent contributions to the population of particles (D_p > 100 nm) from coagulation of the pre-existing aerosol with $n^\dagger$ and self-coagulation of $n^\dagger$ are relatively small (< 5%) compared to the contribution from growth of $n^\dagger$ through 100 nm.

A natural product of this analysis that can be obtained from equation [3] is the CCN production probability defined as n_{100} / n_3, which is the ratio of the size distribution of 100 nm particles at the end of the diameter trajectory to the size distribution of 3 nm particles at the beginning of the trajectory. For the case of constant particle growth rate, the value of n_{100} / n_3 is equivalent to the ratio of particle production rates at 100 and 3 nm. For CCN formation events where there is negligible enhancement from coagulation of smaller particles, n_{100} / n_3 represents the survival probability of a population of 3 nm particles growing to 100 nm. For this case, the aerosol population $n^{\dagger}$ only undergoes loss as it grows and therefore only contains particles that were originally present at 3 nm. The ratio n_{100} / n_3 is then only a function of τ_{loss}, a dimensionless particle lifetime that captures the competing interactions between loss and growth as the particles approach 100 nm. For CCN formation events characterized by a fast growth rate, there is a relatively shorter time over which the various loss mechanisms can act, resulting in a relatively larger CCN population. This dimensionless lifetime is conceptually similar to the L parameter in *McMurry et al.* [2005], which accounts for the survival probability of clusters growing from 1 to 3 nm while being depleted by coagulation.

A related quantity of interest is the enhancement to the pre-existing number concentration of CCN-active particles N_{100} (D_p > 100 nm) due to new particle formation, defined as the ratio of the peak N_{100} after new particle formation to the initial, pre-existing N_{100}. Enhancements to N_{100} due to condensation of the pre-existing aerosol, condensation of the growing aerosol, and coagulation of smaller particles and depletions to N_{100} due to self-coagulation are determined by solving equation [1] for N_{100} from the start of new particle formation to when the peak value of N_{100} occurs.

Analysis of a given CCN formation event begins by identifying the initial distribution of the growing aerosol population, which was defined in this study as the peak value of the distribution function of 3 – 6 nm particles during a new particle formation event. The diameter width for this initial distribution was small enough to be

considered newly formed but large enough to achieve good particle counting statistics. The diameter trajectory $D_p^{\dagger}$ of this initial population was then defined by the time evolution of the peak of the measured distribution which, to a first approximation, ensures that the same aerosol population is being modeled during growth. The diameter trajectory defines both the size and time-dependent sinks and sources (τ_{loss} and F_{coag}) that deplete and increase the particle population as it grows to 100 nm, as well as the length of time over which the effects of these sinks and sources are integrated. Model sensitivity to the initial condition n_3 was explored by starting individual trajectory calculations over an interval of 15 minutes before and after the peak value of n_3 during the period of new particle production.

5.4 Results and Discussion

The diameter trajectory $D_p^{\dagger}$ is a critical quantity in this analysis, defining the various sink and source terms that control the dynamics of $n^{\dagger}$ as it grows. A distinguishing feature of this model is the use of particle trajectories determined by measured growth rates (3 – 22 nm/h for the three measurement campaigns included in this analysis). Previous studies modeling CCN formation from aerosol processes [*Pierce and Adams*, 2007] assume sulfuric acid vapor as the dominant condensing species contributing to particle growth and use either measured or modeled sulfuric acid vapor concentration to estimate growth rates. Studies have shown that growth rates due solely to measured sulfuric acid vapor condensation can significantly underestimate the measured growth rate [*Weber et al.*, 1997], largely because organic compounds are responsible for up to 90% of the growth [*Mäkelä et al.*, 2001; *O'Dowd et al.*, 2002; *Iida et al.*, 2008b; *Smith et al.*, 2008]. This underestimation of the growth rate can lead to overestimation of the particle lifetime and corresponding losses as the population grows up to 100 nm.

The modeled and measured values of n_{100} / n_3 range from 1 – 20% across the three measurement campaigns and are plotted versus the calculated loss parameter τ_{loss} in Figure 5.2. These measured and modeled production probabilities are several orders of magnitude larger than the corresponding probabilities calculated by *Pierce and Adams* [2007]. Their models were initialized with simulated stationary pre-existing aerosol size distributions and particle growth rates based on sulfuric acid condensation, rates which are an order of magnitude smaller than the measured growth rates used in this analysis. The results in Figure 5.2 apply only to those events where growth was strong enough for newly formed particles to reach 100 nm, which represent half of the observed new particle formation events from the three measurement campaigns. For the remaining events, the growing particles did not reach 100 nm in size. Also included on the plot is the model prediction of n_{100} / n_3 versus τ_{loss} assuming no coagulation enhancement (loss-only solution, F_{coag} = 0).

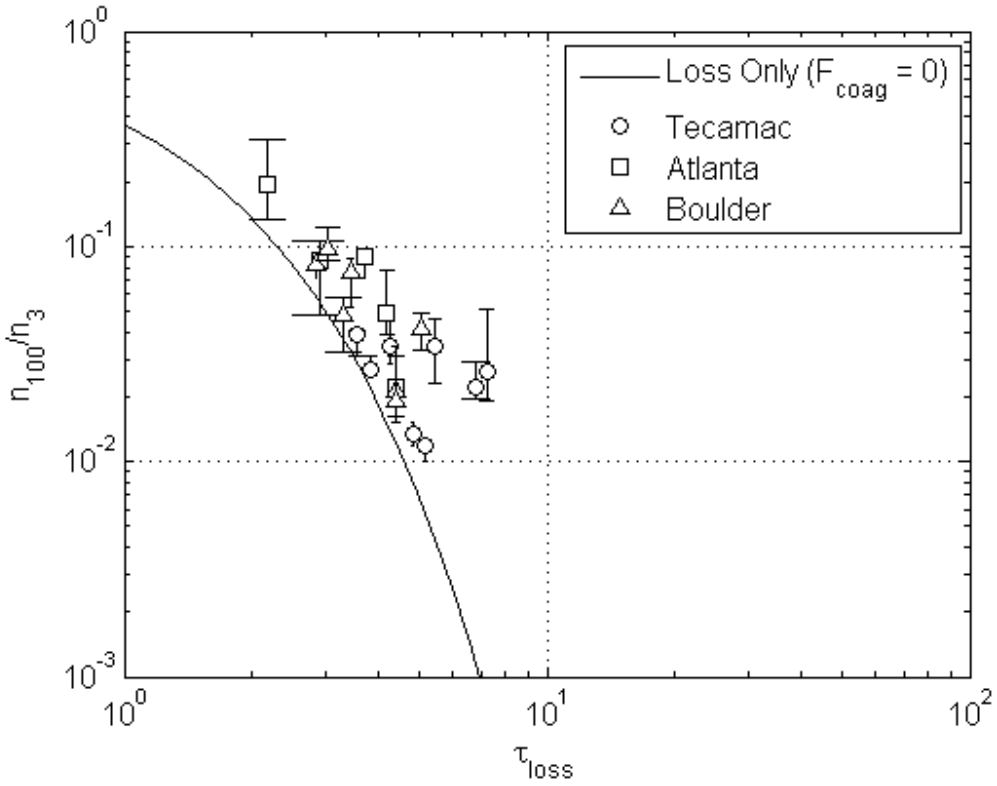

Figure 5.2 Measured n_{100} / n_3 (symbol) versus the dimensionless loss parameter τ_{loss} obtained from the listed measurement campaigns, bounded by modeled n_{100} / n_3 (vertical bar) and τ_{loss} (horizontal bar), representing 95% confidence limits. The loss-only solution ($F_{coag} = 0$) is also shown for reference.

For those events where the modeled and measured n_{100} / n_3 lie on or close to the loss-only solution, n_{100} / n_3 approximates the survival probability of newly formed 3 nm particles growing to 100 nm. For these events, approximately 1 – 10% of newly formed particles survive to 100 nm. It is primarily the competition between loss and growth rates contained within τ_{loss} that controls the CCN survival probability. For those events where the modeled and measured n_{100} / n_3 deviate significantly (at least an order of magnitude) from the loss-only solution, $n^{\dagger}$ contains both particles from the initial growing population and particles formed by coagulation of particles beneath the growing mode. These events were observed in Tecamac and Atlanta and were characterized by sustained periods of particle production with large total aerosol number concentrations (> 1 x 10^5 cm^{-3}).

The pre-existing number concentrations of CCN-active particles (N_{100}) are increased due to new particle formation by factors of 1.6 – 9.1 with a mean value of 3.8, which are plotted as a histogram of enhancement factors in Figure 5.3. The mean and upper range of these enhancement factors are comparable to the maximum CCN concentration enhancements reported by *Spracklen et al.* [2008] when modeled growth rates were increased to match observed growth rates, emphasizing the importance of using measured growth rates when simulating CCN populations. The percent contributions of self-coagulation loss, coagulation production, pre-existing aerosol condensation, and growing aerosol condensation to the N_{100} enhancements are shown in Figure 5.4 along with the pre-existing and peak values of N_{100}, averaged over each measurement campaign. Condensation of the growing aerosol past 100 nm contributes more than 80% to the observed N_{100} enhancement in Tecamac and Atlanta, while the contribution of pre-existing aerosol condensation is comparable to that of the growing aerosol in Boulder. Because of the slower growth rates in Boulder, the contribution from pre-existing aerosol condensation is integrated over a longer time interval, yielding a larger contribution relative to the condensation of the growing aerosol.

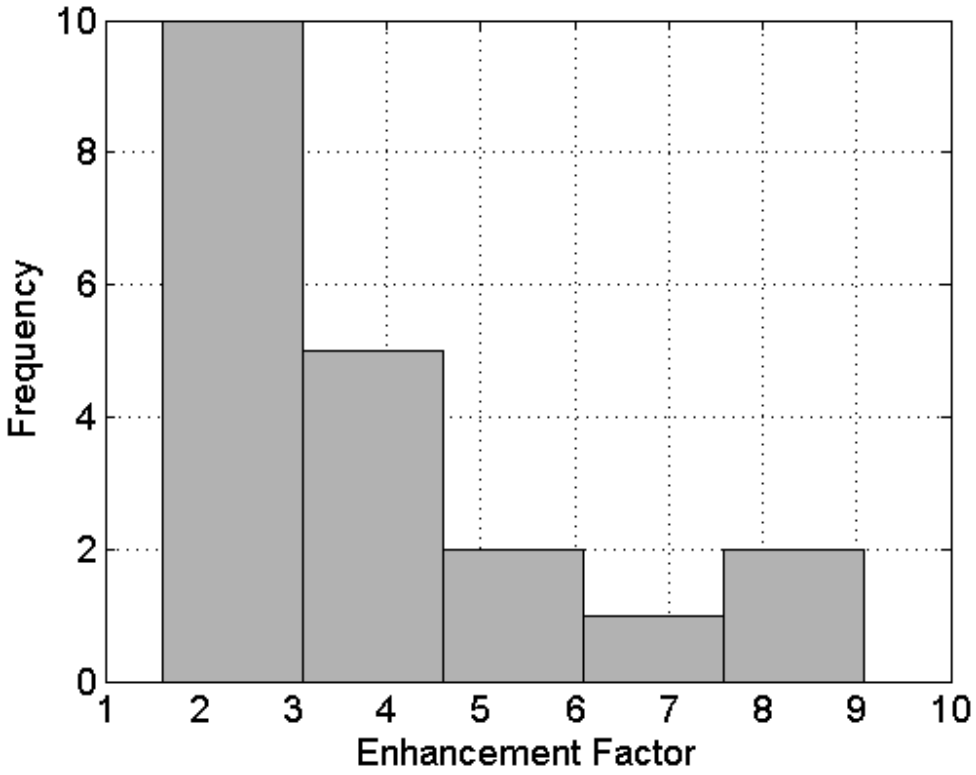

Figure 5.3 Histogram of enhancement factors for CCN number concentration N_{100} (cm^{-3}) (D_p > 100 nm) due to new particle formation.

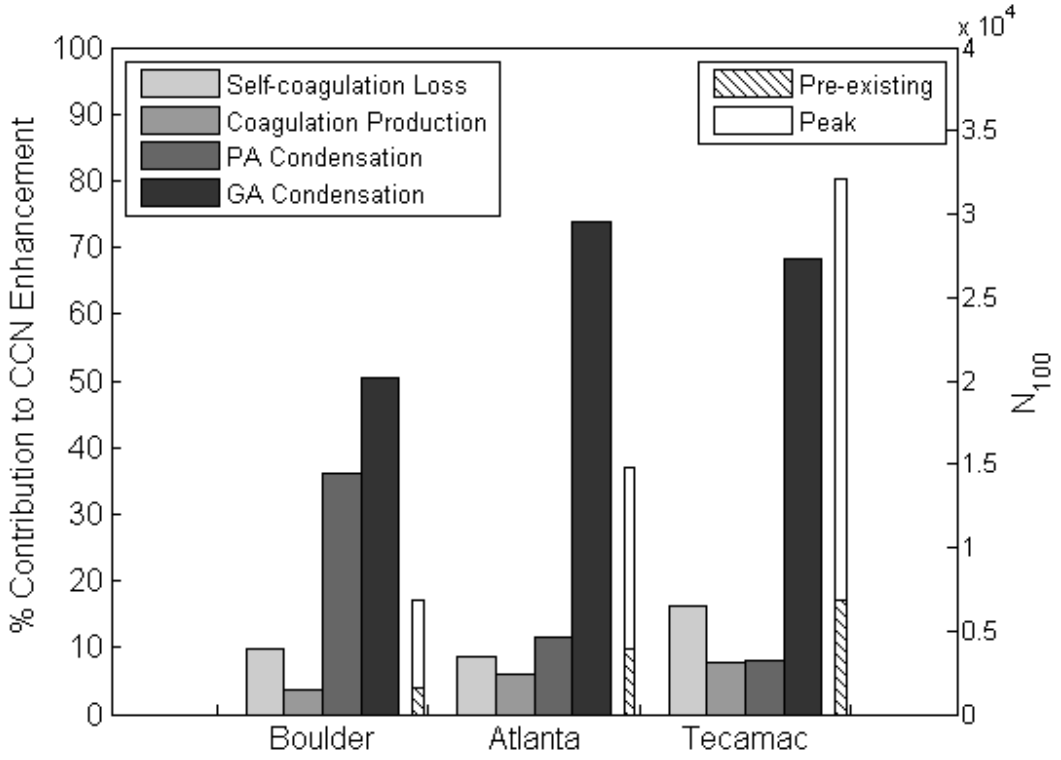

Figure 5.4 Percent contributions of self-coagulation loss, coagulation production, PA (pre-existing aerosol) condensation, and GA (growing aerosol) condensation to the enhancement in N_{100}, along with the pre-existing and peak values of N_{100}, averaged over each measurement campaign.

The relatively narrow distributions of CCN survival probabilities (1 – 10%) and CCN enhancement factors (> 50% are between 2 – 3) suggest a self-regulating process in the atmosphere, as was observed by Spracklen et al. [2008]. High particle growth rates tend to be mitigated by rapid depletion due to a correspondingly large pre-existing aerosol surface area as in Tecamac, and vice versa as in Boulder.

5.5 Conclusions

An analytical model for CCN production was developed by simulating the growth of a subset of an aerosol population from 3 to 100 nm and accounting for various source and sink processes constrained by measured size distributions and growth rates. Modeled production probabilities agreed well with measured values, ranging from 1 – 20%. The analytical model enabled a quantitative comparison of loss processes (scavenging and size-dependent condensation) with coagulation production, which was shown to be significant in Tecamac and Atlanta. For events with relatively little coagulation production, survival probabilities ranged from 1 – 10%. New particle formation increased pre-existing CCN number concentrations by factors of 1.6 – 9.1 with a mean enhancement of 3.8. These enhancements were dominated by contributions from condensation of the growing aerosol.

5.6 Acknowledgements

This work was supported by the NSF IGERT Program (Award No. DGE-0114372), NSF Award No. ATM-050067 and DOE Grant DE-FG02-05ER63997.

Chapter 6 : Future Work

Recent developments in instrumentation have allowed us to approach the measurement of the complete size spectrum of vapors, clusters, and nanoparticles during a nucleation event. A newly developed cluster mass spectrometer [*Zhao et al.*, 2009] has enabled measurements of the sulfuric acid monomer, trimer, and tetramer, while two prototype condensation particle counters [*Iida et al.*, 2008a; *Kuang et al.*, 2009a] have lowered the particle size detection limit down to 1.5 nm mobility diameter (nominally equal to 1.2 nm geometric diameter). These important measurements, combined with the cluster population model developed in *Kuang et al.* [2009e], will enable important estimates of cluster kinetic and thermodynamic properties. Based on these developments, I have identified three areas of future and continuing research: [1] constraining the cluster population balance model [*Kuang et al.*, 2009e] with measurements in order to extract important cluster properties; [2] using the cluster population balance model to develop more accurate nucleation rate parameterization methods, and then applying those methods to combined data sets acquired by researches from the University of Minnesota, the National Center for Atmospheric Research, and the University of Helsinki; and [3] the development and characterization of a condensation particle counter that extends the detection limit towards 1 nm mobility diameter, using oleic acid as a new working fluid.

6.1 Extraction of Cluster Properties with Constrained Cluster Model

6.1.1 Distinguishing Non-Accommodation from Evaporation

The cluster population balance model developed in *Kuang et al.* [2009e] and applied to cluster concentration measurements in *Kuang et al.* [2009c] can, in principle, be used to infer cluster kinetic and thermodynamic properties by constraining the model with measured size distributions of clusters. In certain limiting cases, the model can also be used to help distinguish between processes that have the same qualitative effect on the cluster population, but different physical foundations.

Energy non-accommodation would have the same qualitative effect on cluster concentrations as evaporation, since both processes would lead to reduced net rates of cluster formation. While both processes could in fact be occurring simultaneously, it would be helpful to identify limiting criteria with which we might examine the relative contributions of dimer non-accommodation and dimer evaporation. This can be accomplished by adding the effect of evaporation to the dimensionless dimer population balance equation [*Kuang et al.*, 2009e]:

$$[1] \qquad \frac{d\overline{N}_{k^\dagger}}{d\tau} = \alpha\left(\overline{N}_1\right)^2 - \Gamma c_{1k^\dagger}\overline{N}_1\overline{N}_{k^\dagger} - \overline{N}_{k^\dagger}\sum_{i=k^\dagger}^{\infty} c_{k^\dagger i}\overline{N}_i - \overline{E}_{k^\dagger}\overline{N}_{k^\dagger},$$

where $\overline{N}_k$ is the dimensionless concentration for a cluster of size *k*, c_{ij} is the dimensionless coagulation coefficient between clusters of size i and j, α is an empirical accommodation coefficient, and Γ is a growth enhancement factor calculated as the ratio of the measured growth rate to the growth rate due solely to sulfuric acid condensation. For a single-component aerosol system (only sulfuric acid), $\Gamma = 1$. $\overline{E}_{k^\dagger}$ is a new, dimensionless evaporation parameter, defined as:

$$[2] \qquad \overline{E}_{k^\dagger} = \frac{E_{k^\dagger}}{\beta_{11} N_m},$$

where the quantity $E_{k^\dagger}$ is the dimensional dimer evaporation rate constant, β_{11} is the dimensional monomer-monomer coagulation coefficient, and N_m is the dimensional peak monomer (sulfuric acid) concentration.

This dimensionless parameter $\overline{E}_{k^\dagger}$ provides a means of distinguishing the effects of non-accommodation and evaporation since it is scaled with respect to the maximum sulfuric acid concentration, N_m. This concentration, in principle, can be varied in a controlled manner in the photochemical aerosol generation chamber currently being constructed in the Particle Technology Lab at the University of Minnesota. If dimensionless cluster concentrations (scaled from measured cluster concentrations) are seen to be insensitive to changes in N_m, then dimer evaporation would be seen to

contribute negligibly to cluster dynamics. However, if the dimensionless cluster concentrations change substantially with changes in N_m, then dimer evaporation is likely playing a significant role in reducing net cluster formation rates.

6.1.2 Obtaining Cluster Kinetic and Thermodynamic Parameters

With time-dependent cluster size distributions, one can obtain estimates of the cluster growth rate, and, in certain limiting cases, also obtain the dimer accommodation coefficient or the dimer evaporation rate constant.

Cluster growth rates are important not only because they help determine the probability of cluster survival to CCN-active size [*McMurry et al.*, 2005; *Lehtinen et al.*, 2007], but because they can also give a crude estimate of composition by comparison with growth rates assuming only contributions from sulfuric acid condensation [*Iida et al.*, 2008b; *Smith et al.*, 2008]. Cluster growth rates can be estimated through several methods: [1] tracking the size and time evolution of the peak in the cluster size distribution, a method analogous to that of *Stolzenburg et al.* [2005] who calculated growth rates for nucleation mode particles; or [2] calculating the time required for a cluster to grow to a larger size by determining the time delay between the concentration profiles of the initial and final sizes [*Weber et al.*, 1997; *Fiedler et al.*, 2005].

Two limiting cases regarding the net dimer formation rate can be explored to obtain either the dimer accommodation coefficient or the dimer evaporation rate. In the case where the reduced dimer formation rates can be attributed entirely to the effects of energy non-accommodation, the dimensionless dimer population balance can be written as:

$$[3] \qquad \frac{d\bar{N}_{k^\dagger}}{d\tau} = \alpha\left(\bar{N}_1\right)^2 - \Gamma c_{1k^\dagger}\bar{N}_1\bar{N}_{k^\dagger} - \bar{N}_{k^\dagger}\sum_{i=k^\dagger}^{\infty} c_{k^\dagger i}\bar{N}_i \,.$$

With measured cluster concentrations $\bar{N}_k$ and cluster growth rates inferred from measured cluster distributions (enabling calculation of Γ), the only unknown parameter in equation [3] is the dimer accommodation coefficient α which can be varied empirically until reasonable agreement between measured and modeled cluster

concentrations is achieved. In the case where the reduced cluster concentrations can be attributed entirely to the effects of dimer evaporation (the dimer accommodation coefficient would be unity), the dimensionless dimer population balance can be written as:

$$[4] \qquad \frac{d\bar{N}_{k^\dagger}}{d\tau} = \left(\bar{N}_1\right)^2 - \Gamma c_{1k^\dagger} \bar{N}_1 \bar{N}_{k^\dagger} - \bar{N}_{k^\dagger} \sum_{i=k^\dagger}^{\infty} c_{k^\dagger i} \bar{N}_i - \bar{E}_{k^\dagger} \bar{N}_{k^\dagger} .$$

In this limiting case, the only unknown would be the dimensionless evaporation parameter $\bar{E}_{k^\dagger}$, which can be varied empirically until reasonable agreement between measured and modeled cluster concentrations is achieved. The evaporation rate constant $E_{k^\dagger}$ can then be obtained from equation [2], yielding information regarding the dimer free energy of formation.

6.2 Nucleation Rate Calculations: Method Intercomparisons, Method Validations, and Data Set Linking

Due to particle size detection limits (~ 3 nm), formation rates of freshly nucleated particles (~ 1 nm) currently cannot be directly measured. These nucleation rates at 1 nm, J_1, are usually calculated in two steps: [1] calculation of the particle formation rate J_3 from measured size distributions at the detection limit, followed by [2] extrapolation of J_1 from J_3 by accounting for the probability that a 1 nm particle will grow to 3 nm before being lost by coagulation with the pre-existing aerosol. A number of different methods have been developed to calculate J_3 from measured size distributions [*Weber et al.*, 1996; *Sihto et al.*, 2006; *Riipinen et al.*, 2007], and to calculate the survival probability for a particle growing from 1 to 3 nm [*Weber et al.*, 1997; *Kerminen and Kulmala*, 2002; *Lehtinen et al.*, 2007]. Each of these methods contains approximations in its derivation and therefore has limits of applicability.

The goal of this work is to intercompare the various methods for steps [1] and [2], validate them against the cluster population balance model of *Kuang et al.* [2009e] which exactly solves the aerosol general dynamic equation, and then develop a set of analysis

criteria where certain methods in steps [1] and [2] can be expected to give reasonably accurate results. Such criteria would provide useful operating guidelines for data reduction, enabling the consistent calculation of nucleation rates from diverse measured aerosol size distributions. Once these guidelines for nucleation rate calculation are set, one can then process the combined data sets acquired by researchers from the University of Minnesota, the National Center for Atmospheric Research, and the University of Helsinki for the following measurement campaigns: MILAGRO (Tecamac, Mexico) [*Iida et al.*, 2008b]; ANARChE (Atlanta, Georgia) [*McMurry et al.*, 2005]; Boulder, CO [*Eisele et al.*, 2006]; QUEST II (Hyytiälä, Finland) [*Fiedler et al.*, 2005; *Sihto et al.*, 2006]; and QUEST IV (Hyytiälä, Finland) [*Riipinen et al.*, 2007]. This work will be presented in *Kuang et al.* [2009d].

6.3 Condensational Growth Detection and Sizing of Sub – 3 nm Diameter Aerosols

A new instrument for the detection and sizing of neutral sub – 3 nm aerosols has been developed, has undergone preliminary laboratory characterizations, and has been deployed in several field campaigns. This instrument, known as the nanoparticle growth (NPG) instrument, is based on the principle of condensational growth sizing, which exploits the axial dependence of saturation ratios inside a laminar flow condensation particle counter (CPC) [*Stolzenburg and McMurry*, 1991]. As nanoparticles pass through a CPC, they are exposed to air that is supersaturated with a working fluid (typically butanol), which then condenses onto the nanoparticles, causing them to grow to a size large enough to be detected by light scattering (~ 10 μm).

For small enough particles (< 15 nm), their final droplet size can be used to infer their initial particle size. Due to increasing particle curvature with decreasing size, smaller particles require a higher saturation ratio before they can be activated for growth. These smaller particles must travel farther along the condenser axis before they are exposed to a high enough saturation ratio and can begin to grow. Smaller particles therefore have less time to grow before they exit the condenser, yielding a smaller droplet

size. For small enough particles, the final droplet size exiting the condenser is therefore a function of the initial particle size, yielding information regarding the initial sampled nanoparticle size distribution [*Saros et al.*, 1996; *Weber et al.*, 1998b].

Rather than using butanol however, the NPG instrument uses oleic acid as the working fluid. *Iida et al.* [2008a] showed that, because of its low vapor pressure and high surface tension, oleic acid can activate particles as small as 1.2 nm mobility diameter without undergoing self-nucleation, which occurs when butanol is used to activate particles smaller than about 2.5 nm mobility diameter. This low vapor pressure also enables size-dependent condensational growth, where 1 – 3 nm particles grow to sizes of only 16 – 26 nm within the CPC. The size distribution of "grown" particles are measured by mobility classification [*Wang and Flagan*, 1990], which is then inverted with characterized activation efficiencies and growth laws to obtain the number concentration and size of the initial sampled particles, respectively.

Laboratory experiments showed that this instrument has a 50% activation efficiency for NaCl particles with a mobility diameter of 2.1 nm (about 1.8 nm geometric size) and can detect particles as small as ~ 1 nm geometric size, albeit with a low activation efficiency. Figure 6.1a shows laboratory results for the activation efficiency while Figure 6.1b shows the corresponding relationship bewteen the final "grown" particle size and the initial size of the NaCl particle. The NPG system was deployed for the measurement of new particle formation events in Boulder, CO and in the Manitou Experimental Forest during the summer of 2008. Preliminary analysis of those measurements indicates the detection of particles as small as 2.1 nm mobility diameter.

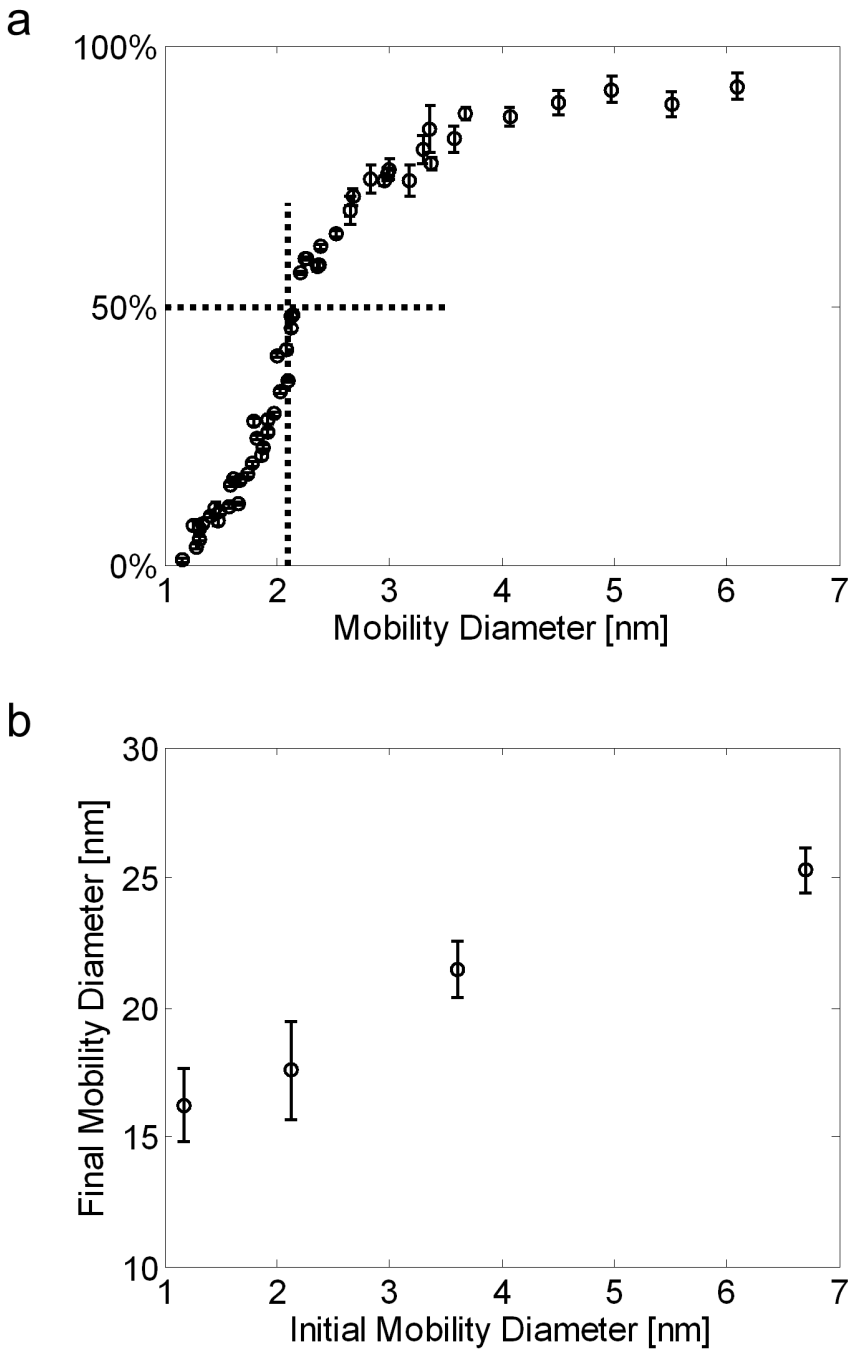

Figure 6.1 NPG characterization of (a) activation efficiencies and (b) size-dependent growth relationships for laboratory-generated neutral sodium chloride particles with oleic acid as the working fluid.

Accurate analysis of those measurements however requires additional work to be performed. Because the activation efficiency of sub 2 nm particles are particle composition dependent [*Iida et al.*, 2008a] and the composition of ambient sub 2 nm particles is currently unknown, there will be uncertainties in the sampled particle concentration. The condensational growth of sub 2 nm particles is likely composition dependent as well, leading to uncertainties regarding the initial particle size. Two approaches to reducing these uncertainties are being pursued: [1] characterizing the NPG instrument with neutral particles of known composition (inorganic, sulfate-based, amine-based, etc.) using established methods of generating mono-disperse aerosol standards; and [2] developing a diffusion sampling inlet (DSI) to be placed upstream of the NPG instrument. In this DSI, the sampling flow rate is varied, and the resulting size-dependent penetration efficiencies of sub 3 nm particles are measured (diffusional losses increase with decreasing flow rate and decreasing particle size). The flow-rate dependence of the penetration efficiency can then be inverted to yield the sampled particle size, providing an independent measure of particle size, unaffected by uncertainties in particle composition.

6.4 Final Remarks

The synergistic relationships between model development, theory development, instrument development, and field campaign measurements have provided insights and testable hypotheses regarding atmospheric nucleation. The cluster population balance model, constrained by ambient measurements, can provide useful upper and lower limits for particle production rates and their effect on the CCN population, for instance. As progress is made in lowering the instrument size detection limit, these model hypotheses regarding cluster formation rates and stability can then be tested and improved upon with these new measurements.

Bibliography

Albrecht, B. A. (1989), Aerosols, cloud microphysics, and fractional cloudiness, *Science*, *245*(4923), 1227-1230.

Becker, R., and W. Doring (1935), Kinetic Treatment of Grain Formation in Supersaturated Vapors, *Ann Physik*, *24*, 719-752.

Benson, S. W. (1968), *Thermochemical kinetics*, Wiley, New York.

Birmili, W., F. Stratmann, and A. Wiedensohler (1999), Design of a DMA-based size spectrometer for a large particle size range and stable operation, *Journal of Aerosol Science*, *30*(4), 549-553.

Boy, M., O. Hellmuth, H. Korhonen, E. D. Nilsson, D. Revelle, A. Turnipseed, F. Arnold, and M. Kulmala (2006), MALTE-model to predict new aerosol formation in the lower troposphere, *Atmospheric Chemistry and Physics*, *6*(12), 4499-4517.

Charlson, R. J., S. E. Schwartz, J. M. Hales, R. D. Cess, J. A. Coakley, J. E. Hansen, and D. J. Hofmann (1992), Climate forcing by anthropogenic aerosols, *Science*, *255*(5043), 423-430.

Chen, D. R., D. Y. H. Pui, D. Hummes, H. Fissan, F. R. Quant, and G. J. Sem (1998), Design and evaluation of a nanometer aerosol differential mobility analyzer (Nano-DMA), *Journal of Aerosol Science*, *29*(5-6), 497-509.

Chin, M., R. A. Kahn, L. A. Remer, H. Yu, D. Rind, G. Feingold, P. K. Quinn, S. E. Schwartz, D. G. Streets, P. Decola, and R. Halthore (Eds.) (2009), *Atmospheric Aerosol Properties and Climate Impacts*.

Dean, A. M. (1985), Predictions of pressure and temperature effects upon radical addition and recombination reactions, *Journal of Physical Chemistry*, *89*(21), 4600-4608.

Eisele, F. L., and D. J. Tanner (1993), Measurement of the gas phase concentration of H_2SO_4 and methane sulfonic acid and estimates of H_2SO_4 production and loss in the atmosphere, *Journal of Geophysical Research-Atmospheres*, *98*(D5), 9001-9010.

Eisele, F. L., and P. H. McMurry (1997), Recent progress in understanding particle nucleation and growth, *Philosophical Transactions of the Royal Society B: Biological Sciences*, *352*(1350), 191.

Eisele, F. L., E. R. Lovejoy, E. Kosciuch, K. F. Moore, R. L. Mauldin, J. N. Smith, P. H. McMurry, and K. Iida (2006), Negative atmospheric ions and their potential role in ion-induced nucleation, *Journal of Geophysical Research, 111*(D4), 11, doi:10.1029/2005jd006568.

Fiedler, V., M. Dal Maso, M. Boy, H. Aufmhoff, J. Hoffmann, T. Schuck, W. Birmili, M. Hanke, J. Uecker, and F. Arnold (2005), The contribution of sulphuric acid to atmospheric particle formation and growth: a comparison between boundary layers in Northern and Central Europe, *Atmospheric Chemistry and Physics, 5*, 1773–1785.

Ford, I. J. (1997), Nucleation theorems, the statistical mechanics of molecular clusters, and a revision of classical nucleation theory, *Physical Review E, 56*(5), 5615-5629.

Frenkel, J. (1946), *Kinetic Theory of Liquids*, Clarendon, Oxford.

Friedlander, S. K. (1977), *Smoke, Dust, and Haze*, Wiley, New York.

Fuchs, N. A. (1964), *The Mechanics of Aerosols*, Pergamon Press, New York.

Fuchs, N. A., and A. G. Sutugin (1971), High-dispersed aerosols, in *Topics in Current Aerosol Research*, edited by G. M. Hidy and J. R. Brock, pp. 1–60, Pergamon, Oxford..

Gaydos, T. M., C. O. Stanier, and S. N. Pandis (2005), Modeling of in situ ultrafine atmospheric particle formation in the eastern United States, *Journal of Geophysical Research, 110*, D07S12, doi:10.1029/2004JD004683.

Gelbard, F., and J. H. Seinfeld (1978), Numerical solution of the dynamic equation for particulate systems, *Journal of Computational Physics*, *28*(3), 357-375.

Gelbard, F., Y. Tambour, and J. H. Seinfeld (1980), Sectional representations for simulating aerosol dynamics, *Journal of Colloid and Interface Science*, *76*(2), 541-556.

Ghan, S. J., R. C. Easter, E. G. Chapman, H. Abdul-Razzak, Y. Zhang, L. R. Leung, N. S. Laulainen, R. D. Saylor, and R. A. Zaveri (2001), A physically based estimate of radiative forcing by anthropogenic sulfate aerosol, *Journal of Geophysical Research, 106*, 5279-5293.

Gilbert, R. G., and S. C. Smith (1990), *Theory of Unimolecular and Recombination Reactions*, Blackwell Scientific, Oxford.

Hanke, M., J. Uecker, T. Reiner, and F. Arnold (2002), Atmospheric peroxy radicals: ROXMAS, a new mass-spectrometric methodology for speciated measurements of HO_2 and RO_2 and first results, *International Journal of Mass Spectrometry*, *213*(2-3), 91-99.

Hanson, D. R., and F. L. Eisele (2002), Measurement of prenucleation molecular clusters in the NH3, H2SO4, H2O system, *Journal of Geophysical Research, 107*(D12), 4158.

Holbrook, K. A., M. J. Pilling, S. H. Robertson, and P. J. Robinson (1996), *Unimolecular Reactions*, Wiley, Chichester.

Iida, K., M. Stolzenburg, P. McMurry, M. J. Dunn, J. N. Smith, F. Eisele, and P. Keady (2006), Contribution of ion-induced nucleation to new particle formation: methodology and its application to atmospheric observations in Boulder, Colorado, *Journal of Geophysical Research, 111*(D23), 16, doi:10.1029/2006JD007167.

Iida, K., M. R. Stolzenburg, and P. H. McMurry (2008a), Effect of Working Fluid on Sub-2 nm Particle Detection with a Laminar Flow Ultrafine Condensation Particle Counter, *Aerosol Science and Technology*, *43*(1), 81-96.

Iida, K., M. R. Stolzenburg, P. H. McMurry, and J. N. Smith (2008b), Estimating nanoparticle growth rates from size-dependent charged fractions: analysis of new particle formation events in Mexico City, *Journal of Geophysical Research, 113*(D5), 15, doi:10.1029/2007JD009260.

IPCC (2007), *IPCC, 2007: Summary for Policymakers*, Cambridge University Press, New York, NY.

Kassel, L. S. (1928a), Studies in Homogeneous Gas Reactions. I, *Journal of Physical Chemistry, 32*(2), 225-242.

Kassel, L. S. (1928b), Studies in Homogeneous Gas Reactions. II. Introduction of Quantum Theory, *Journal of Physical Chemistry, 32*(7), 1065-1079.

Kerminen, V. M., and M. Kulmala (2002), Analytical formulae connecting the "real" and the "apparent" nucleation rate and the nuclei number concentration for atmospheric nucleation events, *Journal of Aerosol Science, 33*(4), 609-622.

Kerminen, V. M., H. Lihavainen, M. Komppula, Y. Viisanen, and M. Kulmala (2005), Direct observational evidence linking atmospheric aerosol formation and cloud droplet activation, *Geophysical Research Letters, 32*(14), L14803, doi:10.1029/2005GL023130.

Korhonen, H., K. E. J. Lehtinen, and M. Kulmala (2004), Multicomponent aerosol dynamics model UHMA: model development and validation, *Atmospheric Chemistry and Physics*, *4*, 757–771.

Ku, B. K., and J. F. de la Mora (2009), Relation between Electrical Mobility, Mass, and Size for Nanodrops 1–6.5 nm in Diameter in Air, *Aerosol Science and Technology*, *43*(3), 241-249.

Kuang, C., P. H. McMurry, A. V. McCormick, and F. L. Eisele (2008), Dependence of nucleation rates on sulfuric acid vapor concentration in diverse atmospheric locations, *Journal of Geophysical Research*, *113*(D10), D10209, doi:10.1029/2007jd009253.

Kuang, C., J. Jiang, and P. McMurry (2009a), Condensational growth detection and sizing of sub - 3 nm particles using oleic acid, *manuscript in preparation*.

Kuang, C., P. H. McMurry, and A. V. McCormick (2009b), Determination of cloud condensation nuclei production from measured new particle formation events, *Geophysical Research Letters*, *36*, L09822, doi:10.1029/2009GL037584.

Kuang, C., P. H. McMurry, A. V. McCormick, and M. R. Zachariah (2009c), Cluster energy non-accommodation and barriers to small cluster formation, *manuscript in preparation*.

Kuang, C., I. Riipinen, S.-L. Sihto, M. Kulmala, and P. McMurry (2009d), Method intercomparisons of nucleation rate parameterizations, *manuscript in preparation*.

Kuang, C., I. Riipinen, S.-L. Sihto, A. V. McCormick, M. Kulmala, and P. McMurry (2009e), An improved criterion for new particle formation in diverse atmospheric environments, *manuscript in preparation*.

Kulmala, M., L. Pirjola, and J. M. Mäkelä (2000), Stable sulphate clusters as a source of new atmospheric particles, *Nature*, *404*(6773), 66-69.

Kulmala, M., L. Laakso, K. E. J. Lehtinen, I. Riipinen, M. Dal Maso, T. Anttila, V. M. Kerminen, U. Hörrak, M. Vana, and H. Tammet (2004a), Initial steps of aerosol growth, *Atmospheric Chemistry and Physics*, *4*, 2553-2560.

Kulmala, M., H. Vehkamäki, T. Petäjä, M. Dal Maso, A. Lauri, V. M. Kerminen, W. Birmili, and P. H. McMurry (2004b), Formation and growth rates of ultrafine atmospheric particles: a review of observations, *Journal of Aerosol Science*, *35*(2), 143-176.

Kulmala, M., K. E. J. Lehtinen, and A. Laaksonen (2006), Cluster activation theory as an explanation of the linear dependence between formation rate of 3 nm particles and sulphuric acid concentration, *Atmospheric Chemistry and Physics*, *6*, 787–793.

Kurten, T., V. Loukonen, H. Vehkamaki, and M. Kulmala (2008), Amines are likely to enhance neutral and ion-induced sulfuric acid-water nucleation in the atmosphere more effectively than ammonia, *Atmospheric Chemistry and Physics*, *8*, 4095-4103.

Kurtén, T., C. Kuang, P. Gomez, P. McMurry, H. Vehkamäki, I. Ortega, M. Salonen, M. Noppel, and M. Kulmala (2009), The role of cluster energy non-accommodation in atmospheric sulfuric acid nucleation, *manuscript in preparation*.

Laaksonen, A., A. Hamed, J. Joutsensaari, L. Hiltunen, F. Cavalli, W. Junkermann, A. Asmi, S. Fuzzi, and M. C. Facchini (2005), Cloud condensation nucleus production from nucleation events at a highly polluted region, *Geophysical Research Letters*, *32*(6), L06812, doi:10.1029/2004GL022092.

Lehtinen, K. E. J., and M. Kulmala (2003), A model for particle formation and growth in the atmosphere with molecular resolution in size, *Atmospheric Chemistry and Physics*, *3*, 251–257.

Lehtinen, K. E. J., U. Backman, J. K. Jokiniemi, and M. Kulmala (2004), Three-body collisions as a particle formation mechanism in silver nanoparticle synthesis, *Journal of Colloid and Interface Science*, *274*(2), 526-530.

Lehtinen, K. E. J., M. Dal Maso, M. Kulmala, and V. M. Kerminen (2007), Estimating nucleation rates from apparent particle formation rates and vice versa: Revised formulation of the Kerminen–Kulmala equation, *Journal of Aerosol Science*, *38*(9), 988-994.

Lihavainen, H., V. M. Kerminen, M. Komppula, J. Hatakka, V. Aaltonen, M. Kulmala, and Y. Viisanen (2003), Production of "potential" cloud condensation nuclei associated with atmospheric new-particle formation in northern Finland, *Journal of Geophysical Research*, *108*(D24), 8.

Mäkelä, J. M., S. Yli-Koivisto, V. Hiltunen, W. Seidl, E. Swietlicki, K. Teinilä, M. Sillanpää, I. K. Koponen, J. Paatero, K. Rosman, and K. Hämeri (2001), Chemical composition of aerosol during particle formation events in boreal forest, *Tellus B*, *53*(4), 380-393.

McGraw, R., and A. Laaksonen (1996), Scaling Properties of the Critical Nucleus in Classical and Molecular-Based Theories of Vapor-Liquid Nucleation, *Physical Review Letters*, *76*(15), 2754-2757.

McMurry, P. H., and S. K. Friedlander (1979), New particle formation in the presence of an aerosol, *Atmospheric Environment*, *13*(12), 1635-1651.

McMurry, P. H. (1980), Photochemical aerosol formation from SO_2: a theoretical analysis of smog chamber data, *J. Colloid Interface Sci.*, *78*, 513-527.

McMurry, P. H. (1983), New particle formation in the presence of an aerosol: rates, time scales, and sub-0.01 μm size distributions, *J. Colloid Interface Sci.*, *95*(1), 72-80.

McMurry, P. H. (2000), A review of atmospheric aerosol measurements, *Atmospheric Environment*, *34*(12-14), 1959-1999.

McMurry, P. H., M. Fink, H. Sakurai, M. R. Stolzenburg, R. L. Mauldin, J. Smith, F. Eisele, K. Moore, S. Sjostedt, D. Tanner, L. G. Huey, J. B. Nowak, E. Edgerton, and D. Voisin (2005), A criterion for new particle formation in the sulfur-rich Atlanta atmosphere, *Journal of Geophysical Research*, *110*(D22), D22S02, doi:10.1029/2005JD005901.

McQuarrie, D. A., and J. D. Simon (1997), *Physical Chemistry: A Molecular Approach*, University Science Books, Sausalito.

O'Dowd, C. D., P. Aalto, K. Hameri, M. Kulmala, and T. Hoffmann (2002), Atmospheric particles from organic vapours, *Nature*, *416*(6880), 497-498.

Okada, Y., and Y. Hara (2007), Calculation of the Sticking Probability of a Water Molecule to a Water Cluster, *Earozoru Kenkyu*, *22*(2), 147-151.

Oxtoby, D. W., and D. Kashchiev (1994), A general relation between the nucleation work and the size of the nucleus in multicomponent nucleation, *The Journal of Chemical Physics*, *100*, 7665.

Oxtoby, D. W. (1998), Homogeneous nucleation: theory and experiment, *Journal of Physics Condensed Matter*, *10*(4), 897-897.

Pierce, J. R., and P. J. Adams (2007), Efficiency of cloud condensation nuclei formation from ultrafine particles, *Atmospheric Chemistry and Physics*, *7*, 1367–1379.

Ramabhadran, T. E., T. W. Peterson, and J. H. Seinfeld (1976), Dynamics of aerosol coagulation and condensation, *Aiche Journal*, *22*(5), 840-851.

Rao, N. P., and P. H. McMurry (1989), Nucleation and growth of aerosol in chemically reacting systems, *Aerosol Science and Technology*, *11*(2), 120-132.

Reiner, T., and F. Arnold (1993), Laboratory Flow Reactor Measurements of the Reaction $SO_3 + H_2O + M$ $H_2SO_4 + M$: Implications for Gaseous H_2SO_4 and Aerosol Formation in the Plumes of Jet Aircraft, *Geophysical Research Letters*, *20*(23).

Rice, O. K., and H. C. Ramsperger (1927), Theories of Unimolecular Gas Reactions at Low Pressures, *Journal of the American Chemical Society*, *49*(7), 1617-1629.

Rice, O. K., and H. C. Ramsperger (1928), Theories of Unimolecular Gas Reactions at Low Pressures. II, *Journal of the American Chemical Society*, *50*(3), 617-620.

Riipinen, I., S.-L. Sihto, M. Kulmala, F. Arnold, M. Dal Maso, W. Birmili, K. Saarnio, K. Teinilä, V. M. Kerminen, and A. Laaksonen (2007), Connections between atmospheric sulphuric acid and new particle formation during QUEST III-IV campaigns in Heidelberg and Hyytiälä, *Atmospheric Chemistry and Physics*, *7*(8), 1899-1914.

Salonen, M., T. Kurtén, H. Vehkamäki, T. Berndt, and M. Kulmala (2009), Computational investigation of the possible role of some intermediate products of SO2 oxidation in sulfuric acid-water nucleation, *Atmospheric Research*, *91*(1), 47-52.

Saros, M. T., R. J. Weber, J. J. Marti, and P. H. McMurry (1996), Ultrafine aerosol measurement using a condensation nucleus counter with pulse height analysis, *Aerosol Science and Technology*, *25*(2), 200-213.

Schenter, G. K., S. M. Kathmann, and B. C. Garrett (1999), Dynamical Nucleation Theory: A New Molecular Approach to Vapor-Liquid Nucleation, *Physical Review Letters*, *82*(17), 3484-3487.

Seinfeld, J. H., and S. N. Pandis (1998), *Atmospheric Chemistry and Physics: From Air Pollution to Climate Change*, John Wiley & Sons, New York.

Sihto, S.-L., M. Kulmala, V. M. Kerminen, M. Dal Maso, T. Petäjä, I. Riipinen, H. Korhonen, F. Arnold, R. Janson, and M. Boy (2006), Atmospheric sulphuric acid and aerosol formation: implications from atmospheric measurements for nucleation and early growth mechanisms, *Atmospheric Chemistry and Physics*, *6*(12), 4079-4091.

Sipilä, M., K. Lehtipalo, M. Attoui, K. Neitola, T. Petäjä, P. P. Aalto, C. D. O'Dowd, and M. Kulmala (2009), Laboratory Verification of PH-CPC's Ability to Monitor Atmospheric Sub-3 nm Clusters, *Aerosol Science and Technology*, *43*(2), 126-135.

Sjostedt, S. J., L. G. Huey, D. J. Tanner, J. Peischl, G. Chen, J. E. Dibb, B. Lefer, M. A. Hutterli, A. J. Beyersdorf, and N. J. Blake (2007), Observations of hydroxyl and the sum of peroxy radicals at Summit, Greenland during summer 2003, *Atmospheric Environment*, *41*(24), 5122-5137.

Smith, J. N., M. J. Dunn, T. M. VanReken, K. Iida, M. R. Stolzenburg, P. H. McMurry, and L. G. Huey (2008), Chemical composition of atmospheric nanoparticles formed from

nucleation in Tecamac, Mexico: evidence for an important role for organic species in nanoparticle growth, *Geophysical Research Letters*, *35*(4), L04808, doi:10.1029/2007GL032523.

Spracklen, D. V., K. S. Carslaw, M. Kulmala, V. M. Kerminen, S.-L. Sihto, I. Riipinen, J. Merikanto, G. W. Mann, M. P. Chipperfield, A. Wiedensohler, W. Birmili, and H. Lihavainen (2008), Contribution of particle formation to global cloud condensation nuclei concentrations, *Geophysical Research Letters*, *35*(6), L06808, doi:10.1029/2007GL033038.

Steinfeld, J. I., J. S. Francisco, and W. L. Hase (1989), *Chemical Kinetics and Dynamics*, Prentice Hall.

Stolzenburg, M. R., and P. H. McMurry (1991), An Ultrafine Aerosol Condensation Nucleus Counter, *Aerosol Science and Technology*, *14*(1), 48-65.

Stolzenburg, M. R., P. H. McMurry, H. Sakurai, J. N. Smith, R. L. Mauldin, F. L. Eisele, and C. F. Clement (2005), Growth rates of freshly nucleated atmospheric particles in Atlanta, *Journal of Geophysical Research*, *110*(D22), D22S05, doi:10.1029/2005JD005935.

Troe, J. (1977a), Theory of thermal unimolecular reactions at low pressures. I. Solutions of the master equation, *The Journal of Chemical Physics*, *66*, 4745.

Troe, J. (1977b), Theory of thermal unimolecular reactions at low pressures. II. Strong collision rate constants. Applications, *The Journal of Chemical Physics*, *66*, 4758.

Troe, J. (1979), Predictive possibilities of unimolecular rate theory, *The Journal of Physical Chemistry*, *83*(1), 114-126.

Venkatesh, R., R. R. Lucchese, W. H. Marlow, and J. Schulte (1995), Thermal collision rate constants for small nickel clusters of size 2–14 atoms, *The Journal of Chemical Physics*, *102*, 7683.

Volmer, M., and A. Weber (1926), Nuclei formation in supersaturated states, *Z. phys. Chem*, *119*, 277-301.

Wang, S. C., and R. C. Flagan (1990), Scanning Electrical Mobility Spectrometer, *Aerosol Science and Technology*, *13*(2), 230-240.

Warren, D. R., and J. H. Seinfeld (1985), Simulation of aerosol size distribution evolution in systems with simultaneous nucleation, condensation, and coagulation, *Aerosol Science and Technology*, *4*(1), 31-43.

Weber, R. J., P. H. McMurry, F. L. Eisele, and D. J. Tanner (1995), Measurement of expected nucleation precursor species and 3–500 nm diameter particles at Mauna Loa Observatory, Hawaii, *Journal of the Atmospheric Sciences*, *52*(12), 2242-2257.

Weber, R. J., J. J. Marti, P. H. McMurry, F. L. Eisele, D. J. Tanner, and A. Jefferson (1996), Measured atmospheric new particle formation rates: Implications for nucleation mechanisms, *Chemical Engineering Communications*, *151*, 53-64.

Weber, R. J., J. J. Marti, P. H. McMurry, F. L. Eisele, D. J. Tanner, and A. Jefferson (1997), Measurements of new particle formation and ultrafine particle growth rates at a clean continental site, *Journal of Geophysical Research*, *102*(D4), 4375-4385.

Weber, R. J., P. H. McMurry, L. Mauldin, D. J. Tanner, F. L. Eisele, F. J. Brechtel, S. M. Kreidenweis, and G. L. Kok (1998a), A study of new particle formation and growth involving biogenic and trace gas species measured during ACE 1, *Journal of Geophysical Research*, *103*(D13), 16,385-316,396.

Weber, R. J., M. R. Stolzenburg, S. N. Pandis, and P. H. McMurry (1998b), Inversion of ultrafine condensation nucleus counter pulse height distributions to obtain nanoparticle (3 – 10 nm) size distributions, *Journal of Aerosol Science*, *29*(5-6), 601-615.

Wehner, B., T. Petäjä, M. Boy, C. Engler, W. Birmili, T. Tuch, A. Wiedensohler, and M. Kulmala (2005), The contribution of sulfuric acid and non-volatile compounds on the growth of freshly formed atmospheric aerosols, *Geophysical Research Letters*, *32*(17), L17810.

Westmoreland, P. R., J. B. Howard, J. P. Longwell, and A. M. Dean (1986), Prediction of rate constants for combustion and pyrolysis reactions by bimolecular QRRK, *Aiche Journal*, *32*(12).

Woo, K. S., D. R. Chen, D. Y. H. Pui, and P. H. McMurry (2001), Measurement of Atlanta aerosol size distributions: observations of ultrafine particle events, *Aerosol Science and Technology*, *34*(1), 75-87.

Wu, J., and R. C. Flagan (1988), A discrete-sectional solution to the aerosol dynamic equation, *Journal of Colloid and Interface Science*, *123*(2), 339-352.

Zahoransky, R. A., J. Hoschele, and J. Steinwandel (1995), Formation of argon clusters by homogeneous nucleation in supersonic shock tube flow, *Journal of Chemical Physics*, *103*(20), 9038-9044.

Zhao, J., F. Eisele, M. Titcombe, C. Kuang, and P. McMurry (2009), Chemical Ionization Mass Spectrometric Measurements of Atmospheric Neutral Clusters using the Cluster-CIMS, *manuscript in submission*.